

Copyright  
by  
Jihyun Park  
2014

**The Dissertation Committee for Jihyun Park Certifies that this is the approved  
version of the following dissertation:**

**Regulation and Function of Two Membrane-Associated Protein Kinases**

**Committee:**

---

Kevin N. Dalby, Supervisor

---

John H. Richburg

---

Karen S. Browning

---

Edward M. Mills

---

Shawn B. Bratton

**Regulation and Function of Two Membrane-Associated Protein Kinases**

**by**

**Jihyun Park, B.S.; M.S.**

**Dissertation**

Presented to the Faculty of the Graduate School of

The University of Texas at Austin

in Partial Fulfillment

of the Requirements

for the Degree of

**Doctor of Philosophy**

**The University of Texas at Austin**

**May 2014**

## **Dedication**

*To the loving memory of my dear grandfather, Tae-San Doo (1926-2014)*

*&*

*To my beloved parents, Sang-Gon Park and Inhye Doo*

## **Acknowledgements**

First and foremost I would like to thank my advisor Dr. Kevin N. Dalby for giving me the opportunity to work in his laboratory. I am sincerely grateful for his guidance, support and patience throughout this study. He has been a real mentor and has inspired me as a scientist during my graduate school years. I will forever be thankful for all the positive things he has brought to my life and all I have learned from him.

I would also like to thank the members of my Ph.D. committee, Dr. John Richburg, Dr. Karen Browning, Dr. Edward Mills, and Dr. Shawn Bratton for their insightful comments, advice, and time over years.

I also thank the past and present members of Dalby's lab who have contributed immensely to my personal and professional development at UT-Austin. The Dalby group has been a source of friendship as well as good advice.

I am deeply grateful to all my friends in Korea and in U.S.A who have supported me along the way in any shape or form as it has all been precious to me.

I would also want to dedicate this work to my boyfriend, Giorgio, who has constantly encouraged me and greatly contributed to my happiness and well-being.

Most importantly, I would like to express my sincerest appreciation to my family, my father and mother, Sang-Gon Park and Inhye Doo, and to my brother, Sungjun Park for their love, support, and sacrifices. They have always believed in me that has enabled me to pursue my goals. Without their caring support, this achievement would not have been possible. I hope that I have made them proud of me.

Specially, this work is dedicated to the memory of my grandfather, Tae-San Doo, who passed down to me a love of reading and the respect for education as a teacher.

Finally, I dedicate this dissertation to all those who believe in the beauty of SCIENCE and the joy of LEARNING.

*Jihyun Park*

*Austin, Texas  
May 2014*

# **Regulation and Function of Two Membrane-Associated Protein Kinases**

Jihyun Park, Ph.D.

The University of Texas at Austin, 2014

Supervisor: Kevin N. Dalby

Protein kinases, many of which are regulated by autophosphorylation, modify their substrates by phosphorylation. Due to their roles in cellular signaling cascades controlling processes such as cellular proliferation, differentiation, metabolism, and apoptosis, protein kinases have caught the attention of scientists. In this study, we characterized the regulation and functions of two human membrane-bound protein kinases, TRPM7 and PERK.

TRPM7 (transient receptor potential melastatin 7) is a non-selective cation channel fused to an atypical kinase domain at the C-terminus that is implicated in cellular magnesium homeostasis. While the channel properties of TRPM7 have been studied extensively, little is known about the mechanisms regulating its kinase activity. Furthermore, to date, no specific small molecule inhibitor of TRPM7 kinase has been identified. Therefore, we characterized the biochemical and functional properties of TRPM7 autoactivity and discovered the first group of small molecule compounds targeting the kinase activity. Through a broad range of biochemical assays, we demonstrated that early autophosphorylation on three serine residues is required for TRPM7 kinase activity.

These phosphorylations promote a tetramer to dimer transition of the catalytic domain, as well as its cellular association with myosin. Aided by the discovery of effective kinase inhibitors a role for the kinase domain in actomyosin contractility and migration was examined.

PERK (PKR-like endoplasmic reticulum kinase) is a serine/threonine kinase, resident in the ER membrane and activated by the unfolded protein response (UPR), which detects the accumulation of unfolded proteins in the ER. The UPR and PERK are up-regulated in a variety of tumor types and may be critical for cancer cell adaptation. Therefore, a goal of this study was to identify PERK inhibitors that will provide new potential therapeutic strategies for treating cancer. We discovered a number of lead compounds and validated their ability to inhibit PERK kinase activity *in vitro*. The most potent PERK inhibitor was further tested to evaluate the modulation of the PERK signaling pathway in pancreatic cancer cells.

## Table of Contents

<b>List of Tables</b> .....	<b>xii</b>
<b>List of Figures</b> .....	<b>xiii</b>
<b>List of Illustrations</b> .....	<b>xvi</b>
<b>Chapter 1: Introduction</b> .....	<b>1</b>
1.1 Functions And Regulation of TRPM7 Channel.....	1
1.2 Characterization of TRPM7 Alpha-Kinase Domain.....	3
1.3 Cellular Functions And Roles of TRPM7 In Cancer.....	5
1.4 The Unfolded Protein Response (UPR) Signaling .....	7
1.5 PERK And Its Regulation.....	9
1.6 PERK: A Key Molecule of The UPR As a Cancer Drug Target.....	11
<b>Chapter 2: Characterization of the Mechanism of TRPM7 Autoactivation: Three Early Phosphorylations Correlate with Autoactivation</b> .....	<b>19</b>
2.1 Abstract.....	19
2.2 Introduction.....	20
2.3 Materials And Methods .....	23
Reagents, Strains, Plasmids and Equipment.....	23
Constructs .....	24
Expression and Purification of Proteins in <i>E.coli</i> .....	26
Analytical Methods .....	29
<i>General kinetic assays</i> .....	29
<i>Autophosphorylation assay using rapid quench flow equipment</i> .....	30
<i>Pre-steady state kinetic assay</i> .....	30
<i>Analysis of the three autophosphorylation-site mutants.</i> .....	31
Dynamic Light scattering .....	32
Mass Spectrometry, Liquid Chromatography, and Automated Spectral Analysis .....	33
Site-Directed Mutagenesis by Overlap Extension Using the Polymerase Chain Reaction.....	34



Western Blotting and Immunoprecipitation Experiments .....	35
2.4 Results And Discussion .....	36
Preparation of phosphate-free TRPM7-KD to facilitate the study of its autophosphorylation mechanism.....	36
Evidence that the inactive kinase domain is tetrameric.....	37
Autophosphorylation is required to activate TRPM7-KD.....	38
Characterization of the mechanism of TRPM7 autophosphorylation .....	38
Pre-steady state kinetic analysis of TRPM7-KD.....	39
Three early phosphorylations are sufficient to fully activate TRPM7 .....	40
The three autophosphorylation sites regulate the association with myosin II B	43
The autophosphorylation on three serine residues induces a conformational change of the TRPM7 kinase domain .....	44
2.5 Conclusion .....	45
<b>Chapter 3: Suppression of Breast Cancer Cell Migration by Novel Inhibitors</b>	
<b>Targeting TRPM7 Kinase Activity .....</b>	<b>60</b>
3.1 Abstract.....	60
3.2 Introduction.....	60
3.3 Materials And Methods .....	63
Biochemical Screening of NCI natural products set and challenge set.....	63
<i>In Vitro</i> Kinase Inhibition Assay .....	64
Cell culture .....	64
Data Analysis.....	65
Immunoprecipitation Experiments .....	67
Cell migration.....	68
3.4 Results And Discussion .....	68
Prioritizing hits and potential mechanisms of inhibition by the identified inhibitors.....	68
Selectivity of the compounds .....	69
Cellular Activity .....	70
TRPM7 kinase domain inhibitors impedes migration of breast cancer cells .....	70

3.5 Conclusion .....	71
<b>Chapter 4: Identification of Small Molecule Inhibitors for PERK through Luminescence High Throughput Screening and Characterization of Novel PERK Inhibitors in Pancreatic Cancer Cells.....</b>	<b>78</b>
4.1 Abstract.....	78
4.2 Introduction.....	79
4.3 Materials And Methods .....	82
Reagents and equipment.....	82
PERK Cloning.....	82
PERK Expression (550-1116) .....	84
PERK Purification (550-1116).....	84
<i>Ni-NTA affinity chromatography</i> .....	84
<i>3C Protease cleavage</i> .....	85
<i>Activation of PERK</i> .....	85
<i>MonoQ 10/10 anion exchange chromatography</i> .....	86
Expression and purification of eIF2 $\alpha$ .....	86
Peptide Synthesis.....	88
Substrate dependence assays .....	88
Compound libraries and Screening Facilities.....	89
Luminescence assay optimization .....	89
DMSO tolerance.....	90
High Throughput Screen (HTS).....	90
Confirmation Screen.....	92
In Vitro Kinase Inhibition Assay.....	93
Cell culture .....	94
Cell Proliferation Assay .....	94
Colony Formation Assay.....	95
Western blot analysis.....	95
4.4 Results And Discussion .....	96
Expression and purification of active human PERK and eIF2 $\alpha$ .....	96
Determination of kinetic parameters of PERK.....	97

Optimization of luminescent kinase assay for screening .....	97
High throughput screening of small molecule libraries .....	99
Hit confirmation screen by radiometric assay .....	100
Effect of compounds (1-4) on PERK autophosphorylation .....	101
Characterization of PERK inhibitors on cellular activity.....	102
Investigating the effect of compound 3 (TG101348) in pancreatic cancer cells .....	104
<i>Effect of compound 3 (TG101348) on cell proliferation and colony     formation.....</i>	<i>104</i>
<i>Effect of compound 3 (TG101348) on PERK downstream signaling pathway     .....</i>	<i>106</i>
<i>Biphasic effects of PERK specific inhibitor (GSK2606414) .....</i>	<i>108</i>
4.5 Conclusion .....	111
4.6 Supplementary Materials .....	135
<b>References .....</b>	<b>136</b>

## List of Tables

Table 3.1. The <i>in vitro</i> kinase assay results of the identified compounds. ....	73
Table 4.1. Inhibition rates of 4 hits from initial HTS using luminescent kinase assay. .	132
Table 4.2. Inhibition rates of 4 hits from validation screening using radiometric kinase assay.....	133
Table 4.3. Summary of PERK inhibition.....	134

## List of Figures

Figure 1.1. Schematic structure of TRPM7 channel.....	16
Figure 1.2. Crystal structure of TRPM7. ....	17
Figure 1.3. Schematic representation of ER stress-induced unfolded protein response (UPR).....	18
Figure 2.1. SDS-PAGE analysis of purified TRPM7-KD (1403-1864). ....	47
Figure 2.2. Dynamic light scattering analysis of phosphate-free TRPM7 kinase domain. ....	48
Figure 2.3. Autoactivity of TRPM7-KD towards peptide substrate. ....	49
Figure 2.4. Effect of different TRPM7 concentrations on its autophosphorylation. ....	50
Figure 2.5. Product release as the rate limiting step in the kinetic mechanism of TRPM7 kinase domain. ....	51
Figure 2.6. Three early autophosphorylation events are required for TRPM7 autoactivation.....	52
Figure 2.7. The effect of Alanine mutation of the early phosphorylation sites on TRPM7-KD autophosphorylation and kinase activity against either peptide and or protein substrate (myosin IIB). ....	54
Figure 2.8. The effect of aspartate mutation of the early phosphorylation sites on TRPM7-KD (A) autophosphorylation and (B) ability to phosphorylate its protein substrate myosin IIb substrate. ....	56
Figure 2.9. The effect of alanine mutation of the early phosphorylation sites on TRPM7 – myosin interaction in HEK293 cells.....	57
Figure 2.10. Dynamic light scattering analysis: Effect of autophosphorylation on the self-association of TRPM7 kinase domain. ....	58
Figure 2.11. Schematic model: Activation of TPRM7 catalytic domain.....	59
Figure 3.1. The effect of compounds 1-5 on the ability of TRPM7 kinase domain to phosphorylate its peptide substrate.....	74
Figure 3.2. Mechanism of TRPM7 inhibition by compound 1.....	75

Figure 3.3. Examining the ability of the tested compounds to modulate TRPM7-myosin interactions in HEK293 cells .....	76
Figure 3.4. TRPM7 kinase domain inhibitors inhibit MDA-MB-231 breast cancer cell migration.....	77
Figure 4.1. Purification of human PERK catalytic domain and eIF2 $\alpha$ that were expressed in <i>E. coli</i> .....	113
Figure 4.2. Analysis of the kinase activity of PERK.....	114
Figure 4.3. Optimization of luminescent kinase assay. ....	115
Figure 4.4. Assay stability in the presence of different concentrations of DMSO. ....	116
Figure 4.5. Examples of hits from Fragment library (Chembridge).....	117
Figure 4.6. Examples of hits from Maybridge library. ....	118
Figure 4.7. Examples of hits from kinase-biased library (Chembridge).....	119
120	
Figure 4.8. Examples of hits from Target focused kinase set.....	120
Figure 4.9. The effect of compounds 1-4 on the ability of PERK kinase domain to phosphorylate eIF2 $\alpha$ substrate. ....	121
Figure 4.10. Preparation of phosphate-free PERK kinase domain by treatment with lambda phosphatase. ....	122
Figure 4.11. The effect of compounds 1-4 on the ability of PERK kinase domain to autophosphorylate.....	123
Figure 4.12. Test the compounds (1-4) on the phosphorylation of eIF2 $\alpha$ <i>in vitro</i> .....	124
Figure 4.13. Cellular effect of compounds (1-4) on the phosphorylation of eIF2 $\alpha$ in HEK293T cells. ....	125
Figure 4.14. Compound 3 induces apoptotic death of pancreatic cancer cells. ....	126
Figure 4.15. Compound 3 inhibits colony formation of MiaPaCa-2 cells.....	127
Figure 4.16. Cellular effect of compound 3 on PERK signaling. ....	128

Figure 4.17. PERK inhibition by GSK2606414 induces biphasic response in pancreatic cancer cell proliferation under ER stress. ....	129
Figure 4.18. GSK2606414 induces biphasic response in colony formation of MiaPaCa-2 cells. ....	130
Figure 4.19. Cellular effect of GSK2606414 on PERK signaling. ....	131
Figure 4.S1. Cellular effect of compound 3 on the phosphorylation of PERK in HEK293T cells. ....	135

## List of Illustrations

Scheme 4.1. The first-in-class inhibitor of PERK (GSK2606414).....	81
Scheme 4.2. Principle of the Kinase-Glo luminescent kinase assay.....	99
Scheme 4.3. Dual inhibition of compound 3 (TG101348). .....	108



## Chapter 1: Introduction

### 1.1 FUNCTIONS AND REGULATION OF TRPM7 CHANNEL

Transient receptor potential (TRP) cation channels constitute a large protein superfamily. Physiologically, TRP channels function as cellular sensors responding to various stimuli such as temperature, taste, pain, sound and mechanical stress <sup>(1-4)</sup>. All TRP members contain six transmembrane segments with the pore loop positioned between the fifth and sixth transmembrane domains, which together form the cation-permeable pore <sup>(3)</sup>. The transient receptor potential melastatin (TRPM) family has eight members representing a wide range of structural features, expression patterns, ion selectivity and gating properties and functions. The TRPM family is divided into four groups based on mammalian sequence homology: TRPM1/3, TRPM6/7, TRPM2/8, and TRPM4/5 <sup>(3, 5)</sup>. TRPM7 consists of 1863 amino acids and was cloned by two groups <sup>(6, 7)</sup>. It is ubiquitously expressed, but with highest mRNA expression levels detected in the brain, heart and kidney <sup>(6, 8, 9)</sup>. Like most TRP channels, TRPM7 channels have six transmembrane domains, with a pore-forming domain between the fifth and sixth transmembrane domains. TRPM7 encodes a divalent cation channel fused to an atypical kinase domain at the C-terminus (figure 1.1) <sup>(10)</sup>. This kinase is a member of a small family of kinases that include elongation factor 2 (eEF2) kinase, and myosin heavy chain kinase A from *Dictyostelium discoideum* <sup>(7)</sup>. How the atypical kinase domain regulates the channel function of TRPM7 remains unclear.

TRPM7 is a non-selective cation channel, which is permeable to divalent cations such as  $Mg^{2+}$  and  $Ca^{2+}$ , as well as other trace metals including  $Zn^{2+}$ ,  $Mn^{2+}$  and  $Ni^{2+}$  (8, 11, 12). Initial studies report that TRPM7 current (flux of ions) is inhibited by the binding of  $Mg^{2+}$  (near the pore) and Mg-ATP (in the kinase domain) (13, 14). Its current is also inhibited by extracellular  $Zn^{2+}$  and  $Gd^{3+}$  (15, 16). In the absence of extracellular divalent cations, TRPM7 has also been reported to conduct monovalent cations such as  $Na^+$  and  $K^+$ , including protons (17). In addition, TRPM7 is known to be regulated by the Src-family kinases, and PIP2 levels have been shown by other groups to be crucial for TRPM7 channel activation (18). It remains controversial whether the receptor-mediated activation of phospholipase C (PLC), promoting hydrolysis of PIP2, leads to activation or inactivation of the TRPM7 channel (19, 20). Other research has also shown that TRPM7 currents are activated following a decrease in extracellular pH from physiological pH (7.4) to pH 4.0 (3, 17).

TRPM channels have diverse C-terminal domains but share a common C-terminal cytoplasmic TRP domain and a coiled-coil domain. Two TRP boxes located within the TRP domain possess significant sequence homology among the members of TRPC, TRPM, and TRPN subfamilies (3). The coiled-coil domain is a widespread protein-protein interaction structural motif that is found in a variety of protein classes including motor proteins, fibrous proteins and membrane fusion proteins. By use of size-exclusion chromatography, Tsuruda et al. demonstrated that a recombinant TRPM8 truncation protein containing the last 50 residues of the C-terminal cytoplasmic domain, forms a coiled-coil that is able to self-assemble into tetramers (21). Furthermore, they demonstrated that this domain is required for the expression of functional channels at the plasma

membrane. Recently, Fujiwara et al. resolved a high resolution crystal structure of the coiled-coil domain of TRPM7, which revealed that its overall structure is a tightly twisted, symmetric, and antiparallel tetramer (figure 1.2A) <sup>(22)</sup>.

Genetic and electrophysiological studies identified a major role of TRPM7 in the regulation of intracellular  $Mg^{2+}$  concentration, by showing that RNA interference or deletion of TRPM7 results in a decrease in intracellular  $Mg^{2+}$ , cell cycle arrest and eventually cell death <sup>(8, 23, 24)</sup>. Recent studies showed that homozygous deletion of the TRPM7 kinase domain caused embryonic lethality while heterozygous mice displayed abnormal absorption of  $Mg^{2+}$  suggesting that TRPM7 is a key regulator of  $Mg^{2+}$  homeostasis <sup>(24)</sup>. Inhibition of TRPM7 channel activity can be achieved by increasing  $Mg^{2+}$  concentration and intracellular Mg-ATP levels. Additionally, recent evidence suggests that TRPM7 activity contributes to various physiological functions in the cell, such as cell proliferation, neuronal cell death, neurotransmitter release, small synaptic-like vesicle fusion, and the regulation of actomyosin contractility <sup>(25-29)</sup>.

## **1.2 CHARACTERIZATION OF TRPM7 ALPHA-KINASE DOMAIN**

TRPM7 contains an atypical functional kinase domain which has specificity for serine and threonine residues <sup>(7, 30)</sup>. While the function and regulation of the TRPM7 channel has been extensively studied, little is known about the molecular mechanisms that regulate the activity of the TRPM7 alpha-kinase domain and the role of the kinase domain in regulating the channel function remains controversial. Runnels et al. reported that kinase-dead and  $Zn^{2+}$ -binding mutants abolished channel activity measured in whole-cell

recording experiments, which suggest that the kinase activity is essential for TRPM7 channel function <sup>(6)</sup>. Another group showed that mutation and deletion of the kinase domain of TRPM7 formed functional channels implying that TRPM7's kinase domain is not essential for activation of its channel <sup>(14)</sup>. Later, using whole-cell patch clamp analysis, Matsushita et al. argued that TRPM7 channel activity is functionally dissociated from its kinase activity, by showing that TRPM7 mutants that were mutated at two major autophosphorylation sites did not alter channel activity or regulation by internal  $Mg^{2+}$  <sup>(31)</sup>.

The TRPM7 alpha-kinase assembles into a dimer through the exchange of a 27-residue-long N-terminal sequence that extends from residue 1551 to residue 1577 (figure 1.2B) <sup>(32)</sup>. By analysis of truncation and site-directed mutants, Crawley et al. further divided the N-terminal segment into two parts; an 'activation sequence', encompassing residues 1553–1562, that is critical for kinase activity, but not dimer formation, and a 'dimerization sequence', encompassing residues 1563–1570, that is required for both dimer formation and TRPM7 kinase activity <sup>(33)</sup>. These findings suggest that TRPM7 alpha-kinase dimer formation plays a pivotal role in regulating enzyme activity.

Like conventional protein kinases, TRPM7 undergoes autophosphorylation, but the functional consequences for kinase activity are not well understood. Clark et al. identified autophosphorylated residues in TRPM7 by mass spectrometry and demonstrated that the cytosolic Ser/Thr-rich domain of TRPM7 is heavily autophosphorylated ( $32 \pm 4$  mol/mol) <sup>(34)</sup>. Recent research has revealed that all three non-muscle isoforms of the myosin II heavy chain (IIA, IIB and IIC) are substrates of TRPM7 kinase <sup>(35, 36)</sup>. Myosin II interacts with actin and forms bipolar filaments, which are important for regulating actomyosin

contractility<sup>(12, 35-37)</sup>. The report that myosin II heavy chain is a downstream substrate of TRPM7 kinase suggests a potential role of TRMP7 in the regulation of the actomyosin cytoskeleton, in a manner which is analogous to the function of myosin II heavy chain kinase (MHCK A) in *Dictyostelium*. *In vitro* biochemical assays were used to show that TRPM7 WT, but not the kinase-dead mutant (TRPM7-D1775A), phosphorylates and associates with myosin IIA in a regulated manner<sup>(36)</sup>. In addition, deletion of the autophosphorylation sites in the Ser/Thr-rich region of TRPM7 completely disrupted the phosphorylation of myosin II heavy chain, suggesting that TRPM7 interacts with the actomyosin cytoskeleton in a kinase-dependent manner to regulate myosin II activity and accordingly actomyosin contractility. TRPM7 is also involved in regulating cytoskeletal dynamics by its association with annexin I<sup>(36, 38)</sup>. Once again, these findings indicate a potential role of the TRPM7 alpha-kinase domain in the regulation of cell adhesion and motility.

### **1.3 CELLULAR FUNCTIONS AND ROLES OF TRPM7 IN CANCER**

As mentioned earlier, TRPM7 has been suggested to play a critical role in cell growth, proliferation and cell death. The expression of TRPM7 is prevalent in the brain, spleen, lung, kidney, heart, liver and microglia. TRPM7 overexpression was also found in cancer cells such as retinoblastoma, neck and head cells, gastric and breast cancer cells<sup>(23, 39-44)</sup>. However, whether TRPM7 activity contributes to cancer progression has not been established.  $\text{Ca}^{2+}$  and  $\text{Mg}^{2+}$  drive several cellular processes, and hence ion channels play a crucial role in the normal physiologic functioning of the cell. However, dysregulation of

channel function has been implicated in promoting a variety of human diseases, including cancer.

As a regulator of cell survival and death, TRPM7 is suggested to be a potential target for the pharmacological treatment of cancer. Research in human gastric cancer cells has shown that blockade of TRPM7 channels or knockdown of TRPM7 expression by siRNA inhibited cancer cell growth and induced the apoptosis of these cancer cells <sup>(40)</sup>. This implies the potential function of TRPM7 in the growth and proliferation of cancer cells. Similarly, pharmacologic inhibition of TRPM7 channels by  $Gd^{3+}$ , a nonspecific TRPM7 channel inhibitor, or knockdown of TRPM7 mRNA, suppressed the growth and proliferation of malignant head and neck tumor cells <sup>(39)</sup>.

Tumor metastasis is a hallmark of cancer and is defined as the ability of tumor cells to change their capacity to migrate, and permits them to adhere to other cells and tissues distant from the original tumor site <sup>(45, 46)</sup>. As TRPM7 is known to be implicated in modulating cell adhesion and migration through regulating cytoskeletal dynamics, researchers including Middelbeek and Guilbert, investigated whether TRPM7 is a key player in cancer cell metastasis <sup>(43, 44, 47)</sup>. Examination of the TRPM7 mRNA expression in the Oncomine database revealed that TRPM7 is closely linked with metastasis and invasive breast cancer <sup>(48)</sup>. Suppression of TRPM7 expression with RNA interference resulted in a significant decrease in the ability of breast cancer cells to migrate. Moreover, a recent study from Guilbert et al. suggested that TRPM7 is involved in estrogen receptor-negative metastatic breast cancer cell migration through its kinase domain. They reported that overexpression of the truncation mutant lacking the kinase domain decreased cell

migration, while the overexpression of the WT TRPM7 significantly increased migration of the weakly metastatic MCF-7 and highly metastatic MDA-MB-231 cells by 2.5 fold <sup>(43)</sup>. However, the molecular mechanisms underlying the contribution of TRPM7 to cancer cell proliferation and migration is still far from being understood. Taken together, these findings increase the possibility that TRPM7 could be a new and potential therapeutic target for the treatment of cancer.

#### **1.4 THE UNFOLDED PROTEIN RESPONSE (UPR) SIGNALING**

The endoplasmic reticulum (ER) is an organelle that has essential roles required for normal cellular functions, including calcium homeostasis, protein secretion and lipid biosynthesis. In eukaryotic cells, the ER provides a unique environment for the proper folding and posttranslational modification of several secretory and transmembrane proteins <sup>(49, 50)</sup>. Approximately one-third of the total proteome is synthesized on the ER. As a protein-folding compartment, this organelle is sensitive to alterations in homeostasis <sup>(51-55)</sup>. Multiple physiological or pathological disturbances that cause ER calcium depletion, nutrient deprivation, oxidative stress, viral infection or DNA damage can interrupt the protein-folding process and trigger accumulation of unfolded or misfolded proteins in the ER, a cellular condition referred to as ER stress <sup>(56-58)</sup>. Under such stress the cell initiates a protective mechanism termed the unfolded protein response (UPR) that is specifically designed to restore homeostasis and normal ER function. The UPR consists of three main signaling systems initiated by three ER resident stress sensors: activating transcription factor 6 (ATF6), inositol requiring kinase 1 (IRE1), and protein kinase R (PKR)-like

endoplasmic reticulum kinase (PERK) (figure 1.3) <sup>(59-61)</sup>. Activation of the UPR leads to adaptation or cellular death <sup>(62)</sup>. During adaptation, the UPR functions to restore ER homeostasis by inducing the expression of chaperones that enhance protein folding. At the same time, protein translation is globally attenuated to reduce the ER folding load, while the degradation of unfolded proteins is increased. On the contrary, if ER stress is prolonged and severe, UPR signaling triggers cell death by apoptosis <sup>(63, 64)</sup>. Thus, ER homeostasis strongly influences many physiological processes including lipid and cholesterol metabolism, energy control and inflammation. The functional significance of UPR signaling is not yet fully understood, but it is known that aberrant protein folding and the UPR have been linked to the development of various disease states such as diabetes, cancer and neurodegenerative disorders <sup>(49, 51, 52, 54, 58, 65-69)</sup>. Therefore, targeting UPR signaling could be a promising therapeutic strategy for the treatment of diseases whose pathogenesis is characterized by a highly activated UPR and ER stress.

Under normal, unstressed conditions, the luminal domains of three UPR sensors (ATF6, IRE1 and PERK) are bound to a chaperone called the glucose regulating protein 78 (GRP78) also known as BiP <sup>(70, 71)</sup>. However, upon ER stress, GRP78 is released from all three transducers and binds to unfolded or misfolded proteins in the lumen of the ER, leading to activation of the UPR and downstream signaling events initiated by all three UPR transducers. As mentioned above, if the ER stress is too severe to be handled, the UPR initiates apoptotic cell death signaling. ER sensor molecules including PERK are responsible for both the adaptive and the proapoptotic pathways of the UPR.



ER stress and UPR signaling are frequently up-regulated in tumor cells as a result of mutant or deregulated protein synthesis and folding<sup>(72, 73)</sup>. They are also up-regulated as a consequence of tumor hypoxia promoted by the tumor's abnormal vasculature, and in some cases due to the protein-damaging effects of agents used in chemotherapy<sup>(74, 75)</sup>. All of these may lead to the accumulation of misfolded proteins in the ER<sup>(76)</sup>. It has been reported that the UPR attenuates overall tumor protein translation, while enhancing the translation of stress survival proteins such as HIF-1 $\alpha$ , c-Myc and VEGF, which are known oncoproteins<sup>(77-83)</sup>. However, how UPR activation contributes to tumor cell survival is not clear.

### **1.5 PERK AND ITS REGULATION**

PERK is an ER transmembrane protein that consists of a luminal domain (bound by the ER chaperone BiP/GRP78 under non-stressed conditions) and a cytoplasmic domain (that possesses kinase activity). PERK is a serine-threonine kinase that belongs to the eIF2 $\alpha$  kinase subfamily (PKR [protein kinase double-stranded RNA-dependent], GCN2 [general control non-derepressible-2] and HRI [heme-regulated inhibitor]) and phosphorylates eIF2 $\alpha$  on Ser51<sup>(59, 84-87)</sup>. When the ER is stressed, BiP/GRP78 binds to the unfolded proteins and releases the luminal domain of PERK, allowing it to oligomerize in ER membranes. This leads to its autophosphorylation and kinase domain activation<sup>(61, 88-90)</sup>. The close vicinity of the cytoplasmic kinase domains of the PERK dimer allows *trans*-autophosphorylation at multiple sites, including residues on the kinase activation loop and the insert loop. PERK is also capable of undergoing autophosphorylation on its tyrosine

residues both *in vitro* and *in vivo* <sup>(91)</sup>. Furthermore, it has been shown that Tyr615, which is located in a highly conserved region of the kinase domain of PERK, is essential for autocatalytic activity <sup>(91)</sup>. PERK is known to be hyperphosphorylated by ER stress in cells; however, very little is known about where the multiple phosphorylation occurs within its kinase domain and how its function is controlled. Using a chimeric FV2E-PERK construct, Avivar-Valderas et al. have demonstrated *in vitro* that dimerization is sufficient to activate the kinase <sup>(92)</sup>. Recently, a crystal structure of the mouse PERK kinase domain was determined to 2.8Å resolution, and its structure revealed a back-to-back N-lobe dimer, which has been shown for the other eIF2 $\alpha$  kinases, GCN2 and PKR <sup>(93)</sup>.

The activation of PERK results in the phosphorylation of its main downstream effector, the eukaryotic initiation factor 2 $\alpha$  (eIF2 $\alpha$ ) and suppression of global mRNA translation by inhibiting its GDP-GTP exchange reaction <sup>(90, 94)</sup>. This mechanism expedites the process of ER homeostasis, by enabling the existing unfolded or misfolded proteins in the lumen to attain their folded conformation. Interestingly, attenuated protein translation is not universal; genes with internal ribosome entry site (IRES) sequences in the 5' untranslated regions escape from this global inhibition of protein synthesis <sup>(95, 96)</sup>. Therefore, some selected mRNAs, such as activating transcription factor 4 (ATF4), are translated. ATF4 acts as a transcription factor regulating multiple genes that contribute to recovering ER functions such as amino acid transport and synthesis, redox reactions and protein secretion <sup>(97, 98)</sup>. ATF4 also induces the expression of genes related to pro-apoptotic functions. Two main target genes driven by ATF4 are CHOP (transcription factor C/EBP homologous protein) and GADD34 (growth arrest and DNA damage-inducible 34) <sup>(99, 100)</sup>.

CHOP is a transcription factor that is associated with apoptotic cell death. However, the link between CHOP expression and cell death is likely more complex than simple down-regulation of pro-survival genes. GADD34 encodes a protein phosphatase 1 (PP1) which counteracts PERK by dephosphorylating the Ser51 residue of eIF2 $\alpha$  <sup>(101)</sup>. In addition, PERK was also reported to phosphorylate the bZIP transcription factor NF-E2 related factor 2 (NRF2), resulting in the activation of genes related to antioxidant response including heme oxygenase 1 and glutathione *S*-transferase <sup>(102, 103)</sup>.

PERK has also been reported to have UPR-independent roles. It regulates proliferation of the insulin-secreting beta cells during early neonatal development and is essential for survival of acinar cells in mouse exocrine pancreas, neither of which is associated with the ER stress response <sup>(104, 105)</sup>. The importance of PERK in this response was first recognized in the human genetic disorder, Wolcott-Rallison syndrome, which is characterized by postnatal retardation, skeletal dysplasia and early onset insulin-dependent diabetes <sup>(106)</sup>. PERK is also required for normal ER functions including pro-insulin trafficking, insulin secretion and quality control of protein synthesis in beta cells <sup>(106-109)</sup>.

Taken together, the PERK-eIF2 $\alpha$  arm of the UPR is strongly protective at modest levels of signaling (varies depending on cell type) by maintaining redox balance during ER stress through activation of ATF4 and NRF2, but can also contribute to apoptotic cell death pathways when activated to a greater extent.

## **1.6 PERK: A KEY MOLECULE OF THE UPR AS A CANCER DRUG TARGET**

The regulation of protein translation is complex, involving 9 eukaryotic initiation factors (eIFs) <sup>(110)</sup>. Eukaryotic translation initiation factor 2 (eIF-2), which consists of three subunits ( $\alpha$ ,  $\beta$  and  $\gamma$ ), is one of the key molecules in the initiation of translation <sup>(87, 111)</sup>. A critical control point is the initiation of protein translation through the alpha subunit of eIF2, which is required for the recruitment of the methionyl-tRNA to the 40S ribosome at the beginning of protein translation. During the initiation phase, eIF2 forms a ternary complex with Met-tRNA<sup>met</sup> and GTP and facilitates generation of 43S preinitiation complex. Before the joining of the 60S ribosomal subunit, the GTP bound to eIF2 is hydrolyzed, then eIF2-GDP is released from the ribosomal subunit. For subsequent rounds of translation, GDP bound to eIF2 must be exchanged for GTP, a process carried out by eIF2B. When eIF2 $\alpha$  is phosphorylated, it prevents the GDP-GTP exchange activity of eIF2B, thus preventing the initiation of protein synthesis, which leads to attenuation of general cap-dependent protein translation <sup>(87, 112, 113)</sup>. In the UPR signaling, the primary mechanism for eIF2 $\alpha$  phosphorylation is through PERK <sup>(61, 88)</sup>. It has been shown that eIF2 $\alpha$  phosphorylation is associated with increased expression of stress response proteins (HIF-1 $\alpha$ , c-MYC, VEGF) <sup>(114)</sup>. Rapidly proliferating cancer cells need increased ER activity to facilitate protein folding, assembly and transport. However, growing tumors suffer from regions of hypoxia and from decreased nutrient supply due to abnormal vascularization and rapid growth <sup>(76, 115)</sup>. These changes disturb ER homeostasis and activate the UPR to overcome stresses by increasing transcription of stress response genes. Thus, in response to ER stress, it was observed that the UPR is activated in a variety of tumor types such as cervical carcinoma, glioblastoma, lung cancer and breast cancer from

both patients and animal models <sup>(57, 116)</sup>. Cells with a compromised PERK-eIF2 $\alpha$ -ATF4 signaling pathway are more sensitive to hypoxic stress *in vitro*, and form tumors that grow more slowly *in vivo* <sup>(117)</sup>. Previous studies by Blais et al. demonstrate that tumors derived from K-Ras-transformed Perk<sup>-/-</sup> mouse embryonic fibroblasts (MEFs) are not only smaller than wild-type tumors but also appear to have severe limitations in their ability to stimulate tumor cell adaptation and angiogenesis <sup>(80, 118)</sup>. Similarly, cell-cycle arrest was observed when PERK expression was knocked down by shRNA in human breast cancer cells and esophageal carcinoma cells. In addition, BiP, a regulator of PERK, was also shown to be required for both tumor growth and conferring drug resistance <sup>(119)</sup>.

Poor oxygenation (hypoxia) is present in the majority of human tumors and is associated with poor prognosis <sup>(74, 115)</sup>. Hypoxia also elicits multiple cellular response pathways that alter gene expression and affect tumor progression, including two separate pathways that strongly suppress the mRNA translation during hypoxia <sup>(74, 120)</sup>. The first pathway is mediated by the UPR and phosphorylation of the eIF2 $\alpha$ , which is required for hypoxic cell survival and tumor growth. Translation during hypoxia is also inhibited through the inactivation of a second eukaryotic initiation complex, eukaryotic initiation factor 4F <sup>(115)</sup>. At least part of this inhibition is mediated through the mammalian target of rapamycin kinase (mTOR). mTOR integrates signals from several upstream pathways that respond to growth factors, nutrients, and energy, to regulate metabolism and cell growth <sup>(120-123)</sup>. Control of mRNA translation via disruption of eIF4F is indeed expected to vary considerably among different tumors because the upstream pathways that control the assembly of this complex are frequently disrupted in cancer <sup>(120)</sup>. In addition, eIF4F has

emerged as an important target during tumor development. Although eIF4F assembly under hypoxia is disrupted, the importance of this effect on tumor growth or hypoxia tolerance has yet to be addressed.

Despite PERK being identified as a therapeutic target for cancer, no selective inhibitors had been reported when this study began. However, recently GlaxoSmithKline research group reported a highly specific small molecule inhibitor of PERK (GSK2606414)<sup>(124)</sup>. GSK2606414 is a high affinity ligand of the PERK kinase domain that hinders kinase activity by binding to the kinase ATP binding pocket, resulting in competition with ATP. GSK2606414 inhibited PERK activation in A549 cells and decreased tumor growth in a xenograft model of pancreatic cancer at a dose of 50-150 mg/kg per day. The same group developed a further optimized PERK inhibitor, GSK 2656157<sup>(125)</sup>, which also blocked PERK activity in cells as shown by a decrease in PERK autophosphorylation, eIF2 $\alpha$  phosphorylation, expression of ATF4 and CHOP. Twice daily oral administration of GSK2656157 also inhibited tumor growth in several mouse xenograft models. Using *in vivo* techniques, including gene expression analysis in pancreatic tumor xenografts and immunohistochemistry, Axten et al. showed that the anticancer activity of the PERK inhibitor (GSK 2656157) correlates with several physiological features including altered amino acid metabolism, decreased blood vessel density, and vascular perfusion<sup>(125)</sup>. However, mechanisms for the observed anti-tumor effect need to be further elucidated.

Together, this evidence suggests a substantial role for PERK and the UPR in tumor survival and adaptation to stress. Therefore, inhibiting PERK activity offer a potentially

effective approach to block the UPR and thus, the synthesis of stress survival oncoproteins, ultimately leading to cancer cell death.

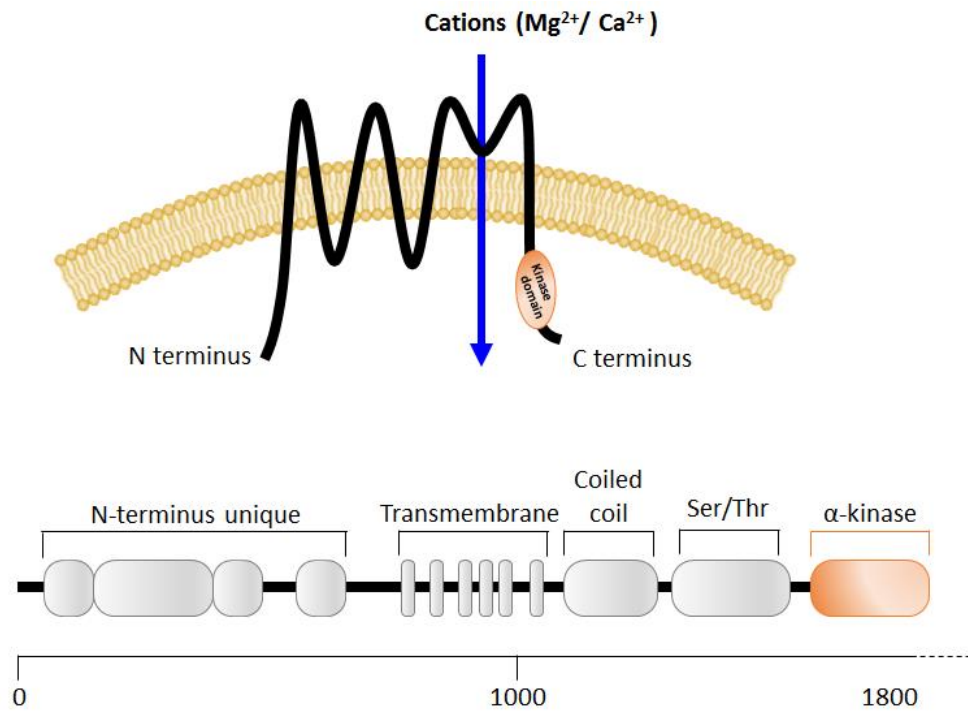


**Figure 1.1. Schematic structure of TRPM7 channel.**

Representation of the domain structure of TRPM7 including the six transmembrane domain, coiled-coil domain, Ser/Thr-rich region and the atypical alpha-kinase domain. (Modified from Wolf et al. <sup>(10)</sup>)



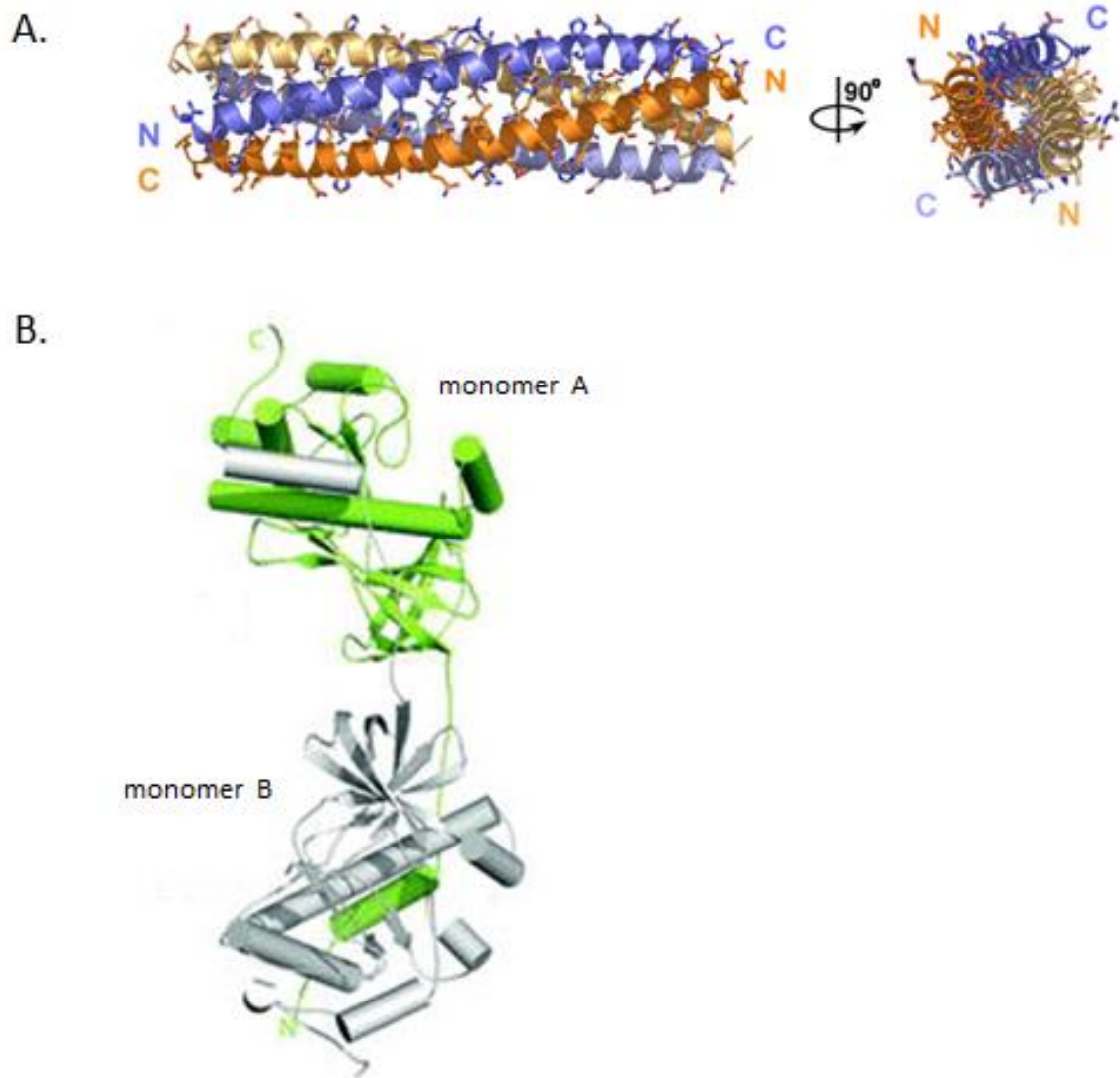


**Figure 1.2. Crystal structure of TRPM7.**

**A,** Structure of the TRPM channel coiled-coil assembly domain (Fujiwara et al.)<sup>(22)</sup>

**B,** Structure of the kinase domain of TRPM7 (residues 1551–1577) (Yamaguchi et al.)<sup>(32)</sup>

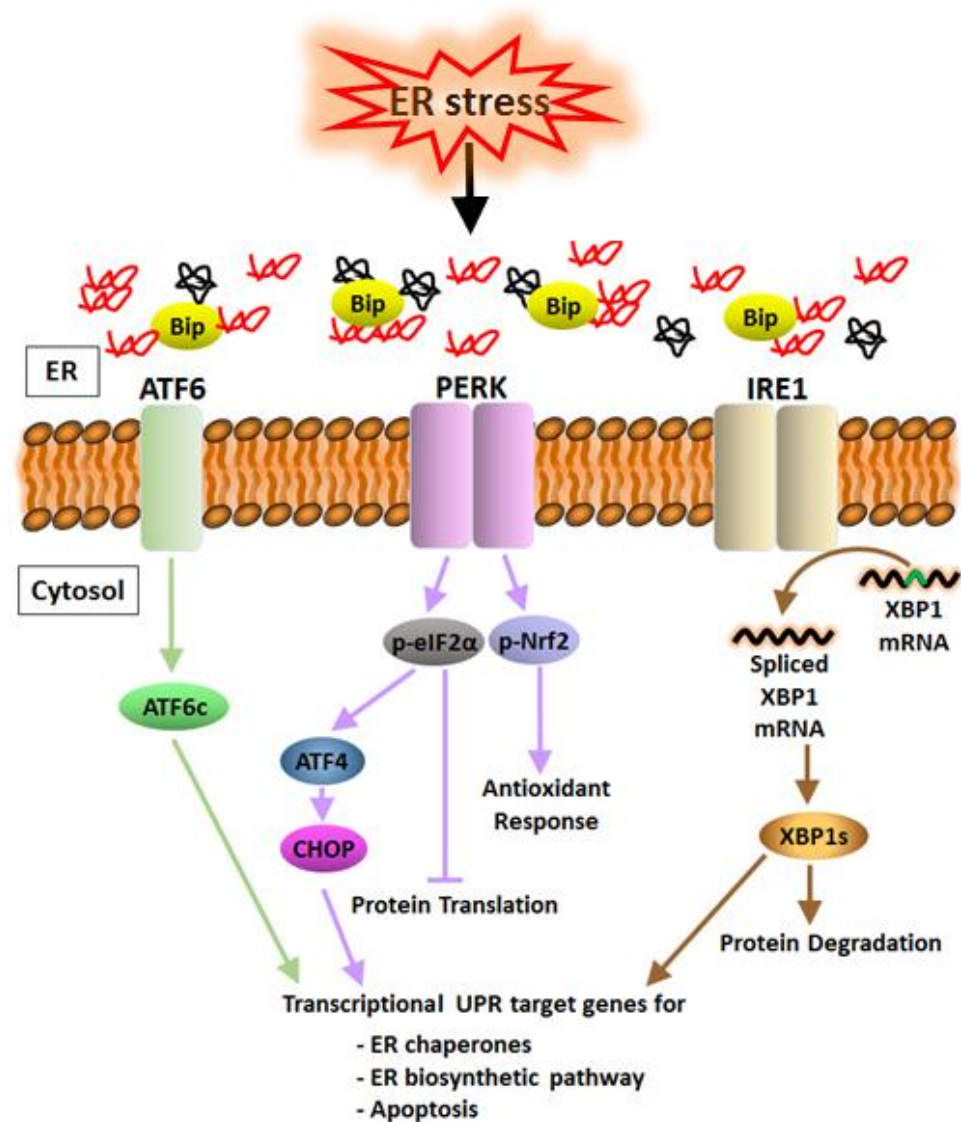


**Figure 1.3. Schematic representation of ER stress-induced unfolded protein response (UPR).**

Accumulation of misfolded or unfolded proteins at the ER triggers an adaptive stress response known as the UPR. The UPR is controlled by three sensor molecules of unfolded proteins in the ER membrane (ATF6, PERK, and IRE1). The ER stress sensors activate transcriptional and translational programs that collectively recover the homeostasis of protein folding in the ER.

## **Chapter 2: Characterization of the Mechanism of TRPM7 Autoactivation: Three Early Phosphorylations Correlate with Autoactivation<sup>†</sup>**

### **2.1 ABSTRACT**

The channel-kinase TRPM7 is a bifunctional protein consisting of a cation channel that is permeable to  $Mg^{2+}$ ,  $Ca^{2+}$  and  $Mn^{2+}$  and is fused to a kinase domain. Electrophysiological characterization of TRPM7 implicates it in cellular magnesium homeostasis. While the channel properties of TRPM7 have been studied extensively, little is known about the mechanisms regulating its kinase activity. In this study, we investigated the biochemical and functional properties of TRPM7 autoactivity. The vigorous autophosphorylation of the TRPM7 kinase domain during its expression in bacterial cells acted as a barrier towards the study of its mechanism of autoactivation. The use of a lambda phosphatase co-expression protocol enabled us to obtain phosphate-free TRPM7. Using this form of TRPM7, we could monitor its autophosphorylation and relate it to its activity against a downstream substrate. Here, using rapid quench-flow kinetics, we demonstrate that the first three phosphates that add to the enzyme (in the first ~30 seconds) are sufficient to fully activate TRPM7 against a peptide substrate and myosin. These three sites were determined by mass spectrometry. Mutation of the three early autophosphorylation sites

---

<sup>†</sup> Contributions to the work described in this chapter: Dr. Tamer S. Kaoud (Analyzed PF-TRPM7 by rapid quench flow device and helped fitting kinetic data); Dr. James A. Madsen and Dr. Jennifer S. Brodbelt (Analyzed early autophosphorylation sites of TRPM7 by mass spectrometry); Dr. Austen F. Riggs (Analyzed TRPM7 by dynamic light scattering).

abolished kinase activity against its substrates and impeded its interaction with actomyosin in the cells. To study the effect of oligomerization of the kinase domain on the autophosphorylation of TRPM7, rapid quench flow was employed over a range of TRMP7 concentrations. The rate of autophosphorylation increased steadily with increasing concentration, consistent with oligomerization-dependent autophosphorylation. Phosphate-free TRPM7 kinase domain exists as a tetramer, while both fully activated and transiently-autophosphorylated (30 seconds) TRPM7 kinase domain is dimeric. Collectively, our results support a model where early autophosphorylation on three residues triggers a conformational change that promotes a tetramer to dimer transition of the catalytic domain and activation of the enzyme to facilitate its association with actomyosin.

## 2.2 INTRODUCTION

The channel-kinase TRPM7 is ubiquitously expressed. This channel is permeable to various cations such as  $Mg^{2+}$ ,  $Ca^{2+}$ ,  $Zn^{2+}$ ,  $Co^{2+}$  and  $Mn^{2+}$ , but preferentially transports  $Mg^{2+}$  (12, 126, 127). Since  $Mg^{2+}$  is an abundant and essential divalent ion in the cell (126), TRPM7 is considered to be an important regulator of cellular  $Mg^{2+}$  homeostasis (6, 8). Magnesium is a critical cation and cofactor in various intracellular functions where it provides structural integrity for numerous proteins and nucleic acids and is a cofactor for many enzymatic reactions (126). However, little is known about the regulation of cellular  $Mg^{2+}$  homeostasis. Recent studies showed that homozygous deletion of the kinase domain caused embryonic lethality while heterozygous mice displayed abnormal absorption of

Mg<sup>2+</sup> suggesting that TRPM7 is a key regulator of Mg<sup>2+</sup> homeostasis <sup>(24)</sup>. On the other hand, another study using primary mammalian cells reported that deletion of the gene *Trpm7* did not affect the absorption of Mg<sup>2+</sup> or the concentration of total cellular Mg<sup>2+</sup> <sup>(128)</sup>. The functional alpha-kinase domain at the carboxyl terminus of TRPM7 has been structurally characterized and displays the unique feature of a zinc finger domain as well as a region involved in the binding of ATP <sup>(32)</sup>. The bifunctional property of TRPM7 to act as an ion channel and as a kinase provides this protein unique abilities to regulate cellular signal transduction <sup>(6, 8)</sup>. The role of the TRPM7 kinase domain in the channel function remains controversial. While some studies reported that the TRPM7 channel activity is dependent on the phosphotransferase activity of the kinase domain by showing for example that mutations of the kinase domain disrupted the channel function in whole cell recordings, others found that the channel function was dissociated from the kinase activity by demonstrating that TRPM7 lacking the kinase domain exhibited the same Mg<sup>2+</sup> sensitivity as wild type TRPM7 <sup>(6, 14, 31, 129)</sup>. Three downstream substrates of TRPM7 kinase have been identified so far. These are annexin-1, myosin II, and calpain <sup>(37, 38, 130)</sup>.

Besides a role in Mg<sup>2+</sup> homeostasis, TRPM7 is involved in other cellular events such as cell proliferation, apoptosis, exocytosis, cell adhesion and actomyosin contractility <sup>(2, 26, 36-38, 130)</sup>. Considering that these substrates and TRPM7 have been implicated in cell migration, cell growth, and cell death, it is possible that the phosphorylation of annexin-1, myosin II, or calpain by the TRPM7 kinase domain is involved in the regulation of cell survival and cell death. However, the biological importance of these signaling events still remains to be addressed. Recent studies suggested that the TRPM7 kinase domain

autophosphorylates extensively (more than 30 sites) within its C-terminus and this extensive autophosphorylation controls substrate recognition and phosphorylation <sup>(34)</sup>. In addition, it was reported that dimerization of TRPM7 is required for its activity <sup>(32, 33)</sup>. To date, little is known regarding the role of autophosphorylation in regulating TRPM7 kinase activity. According to a growing number of studies with clinical significance, TRPM7 has been linked to the pathogenesis of human diseases such as ischemic brain damage, Alzheimer's disease, stroke and cancer <sup>(1, 39, 41, 131, 132)</sup>. Protein kinases are important targets for the treatment of human diseases such as cancer as they are often the result of misregulated kinase-dependent signaling pathways <sup>(133-136)</sup>. Hence TRPM7 can be a candidate target for the treatment of human disease.

In this study, we characterized the mechanisms of TRPM7 autophosphorylation using purified nonphosphorylated TRPM7 catalytic domain and its activity against downstream substrates. We used both peptide and myosin as substrates. A rapid quench-flow kinetic study of its autophosphorylation and autoactivation revealed that the first three phosphates added to the enzyme (within the ~30 seconds) are enough to make the enzyme fully active against its peptide substrate, while the remaining 34 phosphates that are added by further autophosphorylation are not required for its activity. These three autophosphorylation sites have been further studied by MS/MS and site-directed mutagenesis. To study the effect of oligomerization on autophosphorylation of TRPM7, rapid quench-flow was employed to determine the ability of TRPM7 to be autophosphorylated at different concentrations. At a concentration of more than 400 nM the rate of TRPM7 autophosphorylation plateaued. In order to monitor the active state of

this enzyme, dynamic light scattering was used. We also performed a pre-steady state kinetic analysis of the enzyme to obtain the catalytic properties of TRPM7 in detail. We observed an initial burst followed by slower, linear phase. Overall, our results provide a detailed characterization of the kinase activity of TRPM7 and suggest that TRPM7 is autophosphorylated in an oligomerization-dependent manner and requires no more than three phosphates to become active towards other substrates. The autophosphorylation on three sites may play a role promoting a conformational change necessary for enzyme activity and may communicate to regulate the channel.

## **2.3 MATERIALS AND METHODS**

### **Reagents, Strains, Plasmids and Equipment**

Yeast extract, tryptone and agar were purchased from USB Corporation (Cleveland, OH). Isopropyl  $\beta$ -D-1-thiogalactopyranoside (IPTG) and dithiothreitol (DTT) were obtained from US Biological (Swampscott, MA). Qiagen (Valencia, CA) supplied Ni-NTA Agarose, QIAprep Spin Miniprep Kit, QIAquick PCR Purification Kit and QIAquick Gel Extraction Kit. Restriction enzymes, PCR reagents and T4 DNA Ligase were obtained from either New England BioLabs (Ipswich, MA) or Invitrogen Corporation (Carlsbad, CA). Oligonucleotides for DNA amplification and mutagenesis were from Sigma-Aldrich (St. Louis, MO). Stratagene *PfuUltra*<sup>TM</sup> High-Fidelity DNA Polymerase was purchased from Agilent Technologies, Inc. (Santa Clara, CA). BenchMark<sup>TM</sup> Protein Ladder was from Invitrogen Corporation. SIGMAFAST<sup>TM</sup> Protease inhibitor cocktail tablets for purification of His-tagged proteins, ultra-pure grade Tris-HCl, and HEPES were from

Sigma-Aldrich. All other buffer components or chemicals were purchased from either Sigma-Aldrich or Fischer Scientific (Pittsburgh, PA). Amicon Ultrafiltration Stirred Cells, Ultracel Amicon Ultrafiltration Discs and Amicon Ultra Centrifugal Filter Units were from Millipore (Billerica, MA). ATP was purchased from Roche (Indianapolis, IN) and [ $\gamma$ - $^{32}$ P] ATP was purchased from Perkin Elmer (Waltham, MA). *E. coli* strain DH5a for cloning was obtained from Invitrogen Corporation, and BL21 (DE3) and Rosetta-gami<sup>TM</sup> 2(DE3) for recombinant protein expression were from Novagen, EMD4Biosciences (Gibbstown, NJ). The pET-32a vector was obtained from Novagen. The ÄKTA FPLC<sup>TM</sup> System and the following columns Mono Q HR 10/100 anion exchange column and Superdex<sup>TM</sup> 200 prep grade gel filtration column were from Amersham Biosciences GE Healthcare Life Sciences (Piscataway, NJ).

## Constructs

1) Construction of pET32a-TRPM7 1403-1864 : A construct encoding the Trx-His6-tagged kinase domain of TRPM7 was created by PCR amplification of the nucleotide sequence corresponding to the last 462 amino acids (1403-1864) of Homo sapiens channel-kinase 1 (CHAK1, GenBank<sup>TM</sup> accession number AF346629) using the following oligonucleotides: forward (5'-CCGGAATTCATGGCGGCGTCCTCCCTGGAGCAGAAG-3') and reverse (5'-ATGCGGCCGCTCTCAGTGATGATGATGATGATGGGATCCACGCGGAACCAGCCTGAAGAAGGGCAGATGGTGCTG-3'). The PCR product was digested with EcoRI and NotI, and the resulting digested product was ligated into an EcoRI-NotI digested



pET32a vector that has been modified by replacing the sequence coding for the enterokinase cleavage site by the TEV protease cleavage recognition sequence. Then, the construct was transformed into the *E. coli* strain DH5 $\alpha$ . Plasmid DNA was purified and the sequence verified by sequencing.

2) Construction of pGEX4T-myosin1802-1977:

DNA encoding human nonmuscle myosin heavy chain II B in the CMV-EGFP vector was obtained from Addgene (Cambridge, MA). Human myosin heavy chain II B (aa 1802-1977) was created by PCR amplification using the following oligonucleotides, a) forward (5'- GGCAGCGGAGGGATGCAGGAACTCGAG-3') and b) reverse (5'- GACCCAGAGCCACCTTACTCTGACTGGGGTGG-3') and the PCR product was ligated into the linearized pGEX4T-1 vector. Then, the construct was transformed into the *E. coli* strain DH5 $\alpha$ . Plasmid DNA was purified and the sequence verified by sequencing.

3) Construction of mutant TRPM7:

A PCR based site-directed mutagenesis method was employed to generate point mutants, S1492A, S1511A, S1567A, S1492D, S1511D, and S1567D. The wild type pET32a-TRPM7 construct was used as a template, and PCR was carried out for each mutant with a set of sense and antisense mutagenic primers. The PCR products were treated with Dpn1 restriction enzyme and purified through DNA agarose gel electrophoresis. Purified DNA was used to transform *E. coli* strain (Novablue), and transformants were identified. Mutations were confirmed by DNA sequencing.

## **Expression and Purification of Proteins in *E.coli***

### 1) Expression and purification of phosphate-free TRPM7 (PF-TRPM7):

The TRPM7 catalytic domain was undergoing autophosphorylation intensively, which was indicated by a relatively high molecular mass shown on the SDS-PAGE gel (~90 kDa) compared with its actual molecular mass ~73 kDa. The unphosphorylated TRPM7 catalytic domain was prepared by co-expressing with lambda phosphatase, and the plasmid pCDF-Duet  $\lambda$ -phosphatase was given as a generous gift from Dr. Richard Bayliss (Institute of Cancer Research, London UK). The constructs, pET32a-Trx-TRPM7 and pCDF-Duet  $\lambda$ -phosphatase were co-transferred into *E. coli* strain C41 (DE3). A single colony of freshly transformed cells was used to inoculate 100 mL of Luria-Bertani (LB) media containing 50  $\mu$ g/mL ampicillin, 17  $\mu$ g/mL chloramphenicol, and 5  $\mu$ g/mL spectinomycin, and grown overnight at 37 °C on a shaker (250 rpm). The culture was diluted 100-fold into 2x YT media containing the same concentration of antibiotics and incubated at 37 °C on a shaker (250 rpm) until it reached an OD<sub>600</sub> of 0.6-1.0. Protein expression was then induced with 20  $\mu$ M isopropyl  $\beta$ -D-1-thiogalactopyranoside (IPTG) for 16 hours at 22 °C. The cells were harvested by centrifugation (6000g for 10 minutes at 4 °C), flash frozen in liquid nitrogen and stored at -80 °C. The collected cells were lysed in 150 mL of buffer A (20 mM Tris pH 8.0, 0.03% Brij-30, 0.1% (v/v)  $\beta$ -mercaptoethanol, 5 mM imidazole, 1mM benzamidine, 0.1 mM PMSF, and 0.1 mM TPCK) containing 0.5 M NaCl, 20% glycerol, 1 mM MgCl<sub>2</sub> and 0.2 mg/ml lysozyme at 4 °C for 30 minutes. The suspension was sonicated for 10 minutes (5 s pulses) at 4 °C. The lysate was cleared by centrifugation (Sorvall – SS34 rotor) at 27,000g for 30 minutes at 4 °C and the supernatant gently agitated

with 15 mL of Ni-NTA beads (Qiagen) for 1 hour at 4 °C. In a 100 mL chromatography column, the beads were washed with 150 mL of buffer A containing 10 mM imidazole and the Trx-His<sub>6</sub>-TRPM7 was then eluted with 30 mL of Buffer A containing 200 mM imidazole. The eluted protein was applied to a Mono Q HR 10/10 anion exchange column equilibrated in buffer B (20 mM Tris pH 8.0, (v/v) 0.03% Brij-30, (v/v) 0.1% β-mercaptoethanol, and 20% glycerol). The column was developed over 15-17 column volumes of buffer B with a linear gradient of 0-0.5 M NaCl. Eluted fractions of Trx-His<sub>6</sub>-TRPM7 were collected and concentrated to a volume of 10 mL using an Amicon Ultra-15 Centrifugal Filter Unit (Millipore) and applied to a HiLoad™ 16/60 Superdex™ 200 prep grade gel filtration column pre-equilibrated with Buffer D (25 mM HEPES, 2 mM dithiothrietol, 20 mM MgCl<sub>2</sub>, 0.1 mM EDTA, 0.1 mM EGTA, and 20% glycerol pH 7.5). Gel filtration chromatography was performed over 1.5 column volumes (180 mL) at a flow rate of 1 mL/min. Fractions were collected and analyzed for purity using SDS-PAGE. Fractions that contained the TRPM7 catalytic domain were pooled and dialyzed against Buffer E (25 mM HEPES pH 7.5, 50 mM KCl, 0.1 mM EDTA, 0.1 mM EGTA, 2 mM DTT, and 10 % glycerol)

2) Expression and purification of fully phosphorylated TRPM7 kinase domain (TRPM7-KD):

The construct, pET32a-Trx-TRPM7 was transferred into *E. coli* strain Rosetta-gami™ 2(DE3). A single colony of freshly transformed cells was used to inoculate 100 mL of Luria-Bertani (LB) media containing 50 µg/mL ampicillin, 17 µg/mL chloramphenicol, and 5 µg/mL tetracycline, and grown overnight at 37 °C on a shaker (250 rpm). The culture

was diluted 100-fold into 2x YT media containing the same concentration of antibiotics and incubated at 37 °C on a shaker (250 rpm) until it reached an OD<sub>600</sub> of 0.6-1.0. Purification step was same as the one for PF-TRPM7.

3) Expression and purification of GST myosin heavy chain II B (1802-1977):  
pGEX 4T1 containing DNA encoding residues 1802-1977 of myosin heavy chain II B was transformed into *E. coli* strain BL21 (DE3) electro-competent cells. From a single colony of freshly transformed cells, a 10 mL culture of LB containing 50 µg /mL ampicillin was inoculated and incubated with shaking overnight at 37 °C. The culture was diluted 100-fold into LB media containing 50 µg/ mL ampicillin, and incubated at 37 °C with shaking. Once the OD<sub>600</sub> of the culture had reached 0.6, the expression was induced by the addition of 1 mM IPTG. Shaking was continued at 37 °C for 1 hour, before the cells were pelleted (7000×g, 12 minutes). The bacterial pellets were immediately frozen in liquid nitrogen and stored at -80 °C. The frozen wet cells were resuspended in 50 ml of Buffer F (10 mM Na<sub>2</sub>HPO<sub>4</sub>, 1.8 mM KH<sub>2</sub>PO<sub>4</sub>, pH 7.3, 140 mM NaCl, 2.7 mM KCl, 0.1% β-mercaptoethanol, 0.1 mM TPCK, 0.1 mM PMSF and 1 mM Benzamidine) containing 0.2 mg/mL lysozyme. The mixture was incubated at 4 °C for 30 minutes. Then Triton X-100 was added (to a final concentration of 1%) and incubated another 30 minutes at 4 °C. Finally, the cells were sonicated for 5 minutes at 4 °C. The lysate was then centrifuged for 30 minutes at 12,000×g. The supernatant was mixed with 10 mL of Glutathione Sepharose™ High Performance (Amersham Biosciences) equilibrated in Buffer E and shaken gently for 1.5 hours at 4 °C. In a 50 mL column, the beads were washed with 50 mL of Buffer E. The GST-tagged proteins were eluted with 5 mL buffer G (50 mM Tris HCl pH 7.5 containing

20 mM reduced glutathione, 0.1%  $\beta$ -mercaptoethanol, 0.1 mM TPCK, 0.1 mM PMSF and 1 mM Benzamidine).

## **Analytical Methods**

### *General kinetic assays*

In order to assess the correlation between PF-TRPM7 autophosphorylation and its kinase activity, autophosphorylation and activity towards peptide substrate were measured concurrently. After initiating 800 nM PF-TRPM7 autophosphorylation by adding 1 mM [ $\gamma$ - $^{32}$ P] ATP (100-1000 cpm/pmol), the degree of autophosphorylation was determined in 10  $\mu$ l aliquots that were taken from the reaction mixture at set time points. Concurrently, aliquots (30  $\mu$ l) from the TRPM7-KD autophosphorylation reaction mixture were diluted and its ability to phosphorylate its peptide substrate was determined.

TRPM7-KD activity was assayed at 30 °C in assay buffer (25 mM HEPES buffer-pH 7.5, 50 mM KCl, 0.1 mM EDTA, 0.1 mM EGTA, 2 mM DTT and 10  $\mu$ g mL $^{-1}$  BSA), containing 300  $\mu$ M [ $\gamma$ - $^{32}$ P] ATP (100-1000 c.p.m. pmol $^{-1}$ ), 11 mM MgCl $_2$  and 12.5 $\mu$ M of peptide substrate (acetyl-RKKYRIVWKSIFRRFL-amide) in a final total volume of 100  $\mu$ L. At set time points, 10  $\mu$ L aliquots were taken and spotted onto P81 cellulose filters (Whatman, 2  $\times$  2 cm). The filter papers were then washed thrice in 50 mM phosphoric acid (15 minutes, each wash), once in acetone (15 minutes) and finally dried. The amount of labeled peptide associated with each paper was determined by measuring the cpm on a Packard 1500 scintillation counter.

### ***Autophosphorylation assay using rapid quench flow equipment***

Rapid Chemical Quench. Rapid quench experiments were performed on a KinTek RQF-3 rapid quench-flow apparatus. reactions were conducted at 27 °C in assay buffer (25 mM HEPES, 50 mM KCl, 2 mM DTT, 0.1 mM EDTA, and 0.1 mM EGTA, pH 7.4) containing 10 mM MgCl<sub>2</sub>. Experiments were initiated by the rapid mixing of solution A (containing 2 mM [ $\gamma$ -<sup>32</sup>P] ATP (100-1000 cpm/pmol) with an equal volume of solution B (containing various concentrations PF-TRPM7 0-6400 nM). After brief time intervals (0.02-40 seconds), reactions were quenched with 115  $\mu$ L of quenching buffer (20 mM HEPES pH 7.4, 200 mM KCl, 0.1% bovine serum albumin, 50 mM EDTA, 1 mM EGTA). The quenched reaction mixture was collected in 1.5 mL centrifuge tubes followed by heating for 10 minutes at 95 °C and centrifuged briefly at 5000g. Aliquots (30  $\mu$ L) of the quenched reaction mixture were resolved by SDS-PAGE and stained with Coomassie Brilliant Blue. Gels were exposed for 16 hours in a Phosphorimager cassette which was then scanned in a Typhoon Phosphorimager and then analyzed using ImageQuant™ TL software. To determine the stoichiometry of the autophosphorylation, the gels were dried, the pieces containing TRPM7-KD excised, and the associated radioactivity measured with a Packard 1500 liquid scintillation analyzer.

### ***Pre-steady state kinetic assay***

Rapid quench experiments were performed on a KinTek RQF-3 rapid quench-flow apparatus. reactions were conducted at 27 °C in assay buffer (25 mM HEPES, 50 mM KCl, 2 mM DTT, 0.1 mM EDTA, and 0.1 mM EGTA, pH 7.4) containing 10 mM MgCl<sub>2</sub>. Experiments were initiated by the rapid mixing of solution A (containing 2 mM [ $\gamma$ -<sup>32</sup>P]

ATP (100-1000 cpm/pmol) and 25  $\mu$ M peptide substrate mixture) with an equal volume of solution B (containing either 1600 nM fully phosphorylated TRPM7-KD [figure 2.5] or 1600 nM PF-TRPM7 [figure2.3B]). After brief time intervals (0.01-4 seconds), reactions were quenched with 115  $\mu$ L of quenching buffer (20 mM HEPES pH 7.4, 200 mM KCl, 0.1% bovine serum albumin, 50 mM EDTA, 1 mM EGTA). The quenched reaction mixture was collected in 1.5 mL centrifuge tubes followed by heating for 10 minutes at 95  $^{\circ}$ C and centrifuged briefly at 5000g. Aliquots (30  $\mu$ L) of the quenched reaction mixture were resolved by 20% SDS-PAGE and stained with Coomassie Brilliant Blue. Gels were exposed for 16 hours in a Phosphorimager cassette which was then scanned in a Typhoon Phosphorimager and then analyzed using ImageQuant<sup>™</sup> TL software. To determine the peptide substrate phosphorylation, the gels were dried, the pieces containing phosphorylated peptide excised, and the associated radioactivity measured with a Packard 1500 liquid scintillation analyzer. In experiments where both PF-TRPM7 autophosphorylation and peptide substrate phosphorylation were monitored simultaneously (figure 2.6A), the gels were dried, the pieces containing either autophosphorylated TRPM7-KD or phosphorylated peptide excised, and the associated radioactivity measured with a Packard 1500 liquid scintillation analyzer.

***Analysis of the three autophosphorylation-site mutants.***

***a. Assay against peptide substrate:*** Assays were performed in the assay buffer (25 mM HEPES, 50 mM KCl, 2 mM DTT, 0.1 mM EDTA, and 0.1 mM EGTA, pH 7.4) containing 10 mM MgCl<sub>2</sub> using 80 nM of TRPM7-KD WT and mutants that were pre-autophosphorylated following the protocol that mentioned in the general kinetics assays,

12.5  $\mu\text{M}$  peptide substrate and 0.5 mM [ $\gamma$ - $^{32}\text{P}$ ] ATP (100-1000 cpm/pmol) in a final reaction volume of 100  $\mu\text{L}$ . Kinase activity in each case was determined by calculating the rate of phosphorylation of the peptide. ***b. Assay against myosin IIB:*** Assays were performed in the same assay buffer mentioned above using 80 nM of TRPM7-KD WT and mutants, 8  $\mu\text{M}$  myosin IIB and 1 mM [ $\gamma$ - $^{32}\text{P}$ ] ATP (100-1000 cpm/pmol) in a final reaction volume of 50  $\mu\text{L}$ . The reaction mixture was incubated at 30 °C for 10 minutes before the reaction was initiated by addition of 1 mM [ $\gamma$ - $^{32}\text{P}$ ] ATP. The reaction was carried out for 1 minute and quenched by addition of hot SDS-PAGE sample loading buffer. The samples were resolved by SDS-PAGE and stained with Coomassie Brilliant Blue. Gels were exposed for 2 hours in a phosphorimager cassette which was then scanned in a Typhoon Phosphorimager. ***c. Autophosphorylation of TRPM7-KD mutants:*** Assays were performed in the same assay buffer described earlier using 800 nM TRPM7-KD mutants and 1 mM [ $\gamma$ - $^{32}\text{P}$ ] ATP (100-1000 cpm/pmol) in a final reaction volume of 50  $\mu\text{L}$ . The reaction mixture was incubated for 30 and 60 minutes. The samples were analyzed as mentioned above.

### **Dynamic Light scattering**

Dynamic light scattering experiments were performed on phosphate-free TRPM7-KD, 30 seconds autophosphorylated TRPM7-KD and fully phosphorylated TRPM7-KD. Samples were previously dialyzed against light scattering assay buffer (25 mM HEPES (pH 7.5), 100 mM NaCl, 2 mM DTT and 5 mM  $\text{MgCl}_2$ ). The assay buffer, which is freshly



prepared with Nanopure water (~18.3 MΩ cm) and filtered through a 0.02 μm filter (Anodisc 47, Whatman, catalog # 6809-5002) was used to establish the light scattering and refractive index baselines. The TRPM7-KD sample, 40 μL at 3.6 μM, was centrifuged for 30 seconds and injected into the column. Bovine serum albumin monomer (Sigma A1900) was injected to the column at 2 mg/mL for normalization of the light-scattering detectors. Size exclusion 14 chromatography was performed at a flow rate of 0.4 mL/min at room temperature for a run time of ~ 40 minutes. All measurements were made at 25 °C. Size-exclusion chromatography was performed as previously described <sup>(137, 138)</sup> with a TSK-GEL G3000PW<sub>XL</sub> column (300 × 7.8 mm ID, 14 mL column volume, Tosoh Bioscience LLC). Samples were centrifuged for ~ 30 seconds to remove any insoluble components prior to injection. Molar masses, peak concentrations and hydrodynamic radii were determined with Astra software (Wyatt Technology).

### **Mass Spectrometry, Liquid Chromatography, and Automated Spectral Analysis**

TRPM7 samples were reduced, alkylated, and digested with trypsin. A 1:20 enzyme: substrate ratio, a pH of ~8, and an incubation time of 16 hours at 37 °C were used for digestion. All mass spectrometric experiments were undertaken on a Thermo Fisher Scientific LTQ XL (San Jose, CA). Liquid chromatography was performed using a Dionex UltiMate 3000 RSLCnano system (Sunnyvale, CA), and a Dionex Acclaim PepMap RSLC C<sub>18</sub> column (75 μm × 15 cm, 2 μm particle size). Eluent A consisted of 0.1% formic acid in water and eluent B 0.1% formic acid in acetonitrile. A linear gradient from 5% eluent B to 50% eluent B over 120 minutes at 300 nL/min was used. Samples were injected at

approximately one picomole of digested protein. Data-dependent LC-MS/MS was performed as follows: the first event was the full mass scan ( $m/z$  range of 400 - 2000) in the positive mode followed by ten CID events on the ten most abundant ions from the full mass scan. The maximum injection time for full mass scans and MS/MS events was set to 100 ms, the dynamic exclusion duration was 50 s, and the exclusion list size allowed for 500 specified  $m/z$  values. A single repeat count was used. A  $q$ -value of 0.25, an activation time of 30 ms, and normalized collision energy (NCE) of 35% were used for all CID events. MassMatrix was used for automated LC-MS/MS analysis. A precursor mass tolerance of 2.0 Da, and a fragment mass tolerance of 0.8 Da were used for processing. Phosphorylation of serine, threonine, and tyrosine were set as variable side-chain modifications, and carbamidomethyl of cysteine was set as a fixed modification. Experimental CID spectra were searched against a database consisting of the TRPM7 + tag sequence. Peptide hits were filtered based on a minimum pp score of 5, a  $pp^2$  score of 5, or a minimum  $pp_{tag}$  score of 1.3. Peptides with a minimum length of 6 amino acids and a max peptide ranking of one were also filtered out. Phosphorylated peptides were manually verified before calculating peak area ratios.

### **Site-Directed Mutagenesis by Overlap Extension Using the Polymerase Chain Reaction**

A PCR-based site-directed mutagenesis method was employed to generate point mutants, S1492A, S1511A, and S1567A. The full length WT TRPM7 construct containing Myc and FLAG tags (Origene) was used as a template, and PCR was carried out for each

mutant with a set of sense and antisense mutagenic primers. The PCR products were treated with DpnI restriction enzyme to get rid of methylated template plasmid and purified through agarose gel electrophoresis. The mutated plasmid remains intact in the reaction. Purified DNA was used to transform *E. coli* (novablue), and transformants harboring mutant constructs were identified. Mutations were confirmed by DNA sequencing.

### **Western Blotting and Immunoprecipitation Experiments**

The full length of Myc-FLAG tagged TRPM7 in pCMV vector was purchased from Origene. HEK293 cells were transfected with full length of Myc-FLAG tagged TRPM7 (both WT and alanine mutants) using lipofetamine 2000 (Invitrogen). At 72 hours after transfection, cells were lysed on ice for 20 minutes in lysis buffer (50 mM Tris pH 7.5, 300 mM NaCl<sub>2</sub>, 0.5 mM DTT, 1.5 mM MgCl<sub>2</sub>, 0.2 mM EDTA, 1% Triton X-100 supplemented with protease inhibitors) and the extract was cleared by centrifugation. The protein concentration was measured by Bradford analysis (Bio-Rad). For immunoprecipitation of exogenously expressed TRPM7, Myc-Tag (9B11) Mouse mAb (Sepharose Bead Conjugate) (Cell Signaling Technology) was added to the lysates of WT and mutant TRPM7, the samples were incubated at 4 °C overnight. Subsequently, the beads were washed three times with lysis buffer, protein complexes were solubilized in Laemmli sample buffer and separated by SDS-PAGE. Proteins were fractionated on a 10% SDS polyacrylamide gel (Bio-Rad) and transferred to Hybond-P PVDF Membrane (GE Healthcare). Primary antibodies were incubated overnight at 4 °C using 1:1000 anti-FLAG antibody (Sigma-Aldrich); 1:1000 anti-myosin IIB rabbit polyclonal antibodies (Cell

Signaling Technology); anti-rabbit (Bio-Rad) horseradish peroxidase-conjugated secondary antibodies and ECL Plus™ Western blotting reagents (GE Healthcare) were employed to develop the blots.

## 2.4 RESULTS AND DISCUSSION

### **Preparation of phosphate-free TRPM7-KD to facilitate the study of its autophosphorylation mechanism**

All alpha-kinases including eEF2K, MHCKs, TRPM6, and TRPM7 have been reported to autophosphorylate, and this autophosphorylation is considered to be an important regulatory mechanism for their activity <sup>(1)</sup>. The *in vitro* study of the autophosphorylation mechanism of these enzymes is challenging due to its uncontrollable autophosphorylation upon expression in bacterial or mammalian cells. For example, a recent study has shown that the cytosolic C-terminal kinase domain of TRPM7 undergoes extensive autophosphorylation during expression in HEK293 cells <sup>(34)</sup>. Herein, we introduced a novel co-expression system to co-express both lambda phosphatase and residues 1403-1864 of TRPM7 (TRPM7-KD) in *E. coli* in order to prepare the phosphate-free TRPM7 kinase domain (PF-TRPM7).

The SDS-PAGE experiments shown in figure 2.1A and B demonstrate the difference in apparent molecular weight when assessed by SDS PAGE (72 versus 90 kDa) between TRPM7-KD when expressed in *E. coli*, in the presence and absence of lambda phosphatase. When TRPM7-KD is treated with lambda phosphatase *in vitro* a similar molecular weight band is observed supporting the notion that this system can produce

phosphate-free TRPM7-KD (PF-TRPM7). The phosphorylation status of PF-TRPM7 was further examined. A mass spectrometry analysis of proteolytically cleaved PF-TRPM7 revealed only trace phosphorylation (figure 2.6 B, D).

To test the capability of PF-TRPM7 to autophosphorylate *in vitro* after removal of the phosphates during bacterial expression, 800 nM of PF-TRPM7 was incubated with 1 mM [ $\gamma$ - $^{32}$ P] ATP in the presence of 11 mM MgCl<sub>2</sub> and phosphate addition detected by autoradiography and quantified by phosphorimager analysis. PF-TRPM7 was successfully autophosphorylated with high efficiency *in vitro* (figure 2.1C), which validates this form of the enzyme as a suitable tool to study the TRPM7-KD autophosphorylation mechanism.

### **Evidence that the inactive kinase domain is tetrameric**

A shorter form of TRPM7 (residues 1548-1863) has been reported by Scott W. Crawley et al. <sup>(33)</sup> to be a dimer, while the structure of residues 1230-1282 (TRPM7cc) that corresponds to a coiled-coil domain has been recently resolved by Yuichiro Fujiwara et al. <sup>(22)</sup> to be an antiparallel tetramer in both crystal and solution. The availability of a phosphate-free form of the kinase domain TRPM7 enhances the chance to characterize the oligomerization state of this domain in both its non-phosphorylated and fully phosphorylated form using dynamic light scattering <sup>(139)</sup>. Figure 2.2 shows that PF-TRPM7 has an approximate molecular mass that is 4-fold the expected molecular mass (72kDa), suggesting that PF-TRPM7 is a tetramer in solution.

### **Autophosphorylation is required to activate TRPM7-KD**

To compare the autoactivation of PF-TRPM7 and TRPM7-KD, we monitored their activities towards a peptide substrate (RKKYRIVWKSIFRRFL) <sup>(140)</sup> utilizing a P81-based kinase assay (figure 2.3A). Kinase activity was measured as a function of autophosphorylation time. The kinase activity of both PF-TRPM7 (figure 2.3A) and TRPM7-KD (data not shown) was maximal within the first minute of autophosphorylation, suggesting that either autophosphorylation is not required for its kinase activity or the autophosphorylation is rapid.

To test if autophosphorylation is required for its kinase activity, we used a rapid quench-flow device to monitor phosphate incorporation into either the peptide substrate or myosin IIB protein substrate <sup>(35)</sup>. We compared PF-TRPM7 and fully phosphorylated TRPM7-KD. We reasoned that if autophosphorylation regulates TRPM7-KD activity, fully phosphorylated TRPM7-KD will initially phosphorylate its substrates more rapidly than the PF-TRPM7. The comparison between the ability of fully phosphorylated TRPM7-KD and PF-TRPM7 to phosphorylate the peptide substrate (figure 2.2B) demonstrated that autophosphorylation is essential to activate TRPM7-KD as PF-TRPM7 exhibits a lower initial rate of peptide phosphorylation than the fully phosphorylated TRPM7-KD.

### **Characterization of the mechanism of TRPM7 autophosphorylation**

As previously established, the early autophosphorylation of PF-TRPM7 is sufficient for its full autoactivation. To determine the effect of PF-TRPM7 concentration on its autophosphorylation, we examined how the rate of autophosphorylation varied with

the TRPM7 concentration. Using a rapid quench flow kinetic assay, we were able to quantify the initial rate of  $^{32}\text{P}$  incorporation into PF-TRPM7 at different concentrations and determine the relationship between the rate of autophosphorylation and TRPM7 concentration. Rapid quench-flow kinetic experiments were performed at 7 different concentrations of TRPM7 between 50–3200 nM (figure 2.4). The observed rate constant  $k_1$  for the initial rate of autophosphorylation varied from 0.01 to 0.08  $\text{sec}^{-1}$  and plateaued above 800 nM PF-TRPM7.

### **Pre-steady state kinetic analysis of TRPM7-KD**

Our previous rapid quench data showed that fully active TRPM7 exhibits a transient pre-steady-state "burst" of a phosphorylated substrate. Therefore, we studied kinetic transients on the catalytic reaction pathway of TRPM7 in detail. Experiments were performed on a Rapid Quench-Flow apparatus as described in Materials and Methods. To observe a burst of product formation, the concentration of substrate must exceed that of the enzyme and must exceed the dissociation constant, such that the majority of the enzyme will be bound to the substrate before initiation of the catalytic reaction. For experiments, final concentrations of 3 mM MgATP, 25  $\mu\text{M}$  peptide, and 0.5-1  $\mu\text{M}$  TRPM7 were used. Both peptide and MgATP were incubated together in syringe A before rapid mixing with an equal volume of TRPM7 from syringe B. At varying times, the reaction was stopped by the addition of a quench solution (400 mM EDTA). Figure 2.5A shows 8 time courses, for the formation of peptide~p, obtained at two different concentrations of TRPM7 (0.5, 1  $\mu\text{M}$ ). The progress curve for each time course exhibited an initial burst followed by a

slower linear phase. Data were fitted to an equation describing a single exponential followed by a steady-state rate (equation. 2.1). The formation of the burst occurred with a rate constant of  $k_2 = 27 \text{ s}^{-1}$  followed by a slow product release from the enzyme with a rate constant of  $k_3 = 1.9 \text{ s}^{-1}$ . The amplitude of the burst exhibited a proportional dependence on the enzyme concentration when the experiments were performed at two different enzyme concentrations, 0.5 and 1  $\mu\text{M}$ , respectively. The burst amplitude indicates the quantity of active enzyme that is present in the reaction mixture. The observed burst amplitudes ( $\alpha$ ) for each curve fit represented approximately 80% of the total enzyme concentration ( $[\text{E}]_t$ ,  $\alpha [\text{E}]_t$ : 0.5, 0.43; 1, 0.75  $\mu\text{M}$ ).

$$\frac{[\text{EAP}] + [\text{P}]}{[\text{EA}]_0} = \left(\frac{k_2}{k_2 + k_3}\right)^2 [1 - e^{-(k_2 + k_3)t}] + \left(\frac{k_2 k_3}{k_2 + k_3}\right) t \quad \text{Equation 2.1}$$

### Three early phosphorylations are sufficient to fully activate TRPM7

To further understand the mechanism we simultaneously monitored autophosphorylation and substrate phosphorylation using a rapid quench kinetic assay. Data were fitted to the following model (where E is PF-TRPM7 and EA is phosphorylated TRPM7-KD, S is the peptide substrate and P is the phosphorylated peptide substrate) using Kintek Explorer software:

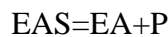
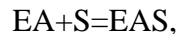
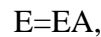




Figure 2.6A shows the fitted data, PF-TRPM7 exhibits a lag phase in its ability to phosphorylate the peptide substrate, which corresponds to the incorporation of 3 phosphates into PF-TRPM7 (closed circles represents mole phosphate per mole TRPM7 and closed squares present phosphorylated peptide) and as shown in figure 2.6A, fully phosphorylated TRPM7 does not exhibit such a lag phase. Interestingly, after ~40-50 seconds of autophosphorylation, the rate of myosin (TRPM7-KD protein substrate) phosphorylation by PF-TRPM7 became similar to the rate of phosphorylation by fully phosphorylated TRPM7-KD (data not shown), suggesting that early three autophosphorylation sites are sufficient for its kinase activity towards myosin. These three autophosphorylation sites have been further determined by mass spectrometry analysis (figure 2.6B-D). To determine these early autophosphorylation sites purified PF-TRPM7 was allowed to autophosphorylate in the presence of MgATP for 30 seconds. The sample was reduced, alkylated, and digested with trypsin as described under '2.3 Materials and Method'. The relative degree of phosphorylation of the TRPM7 sites based on peak area ratios of phosphorylated and non-phosphorylated peptides from TRPM7-KD after 0 or after 30 seconds of autophosphorylation was compared and the results (which have been summarized in figure 2.6D), revealed three major sites after 30 seconds of autophosphorylation in recombinant human TRPM7-KD - Ser1492, Ser1511 and Ser1567. It should be noted that only trace phosphorylation was detected in PF-TRPM7.

Previously, Matsushita et al. reported that Ser<sup>1511</sup> and Ser<sup>1567</sup> are the major sites of TRPM7 autophosphorylation <sup>(31)</sup>. Accordingly, we investigated the contribution of the three autophosphorylation sites to TRPM7 kinase activity by generating mutant constructs.

In order to confirm these phosphorylation sites are important for TRPM7 activity, we mutated Ser<sup>1492</sup>, Ser<sup>1511</sup> and Ser<sup>1567</sup> individually to alanine and tested whether mutation of these autophosphorylation sites abolishes kinase activity. Mutation of Ser<sup>1492</sup>, Ser<sup>1511</sup> or Ser<sup>1567</sup> to alanine resulted in almost no autophosphorylation compared with wild-type TRPM7-KD (figure 2.7A). We also assessed the ability of these mutants that were autophosphorylated for different times (0.5–45 minutes) to phosphorylate a TRPM7 peptide substrate. None of the mutants showed significant peptide phosphorylation, as compared to the wild-type enzyme or any enhancement of enzyme activity following incubation with MgATP (figure 2.7B). Myosin IIB exhibited similar results to the peptide substrate (figure 2.7C). In addition, we mutated Ser<sup>1492</sup>, Ser<sup>1511</sup> and Ser<sup>1567</sup> to aspartic acid to mimic phosphorylation and investigated the ability of these mutants to autophosphorylate or phosphorylate myosin IIB. The aspartic acid mutants showed a similar autophosphorylation level to the wild type TRPM7-KD (figure 2.8A) but only one of them (S1567D) rescued myosin IIB phosphorylation (figure 2.8B).

As described in Chapter 1, by LC-MS/MS, Clark et al. identified 46 residues autophosphorylated in WT-TRPM7 including Ser<sup>1511</sup> and Ser<sup>1567</sup> which were identified earlier by Matsushita et al <sup>(31, 34)</sup>. However, Clark et al. reported that mutation of these residues to alanine either individually or in combination had no effect on TRPM7 autophosphorylation or activity towards myosin II. Their results are consistent with neither those of Matsushita's nor our studies. Their HA-tagged TRPM7 kinase domain was obtained from HEK293 cells by immunoprecipitation and subjected to an *in vitro* kinase assay. These experiments raise the possibility that TRPM7 can undergo extensive

autophosphorylation and function normally in spite of mutation of Ser<sup>1511</sup> and Ser<sup>1567</sup> to alanine by unknown factors in the cells. By taking advantage of a rapid quench kinetic assay using PF-TRPM7, we demonstrated that Ser<sup>1492</sup>, Ser<sup>1511</sup> and Ser<sup>1567</sup> residues are absolutely essential for TRPM7 activity. Autophosphorylation on these residues are required for further autophosphorylation of TRPM7 implying that their phosphorylation is an important priming event that would control TRPM7 autophosphorylation and kinase activity.

### **The three autophosphorylation sites regulate the association with myosin II B**

As previously described in Chapter 1.2., the protein kinase domain of TRPM7 phosphorylates actin filament interacting proteins: myosin II. Clark et al. demonstrated that TRPM7 associates with myosin II in a kinase-dependent manner by showing that a kinase dead mutant (TRPM7-D1775A) did not interact with myosin IIA heavy chain <sup>(36)</sup>. Interaction with the actomyosin cytoskeleton suggests that TRPM7 kinase activity might regulate the stability of actomyosin filaments and affect cytoskeletal remodeling. Therefore, we investigated whether the three early autophosphorylation sites influence the association of TRPM7 with the actomyosin cytoskeleton in the cells. Accordingly, we co-precipitated Myc-TRPM7 complexes (WT and three alanine mutants) with anti-Myc antibodies and detected the presence of associated myosin IIB by western blotting. As seen in figure 2.9, myosin IIB heavy chain was present in a complex with WT TRPM7, but not in a complex with the mutants. These results indicate that the interaction between TRPM7

and myosin IIB is strictly kinase activity-dependent and further confirm that the three autophosphorylation residues are the main regulators of the kinase activity.

### **The autophosphorylation on three serine residues induces a conformational change of the TRPM7 kinase domain**

As mentioned earlier, TRPM channels have diverse C-terminal domains but share a common coiled-coil domain located at the C-terminus of the transmembrane domain. When recombinant proteins containing putative coiled-coils from TRPM channels are expressed by themselves, the coiled-coil domains are able to self-assemble into tetramers, as observed using biophysical techniques. The deletion or point mutated coiled-coil domain was shown to result in a non-functional channel by abolishing multimeric channel assembly, suggesting that the tetramerized coiled coil is important for functional TRPM channels. Moreover, recent X-ray crystallography of the TRPM7 coiled-coil domain (residues 1230-1282) demonstrated that TRPM7 coiled-coils were capable of forming tetrameric antiparallel structure <sup>(22)</sup>. The structure of the short TRPM7 alpha-kinase domain (residues 1548-1863) expressed in *E.coli*, determined by X-ray crystallography, revealed that TRPM7 alpha-kinase assemble into a dimer through the interaction of the N-terminal alpha-helix of one subunit with the second subunit <sup>(33)</sup>. Taken together based on previous structural studies, there would be two kinase dimers in a tetrameric TRPM7 channel. The successful preparation of a phosphate-free form of the kinase domain of TRPM7 allowed us to determine the oligomerization state of this domain in both its non-phosphorylated and fully phosphorylated form. Using dynamic light scattering we found

that a phosphate-free form of TRPM7 exists as a tetramer in solution (figure 2.2 and 2.10). This observation increased the possibility that the TRPM7 oligomerization state can be influenced by autophosphorylation. Therefore, we also performed dynamic light scattering on fully phosphorylated TRPM7-KD and autophosphorylated TRPM7-KD (30 seconds) in order to compare with tetrameric inactive TRPM7-KD. The molar mass distribution, as a function of elution volume, is shown for each sample in figure 2.10. The molecular mass of fully phosphorylated TRPM7-KD and autophosphorylated TRPM7-KD (30 seconds) is estimated to be 150 kDa in solution. This is about twice the sequence derived mass of ~72 kDa, which suggests that both fully phosphorylated and 30 second-autophosphorylated TRPM7-KD exist in a dimeric state. These data support the notion that early autophosphorylation on three serine residues causes a conformational change to promote a tetramer to dimer transition of the kinase domain leading to an active enzyme. As expected, alanine mutants which do not have an ability to be autophosphorylate and harbor kinase activity could not form a dimer (data not shown) and remained a tetramer. Our data provide evidence that the active TRPM7 kinase domain is dimeric under physiological conditions. As a result, our findings propose a schematic model for the regulation of TRPM7 conformational change as seen in figure (figure 2.11). In the inactive state, the TRPM7 kinase domain is tetrameric. Activation of the kinase domain by autophosphorylation results in the structural transition of the kinase from the tetramer to dimer, potentially regulating the channel.

## **2.5 CONCLUSION**

We provide evidence that three early autophosphorylation sites of TRPM7 (Ser<sup>1492</sup>, Ser<sup>1511</sup> and Ser<sup>1567</sup>) regulate its autoactivity and its interaction with myosin II using a range of biochemical experimental techniques. The evidence includes i) a concentration-dependent autophosphorylation mechanism, ii) *in vitro* rapid quench kinetic analysis and MS/MS demonstrating that TRPM7 requires the early three phosphates to activate the kinase domain towards downstream substrates, iii) biochemical analyses of the TRPM7 complex showing that TRPM7 associates with myosin II in a kinase dependent manner in cells and iv) dynamic light scattering analysis revealing that early autophosphorylation induces a conformational change of the TRPM7 kinase domain.

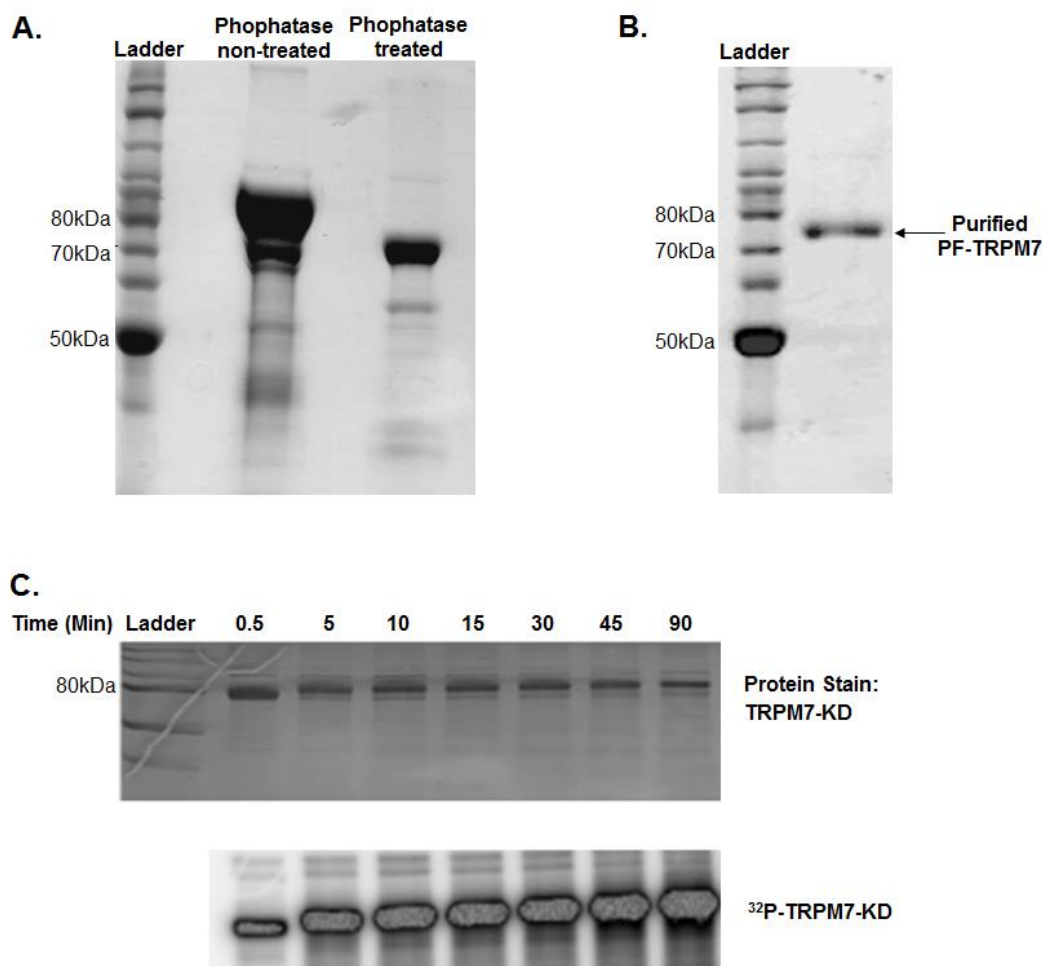


**Figure 2.1. SDS-PAGE analysis of purified TRPM7-KD (1403-1864).**

**A**, *In vitro* treatment of purified TRPM7-KD with lambda phosphatase. **B**, Purified PF-TRPM7 kinase domain which was co-expressed with lambda phosphatase in *E.coli*. Proteins were expressed in *E.coli* (Rossita Gami 2 cells), purified and analyzed by 10% SDS-PAGE in tris-glycine running buffer using BenchMark Protein Ladder (Invitrogen), and stained with coomassie blue. **C**, Autophosphorylation of PF-TRPM7. PF-TRPM7 (800 nM) was allowed to autophosphorylate in the presence of 11  $\mu$ M MgCl<sub>2</sub>. At the indicated times, the reaction quenched with hot SDS-PAGE sample loading buffer. The samples were then analyzed as described under '2.3. Materials and Methods'. (*upper*) Coomassie-stained gel. (*down*) Autoradiograph.

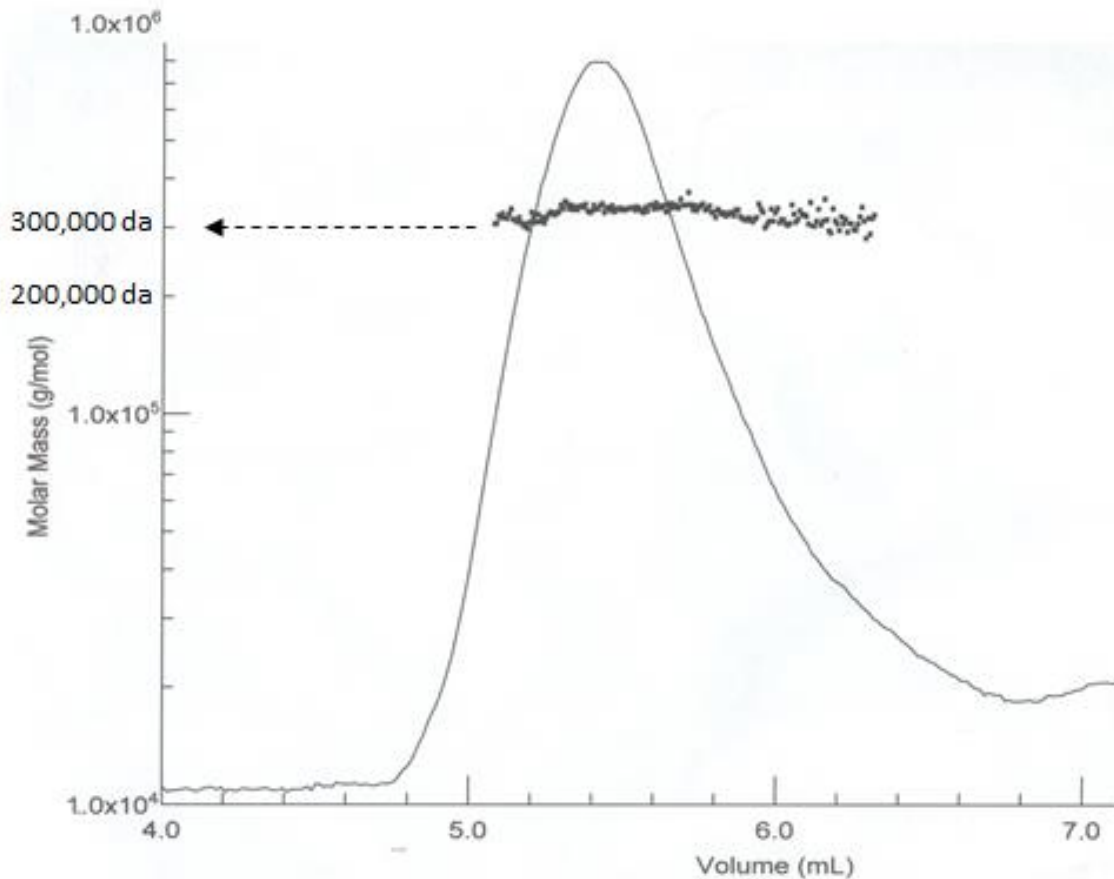


**Figure 2.2. Dynamic light scattering analysis of phosphate-free TRPM7 kinase domain.**

Fractionation of 3.6  $\mu\text{M}$  phosphate-free TRPM7 kinase domain using size exclusion chromatography followed by quasi-elastic light scattering (QELS) analysis shows that phosphate-free TRPM7 self-association causes tetramerization. The chromatographic conditions are given in the '2.3. Materials and Methods'. The patterns represent the relative concentrations determined by measurement of the refractive index differences, the molar mass distribution and the hydrodynamic Stokes radius ( $R_H$ ), as a function of elution volume.



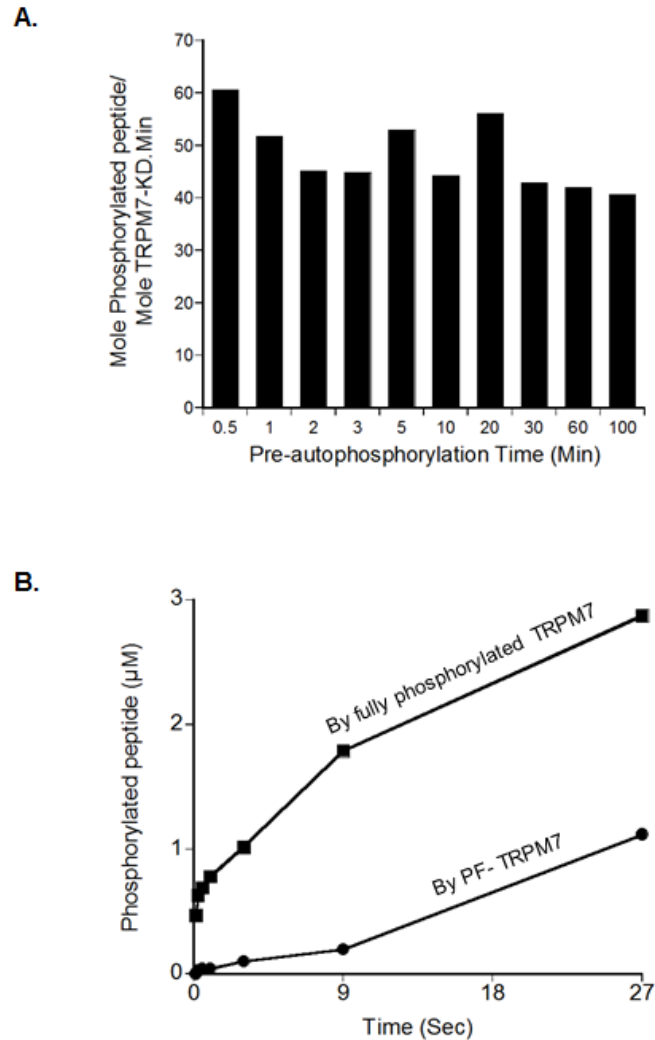


**Figure 2.3. Autoactivity of TRPM7-KD towards peptide substrate.**

**A**, Activity of PF-TRPM7 pre-phosphorylated for designated time against peptide substrate. The incorporation of phosphate into 12.5  $\mu$ M peptide substrate by PF-TRPM7 pre-phosphorylated for different time points (0.5-100 min) monitored by general kinase assay using p81 paper. **B**, Rapid quench flow kinetics experiment compares the ability of PF-TRPM7 and fully phosphorylated TRPM7-KD to phosphorylate 12.5  $\mu$ M peptide substrate. Closed squares represent the activity of 800 nM of fully phosphorylated TRPM7-KD towards its peptide substrate in the presence of a saturating ATP concentration. Closed circles represent activity of 800 nM PF-TRPM7 towards its peptide substrate in the presence of a saturating ATP concentration.

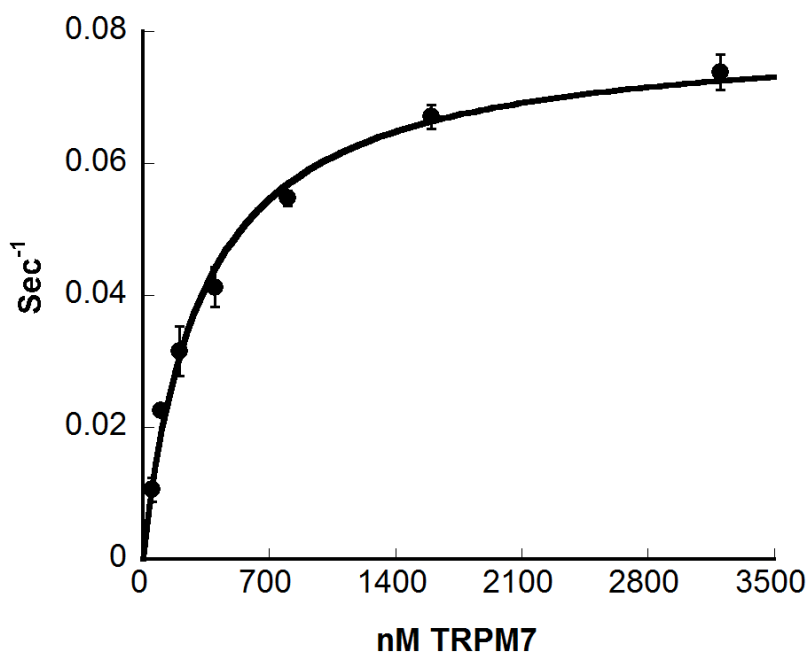


**Figure 2.4. Effect of different TRPM7 concentrations on its autophosphorylation.**

It was studied by investigating the concentration dependence of TRPM7-KD autophosphorylation rate constant. Plotted is the observed rate constant ( $\text{sec}^{-1}$ ) for autophosphorylation versus TRPM7-KD concentration (nM). The incorporation of phosphate into different concentrations of PF-TRPM7 was monitored by rapid quenched flow kinetics. The lines are the best fits of each data set to the following equation  $k_{\text{obs}} = k_{\text{max}} + [E]/[E] + ^\wedge K_d$  where  $k_{\text{obs}}$  is the observed rate constant,  $k_{\text{max}}$  is the maximum observed rate constant,  $[E]$  is TRPM7-KD concentration and  $^\wedge K_d$  is the apparent dissociation constant.

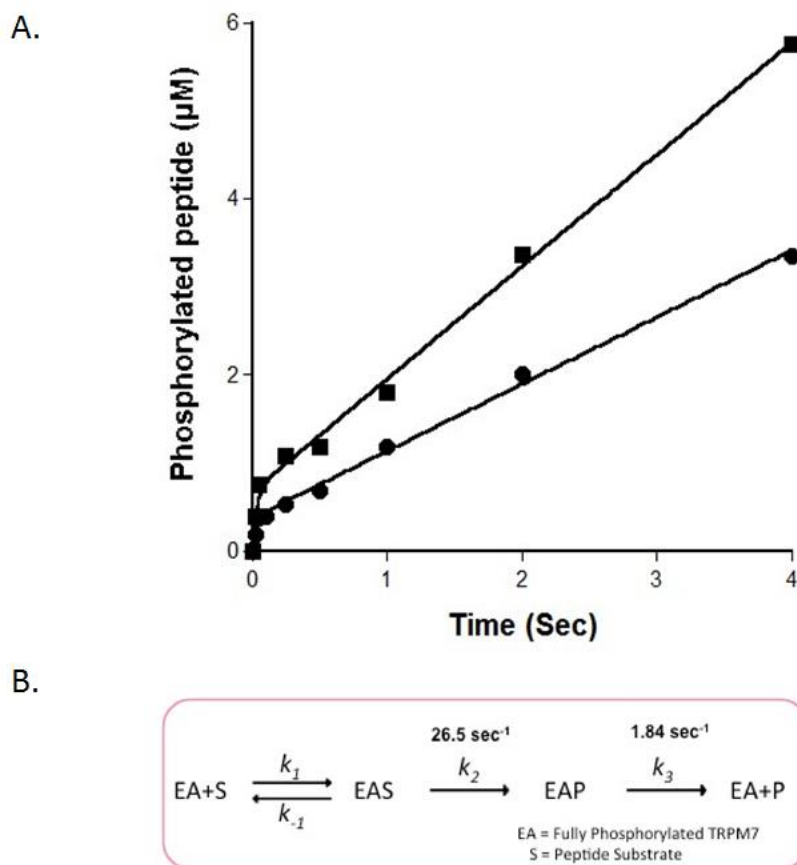


**Figure 2.5. Product release as the rate limiting step in the kinetic mechanism of TRPM7 kinase domain.**

**A**, Rapid mixing of MgATP with TRPM7-KD•Peptide substrate. Rapid quench-flow experiments were conducted at 27 °C and pH 7.5 in assay buffer (25 mM HEPES, 50 mM KCl, 2 mM DTT, 0.1 mM EDTA, and 0.1 mM EGTA) containing 10 mM MgCl<sub>2</sub>. [ $\gamma$ -<sup>32</sup>P] ATP (100-1000 cpm/pmol) and peptide substrate mixture were loaded into sample loop A, while TRPM7-KD were loaded into sample loop B. Final concentrations were 1 mM MgATP<sub>2</sub><sup>-</sup>, 25  $\mu$ M peptide substrate, and 0.5 (circle), 1  $\mu$ M (square) TRPM7-KD. At set times, reactions were quenched by the addition of quenching buffer (20 mM HEPES pH 7.4, 200 mM KCl, 0.1% bovine serum albumin, 50 mM EDTA, 1 mM EGTA) and product formation (EAP + P) was quantified as described in ‘2.3 Materials and Methods’. The lines through the data correspond to the best fit to equation 2.1 according to an average  $k_2$  of 26.5 s<sup>-1</sup> and  $k_3$  of 1.84 s<sup>-1</sup>. **B**, Reaction scheme.

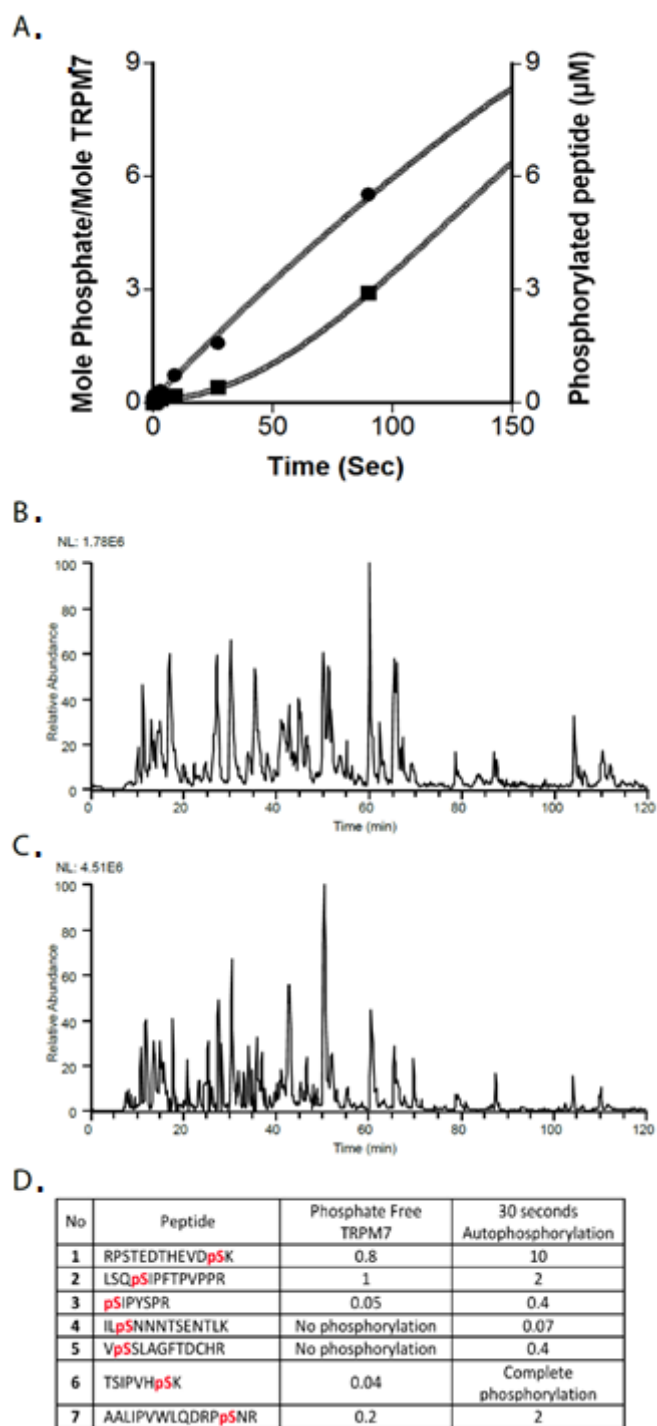


**Figure 2.6. Three early autophosphorylation events are required for TRPM7 autoactivation.**

**Figure 2.6 continued.**

**A**, Fitted rapid quench kinetic data showed that PF-TRPM7 became active towards substrates after incorporation of the first 2-3 phosphates which was confirmed by lag phase of peptide phosphorylation until TRPM7 gets ~3 phosphates. (Closed circle curve represents mole phosphate per mole TRPM7 and closed square curve presents phosphorylated peptide). Data were fitted using Kintek explorer software to the following model ( $E=EA$ ,  $EA+S=EAS$ ,  $EAS=EA+P$ ). **B-D**, Mass spectrometric analysis of autophosphorylation sites in TRPM7-KD. Base peak ion chromatogram of B, PF-TRPM7 and C, after 30 seconds of autophosphorylation. D, Relative degree of phosphorylation of TRPM7 sites based on peak area ratios of phosphorylated and non-phosphorylated peptides from TRPM7 after 0 or after 30 seconds of autophosphorylation. Peak area ratio = peak area for phosphorylated peptide / peak area for non-phosphorylated peptide. The ratios were calculated using the highest peak area for each peptide and corresponding phosphorylated peptide.

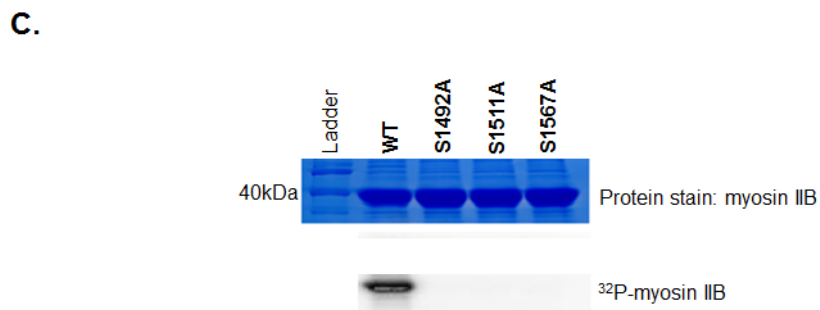
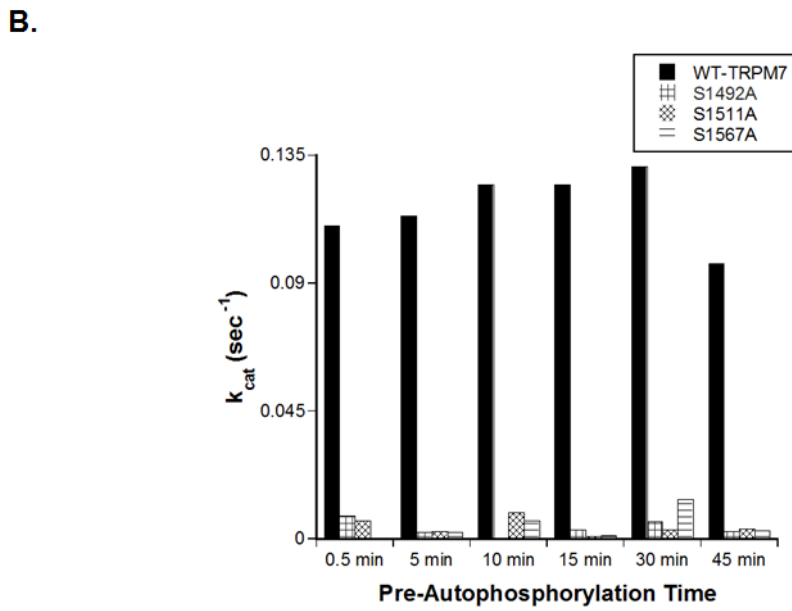
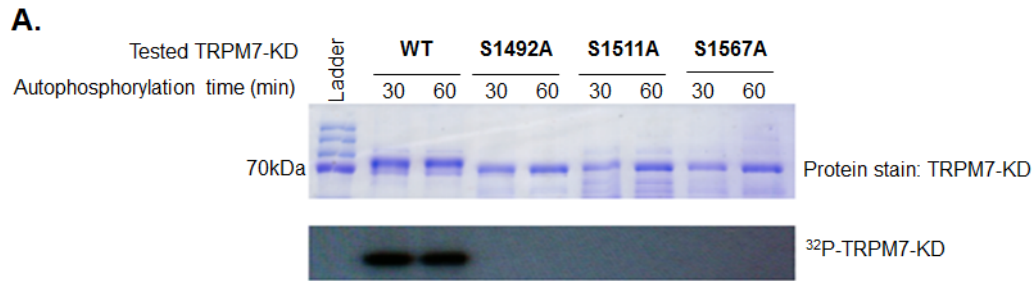


**Figure 2.7. The effect of Alanine mutation of the early phosphorylation sites on TRPM7-KD autophosphorylation and kinase activity against either peptide and or protein substrate (myosin IIB).**

**Figure 2.7 continued.**

**A**, Autophosphorylation of wild type PF-TRPM7 and mutant TRPM7 in which Ser1492, Ser1511, and Ser1567 were changed to alanine residues. Either WT PF-TRPM7 or each mutant was incubated with [<sup>32</sup>P] MgATP for 30 min and 60 min. Samples were separated by SDS-PAGE (upper) and analyzed by autoradiography (lower). **B**, Activity of PF-TRPM7 and each alanine mutant that were pre-autophosphorylated for different time points against 12.5 μM peptide substrate and saturating concentration of ATP. **C**, Kinase activity of PF-TRPM7 and each alanine mutant against myosin IIB. Either wild type PF-TRPM7 or each alanine mutant was incubated with [<sup>32</sup>P] MgATP and myosin IIB for 30 min. Samples were separated by SDS-PAGE (upper) and analyzed by autoradiography (lower).

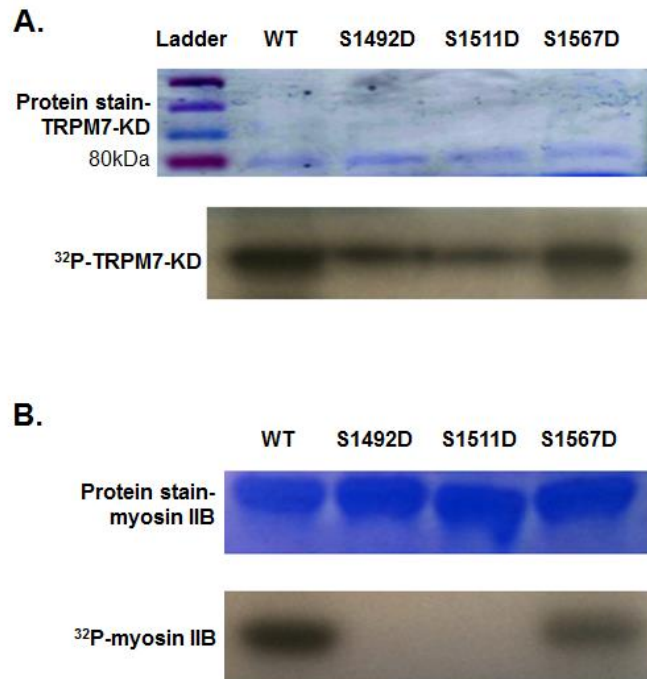


**Figure 2.8. The effect of aspartate mutation of the early phosphorylation sites on TRPM7-KD (A) autophosphorylation and (B) ability to phosphorylate its protein substrate myosin IIB substrate.**

**A**, Autophosphorylation of wild type PF-TRPM7 and three mutants in which Ser1492, Ser1511, and Ser1567 were changed to aspartic acid residues. Either wild type PF-TRPM7 or mutant was incubated with [<sup>32</sup>P] MgATP for 60 min. Samples were separated by SDS-PAGE (upper) and analyzed by autoradiography (lower). **B**, Either wild type PF-TRPM7 or each aspartate mutant was incubated with [<sup>32</sup>P] MgATP and myosin IIB for 30 min. Samples were separated by SDS-PAGE (upper) and analyzed by autoradiography (lower).



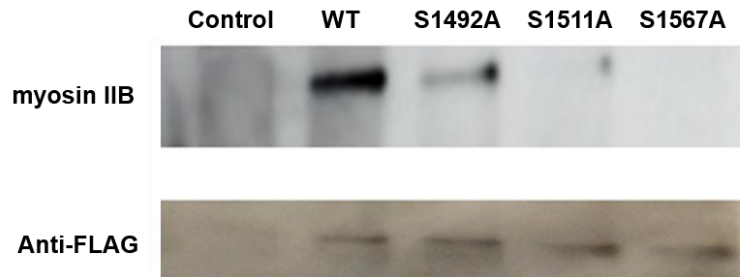


**Figure 2.9. The effect of alanine mutation of the early phosphorylation sites on TRPM7 –myosin interaction in HEK293 cells.**

Full length of Myc-FLAG tagged TRPM7 WT and Alanine mutants were transfected into HEK293 cells and immunoprecipitated with anti-Myc antibody-containing beads according to the protocol described in ‘2.3 Materials and Methods’ and associating myosin IIB heavy chain was detected by western blotting.

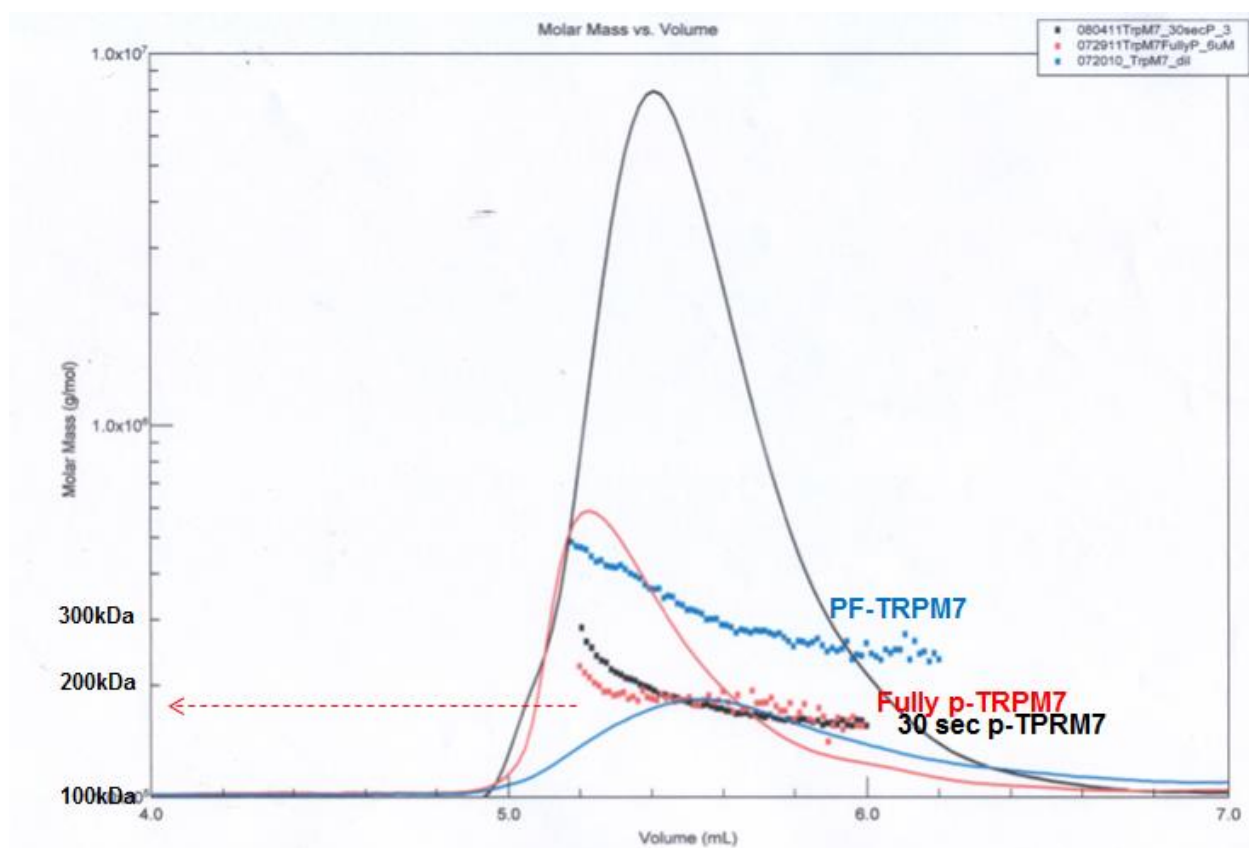


**Figure 2.10. Dynamic light scattering analysis: Effect of autophosphorylation on the self-association of TRPM7 kinase domain.**

Fractionations of inactive TRPM7 (PF-TRPM7) and active TRPM7 (Fully phosphorylated TRPM7-KD and 30 sec-autophosphorylated TRPM7-KD) show that early TRPM7-KD autophosphorylation as well as TRPM7-KD full phosphorylation induces its dimerization.

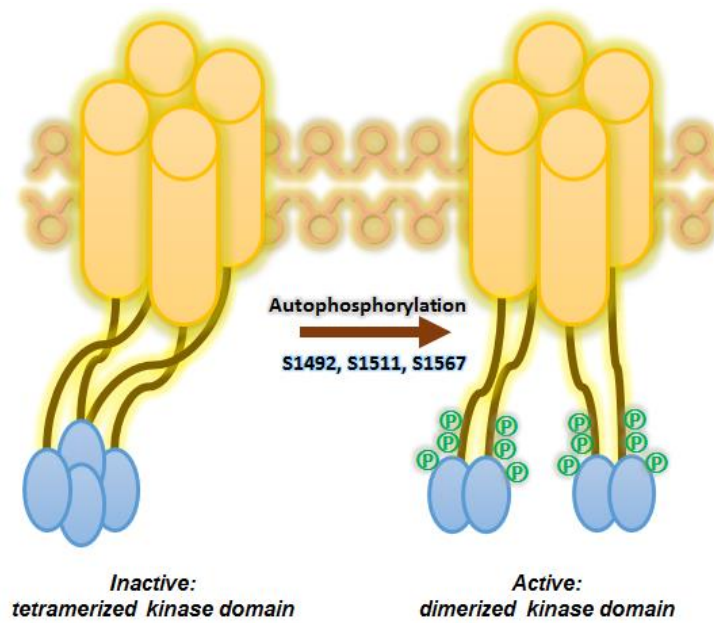


**Figure 2.11. Schematic model: Activation of TPRM7 catalytic domain.**

## **Chapter 3: Suppression of Breast Cancer Cell Migration by Novel Inhibitors Targeting TRPM7 Kinase Activity<sup>‡</sup>**

### **3.1 ABSTRACT**

TRPM7 (transient receptor potential melastatin 7) is a non-selective cation channel that is permeable to both Ca<sup>2+</sup> and Mg<sup>2+</sup> and is implicated in cell adhesion and magnesium homeostasis. The TRPM7 channel possesses a protein kinase domain at the C-terminus whose activity is linked to the control of actomyosin contractility. TRPM7 mediates proliferation, adhesion and migration of breast cancer cells and recently has been reported to promote breast tumor cell metastasis. The lack of cell-permeable pharmacological inhibitors of the kinase domain represents a barrier to fully understanding its kinase function. Herein, we describe the discovery of the first group of small molecule compounds that target TRPM7 kinase activity and characterize their mechanism of inhibition *in vitro* and *in cells*. These compounds were shown to decrease the binding of myosin IIB to TRPM7 in cells transfected with pCMV6-TRPM7. Interestingly, two of the inhibitors significantly inhibited MDA-MB-231 breast cancer cell migration, which is reportedly regulated by TRPM7 kinase activity.

### **3.2 INTRODUCTION**

---

<sup>‡</sup> Contributions to the work described in this chapter: Dr. Tamer S. Kaoud (Performed biochemical screening assays); Dr. Shreya Mitra (Analyzed breast cancer cell migration assay); Anna Tseng (Helped biochemical assays).

As described above, TRPM7 (transient receptor potential melastatin 7) is a non-selective cation channel that is permeable to both  $\text{Ca}^{2+}$  and  $\text{Mg}^{2+}$  as well as metal ions and is fused to a protein kinase domain at the C-terminus whose activity is linked to the control of actomyosin contractility. The ion-conducting properties of TRPM7 can be modulated by different stimuli, resulting in a variety of cellular responses. The expression of the TRPM7 channel is widespread and is found in cancer cells such as retinoblastoma, neck and head, gastric and breast<sup>(39, 41, 42)</sup>. Whether TRPM7 activity contributes to cancer progression has not been delineated in detail. Central to tumor metastasis is the capacity of tumor cells to adhere to cells and tissue that differ from the original site. Metastasis occurs through a complicated multistep process including tumor cell dissemination, cell invasion, entry into the bloodstream and outgrowth of secondary tumors in distant organs<sup>(45)</sup>. The continuous  $\text{Ca}^{2+}$ -mediated regulation of actomyosin contractility, as well as cytoskeletal dynamics is required for each step of metastasis. Therefore, as a regulator of actomyosin contractility, cell motility and proliferation, TRPM7 was suggested to be a potential target for the pharmacological treatment of cancers.

Earlier studies in human gastric cancer cells showed that blockade of TRPM7 channels or knockdown of TRPM7 expression by siRNA inhibited cancer cell growth and induced apoptosis, implying the potential function of TRPM7 in the growth and proliferation of cancer cells. In breast cancer cells, previous studies have shown that calcium is involved in the control of proliferation and apoptosis. It has been reported that there is a clinically relevant link between TRPM7 levels and metastatic disease in breast cancer patients<sup>(44)</sup>. The TRPM7 channel was overexpressed in grade III breast cancer

samples and associated with tumor size. In earlier work, Middelbeek et al. showed that knocking down TRPM7 expression by siRNA transfection in invasive human breast cancer cells impaired their ability to migrate *in vitro* and their metastatic potential in a mouse xenograft model of human breast cancer<sup>(44)</sup>. Moreover, a recent study from Guilbert et al. suggested that TRPM7 is involved in estrogen receptor-negative metastatic breast cancer cells migration through its kinase domain by showing that overexpression of the kinase domain-truncated TRPM7 decreased the number of adherent cells and strongly inhibited cell migration while the overexpression of the WT TRPM7 significantly increase it<sup>(43)</sup>.

Taken together, these findings suggest that TRPM7 is a key player in modulating adhesion and migration of MDA-MB-231 cells and suggest that TRPM7 could be a potential therapeutic target for limiting the metastatic potential of cancer cells. However, molecular mechanisms underlying the contribution of TRPM7 to cancer cell proliferation and migration is still not fully elucidated. In addition, the lack of cell-permeable pharmacological inhibitors of the TRPM7 kinase domain represents a barrier to fully understand the kinase domain's function.

In this study, we discovered small molecule inhibitors that target TRPM7 kinase activity by screening a compound collection from NCI and characterized their mechanism of inhibition. The compounds inhibited the association between TRPM7 and myosin in HEK293 cells. Furthermore, some compounds were shown to significantly suppress MDA-MB-231 breast cancer cell migration. Our results support a previous study suggesting that TRPM7 plays a role in breast cancer cell migration through its kinase

domain. These small molecule compounds represent the first group of inhibitors to target the kinase activity of TRPM7, resulting in the inhibition of breast cancer cell migration.

### **3.3 MATERIALS AND METHODS**

#### **Biochemical Screening of NCI natural products set and challenge set**

Four 96-well plates were provided by NCI and used for the kinase screening. Phosphorylation of 10  $\mu\text{M}$  of TRPM7 peptide substrate (acetyl-RKKYRIVWKSIFRRFL-amide) were tested using 25 nM of fully phosphorylated TRPM7 in kinase assay buffer (25 mM HEPES (pH 7.6), 10 mM  $\text{MgCl}_2$ , 50 mM KCl, 2 mM DTT, 0.1 mM EDTA, 0.1 mM EGTA, 0.03 % Brij-35, 5-10% DMSO and 10  $\mu\text{g/ml}$  BSA) in the presence of 10  $\mu\text{M}$  of each compound. Each reaction mixture was incubated in a volume of 90  $\mu\text{L}$  per well in 96-well plate at room temperature for 30 minutes. The reactions were initiated by the addition of 10  $\mu\text{L}$  [ $\gamma$ - $^{32}\text{P}$ ] ATP, adjusting the ATP concentration to 200  $\mu\text{M}$  (100-1000 c.p.m.  $\text{pmol}^{-1}$ ). The reaction was incubated at room temperature for 10 minutes and then quenched by transferring 80  $\mu\text{L}$  of reaction mixture to each well of a P81 96-well filter plate (Unifilter, Whatman) containing 200  $\mu\text{L}$  of 0.1 M phosphoric acid solution. The P81 filter plate was washed 7-8 times with 200-300 mL of 0.1 M phosphoric acid solution and one time with pure acetone, followed by the addition of 20 mL of scintillation cocktail. A MicroBeta TriLux liquid scintillation counter (PerkinElmer) was used for screening.

### ***In Vitro* Kinase Inhibition Assay**

Kinase inhibition assays were conducted at 30 °C in assay buffer (25 mM HEPES buffer-pH 7.5, 50 mM KCl, 0.1 mM EDTA, 0.1 mM EGTA, 2 mM DTT and 10 µg mL<sup>-1</sup> BSA), containing 300 µM [ $\gamma$ -<sup>32</sup>P] ATP (100-1000 c.p.m. pmol<sup>-1</sup>), 11 mM MgCl<sub>2</sub> and different concentrations of each compound in a final total volume of 70 µL, containing 5-10 % DMSO and 0.03% Brij-35 surfactant.

For TRPM7 assays, 25 nM of fully phosphorylated TRPM7 were assayed with 10 µM of TRPM7 peptide substrate (acetyl-RKKYRIVWKSIFRRFL-amide). For eEF2K, 2 nM eEF2K were assayed with 50 µM eEF2K peptide substrate (acetyl-RKKYKFNEDTERRRFL-amide) <sup>(142)</sup>. Activity was assessed at different compound concentrations by the measurement of initial rates, where the total product formation represented less than 10% of the initial substrate concentrations. Every reaction was initiated by the addition of ATP. At set time points (0.5, 1, 1.5, 2, 4 min), 10 µl aliquots were taken from every reaction and spotted onto 2×2 cm<sup>2</sup> squares of P81 cellulose paper; the papers were washed 3 times for 15 minutes each in 50 mM phosphoric acid (H<sub>3</sub>PO<sub>4</sub>), followed by a pure acetone wash, then dried. The amount of labeled protein was determined by counting the associated c.p.m. on a Packard 1500 scintillation counter at a sigma value of 2.

### **Cell culture**

HEK293T cells were maintained in DMEM (Invitrogen) supplemented with 2 mM L-glutamine (Invitrogen), 10% (v/v) FBS-US grade (Invitrogen), 100 g mL<sup>-1</sup> streptomycin (Sigma) and 100 U mL<sup>-1</sup> penicillin (Sigma). Cells were cultured at 37 °C in a humidified



5% CO<sub>2</sub> incubator. For myosin co-immunoprecipitation experiments, cells were seeded in a 12-well plate at 400,000 cells per well and the pCMV6-Entry vector containing DNA encoding for full length TRPM7 (Myc-DDK-tagged)-Human transient receptor potential cation channel, subfamily M, member 7 (Origene) was transfected into HEK293T cells by lipofectamine 2000 (Invitrogen, California, USA) according to the manufacturer's protocol. After 48 hours of transfection, cells were incubated with different concentrations of the compounds for additional 16 hours in serum free media except the compound 5 which was incubated for 3 hours and finally, cells were treated with bradykinin (10-50 nM) for 30 minutes in full media. For cell migration experiment, MDA-MB-231 cells were maintained in RPMI media (Cellgro, Mediatech) with 5% (v/v) FBS (Gemini Bio-Products) 100 U mL<sup>-1</sup> penicillin (Sigma), and 100 g mL<sup>-1</sup> streptomycin (Sigma). Cells were pre-incubated with 10 μM of each tested compound for overnight, prior to the migration assays. The compounds were maintained in the culture media for the duration of the experiment.

## **Data Analysis**

*Steady-state kinetic experiments* - Reactions were carried out as mentioned in the kinase activity assay except in the kinetic mechanism study, where we varied concentrations of substrate (ATP) and compound 2. Initial rates were determined by linear least squares fitting to plots of product against time. Reciprocal plots of 1/v against 1/s were checked for linearity, before the data were fitted to equation 3.1 using a non-linear least squares approach, assuming equal variance for velocities, using the program

Kaleidagraph 3.5 (Synergy software). Values for kinetic constants were then obtained using the program Sigma plot by fitting the kinetic data to the relevant over-all equation. Data conforming to linear competitive inhibition were fitted to equation 3.2; data conforming to hyperbolic mixed inhibition were fitted to equation 3.3. Dose-response curves for data conforming to inhibition were fitted to equation 3.4.

$$\frac{V_0}{V_{\max}^{\text{app}}} = \frac{s}{K_{\text{mS}}^{\text{app}} + s} \quad \text{Equation 3.1}$$

$$\frac{V_0}{V_{\max}^{\text{app}}} = \frac{s}{K_{\text{mS}}^{\text{app}} \left(1 + i/K_{\text{ic}}^{\text{app}}\right) + s} \quad \text{Equation 3.2}$$

$$\frac{V_0}{V_{\max}^{\text{app}}} = \frac{s}{K_{\text{mS}}^{\text{app}} \left( \frac{1 + \frac{i}{K_i^{\text{app}}}}{1 + \frac{\beta i}{\alpha K_i^{\text{app}}}} \right) + s \left( \frac{1 + \frac{i}{\alpha K_i^{\text{app}}}}{1 + \frac{\beta i}{\alpha K_i^{\text{app}}}} \right)} \quad \text{Equation 3.3}$$

$$V_0 = V_{\infty} - \left( V_{\infty} \frac{i}{i + (K50)} \right) + V' \quad \text{Equation 3.4}$$

The parameters used in deriving equations are defined as follows;  $V_o$ , observed rate;  $V_{max}^{app}$ , apparent maximum rate;  $s$ , concentration of substrate S;  $K_{mS}^{app}$ , apparent Michaelis constant for substrate S;  $i$ , concentration of inhibitor I;  $K_i^{app}$  or  $K_{ic}^{app}$ , apparent competitive inhibition constant for inhibitor I;  $\alpha K_i^{app}$ , apparent uncompetitive inhibition constant for inhibitor I;  $\beta V_{max}^{app}$ , apparent maximum rate for enzyme inhibitor complex;  $V_\infty$ , is the observed rate in the absence of inhibitor,  $V'$  is the observed rate constant at saturating inhibitor, I;  $K_{50}$  is the concentration that leads to half the maximal change in  $V_o$ .

### **Immunoprecipitation Experiments**

After washing the cells with PBS (Invitrogen), the lysates were prepared in lysis buffer containing 50 mM Tris pH 7.5, 300 mM NaCl, 0.5 mM NaCl, 0.5 mM DTT, 1.5 mM MgCl<sub>2</sub>, 0.2 mM EDTA, 1% Triton X-100 supplemented with protease and phosphatase inhibitors and then cleared by centrifugation. The protein concentration was measured by Bradford analysis (Bio-Rad). For immunoprecipitation of exogenously expressed TRPM7, Myc-Tag (9B11) Mouse mAb (Sepharose Bead Conjugate) (Cell Signaling Technology) were added to the lysate, the samples were incubated at 4 °C overnight. Subsequently, the beads were washed three times with lysis buffer, protein complexes were solubilized in Laemmli sample buffer and separated by SDS-PAGE. Proteins were fractionated on a 10% SDS polyacrylamide gel (Bio-Rad) and transferred to Hybond-P PVDF Membrane (GE Healthcare). Primary antibodies were incubated overnight at 4 °C using 1:1000 anti-myosin IIB rabbit polyclonal antibodies (Cell Signaling

Technology); anti-rabbit (Bio-Rad) horseradish peroxidase-conjugated secondary antibodies and ECL Plus™ Western Blotting Reagents (GE Healthcare) were employed to develop the blots.

### **Cell migration**

A modified Boyden chamber (Millipore) was used to measure cell migration. About 50,000 cells, rinsed and resuspended in serum free RMPI, were added into the upper chamber of trans-well separated by inserts with 8 µm pores. A chemotactic gradient was created by adding HBSS (Hank's Buffered Salt Solution) medium containing 1% (v/v) FBS to the lower chamber. Cells were allowed to migrate for 6 hours. After fixing the migrated cells with 4% paraformaldehyde, they were stained with 0.5% (w/v) crystal violet, and quantified by counting four randomly chosen fields (at an objective of 10 ×).

## **3.4 RESULTS AND DISCUSSION**

Our biochemical screening identified five compounds (Table 3.1) exhibiting considerable inhibition of TRPM7 kinase activity when assayed at a concentration of 10 µM.

### **Prioritizing hits and potential mechanisms of inhibition by the identified inhibitors**

To prioritize the 5 hits identified in the biochemical screening we performed dose-response curves, examining the ability of the compounds to inhibit the phosphorylation of a peptide substrate by the TRPM7 kinase domain in an *in vitro* kinase assay (table 3.1 and

figure 3.1). To further understand the mechanism of TRPM7 kinase domain inhibition by these compounds we tested the ability of these compounds to suppress TRPM7 autophosphorylation. Three compounds (1-3) were able to inhibit TRPM7 kinase domain autophosphorylation, while the other two compounds did not affect autophosphorylation (table 3.1).

We determined  $k_{\text{obs}}$  over a range of Mg-ATP concentrations at different fixed concentrations of compound 1, in the presence of a saturating concentration of peptide-substrate. The double reciprocal plot derived from this study (figure 3.2) is consistent with a mechanism of competitive inhibition (figure 3.2, where  $K_i \sim 0.7 \pm 0.04 \mu\text{M}$ ). According to this model, compound 1 binds TRPM7 and alters its affinity for ATP without affecting  $k_{\text{cat}}$ .

### **Selectivity of the compounds**

To profile the selectivity of the five compounds towards the TRPM7 kinase domain, the  $\text{IC}_{50}$  of each compound was determined against another atypical alpha kinase eEF2K that has been reported to be structurally similar to the TRPM7 kinase domain<sup>(143)</sup>. Dose response inhibition assays against eEF-2K were performed using 2 nM eEF-2K, 50  $\mu\text{M}$  [ $\gamma$ - $^{32}\text{P}$ ] ATP, 30  $\mu\text{M}$  Pep-S (acetyl-RKKYKFNEDTERRRFL-amide), and various concentrations of each compound. Most notably, compound 1 exhibits a 700-fold selectivity for TRPM7 over eEF2K. The selectivity profile of these compounds strongly demonstrates the ability of the screening protocol to identify molecules that target TRPM7 kinase domain with selectivity.

## **Cellular Activity**

It has been reported that myosin binding to TRPM7 is triggered by kinase domain autophosphorylation. Unlike TRPM7–WT, TRPM7-D1775A (Kinase dead TRPM7) does not interact with myosin IIA heavy chain <sup>(36)</sup>. The ability of the five compounds to inhibit the TRPM7 interaction with myosin IIB were examined in HEK293 cells following stimulation by bradykinin <sup>(36)</sup> and visualized through western blot analysis (figure 3.3). Compounds 1, 2 and 5 showed inhibition of the TRPM7-myosin interaction in HEK293 cells, with compound 1 exhibiting ~75% inhibition at a concentration of 50  $\mu\text{M}$ . It should be noted that the protein substrates concentration in the cell is significantly lower than MgATP. Thus, a non-ATP competitive inhibitor does not have to be as potent as an-ATP competitive inhibitor to achieve an acceptable effective dose-50 ( $\text{ED}_{50}$ ) in cells. For example, in figure 3.3, compare the degree of inhibition of 50  $\mu\text{M}$  of compound 1 (an ATP-competitive inhibitor of TRPM7 kinase domain whose  $\text{IC}_{50}$  is 0.5  $\mu\text{M}$ ) with that of compound 5 (a non ATP-competitive inhibitor whose  $\text{IC}_{50}$  is 3.5  $\mu\text{M}$ ).

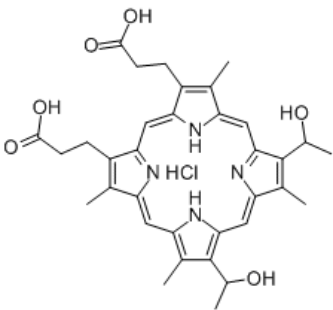
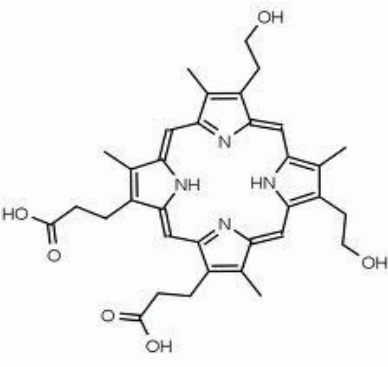
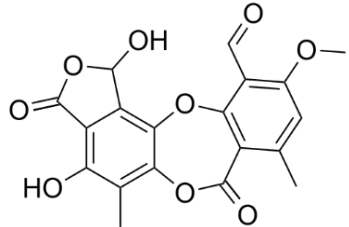
## **TRPM7 kinase domain inhibitors impedes migration of breast cancer cells**

The invasion-metastatic cascade involves a series of events whereby tumor cells leave the primary tumor, intravasate into the circulation, extravasate at distant tissues, and establish micrometastases that may grow into macroscopic secondary tumors <sup>(144)</sup>. Cell migration is an early requirement for tumor metastasis, so inhibition of cell migration provides a potential strategy to inhibit metastasis <sup>(145)</sup>. A recent study has reported the importance of TRPM7 for breast tumor cell metastasis as TRPM7 knockdown inhibits the

migration of invasive human triple negative breast cancer cells (MDA-MB-231)<sup>(44)</sup>, although the effect was significant but the absence of inhibitors that specifically inhibit TRPM7 kinase domain acted as a barrier to determine if this effect on metastasis returns to the channel or the kinase domain. Interestingly, Guilbert et al. has finally reported that TRPM7 is involved in oestrogen receptor-negative metastatic breast cancer cells migration through its kinase domain <sup>(43)</sup>. We examined whether any of the identified compounds inhibited chemotactic cell migration of a highly metastatic human breast cancer cell line namely MDA-MB-231 in a trans-well assay. MDA-MB-231 cells were treated with DMSO, or compounds 1-5 (10  $\mu$ M) (figure 3.4) overnight. Cell viability was monitored during the migration assay and found to be unaffected by the addition of the compounds. Untreated MDA-MB-231 cells showed robust migration in response to serum, while cells treated with 10  $\mu$ M of compounds 1 and 5 exhibited approximately 80% inhibition of migration (figure 3.4).

### **3.5 CONCLUSION**

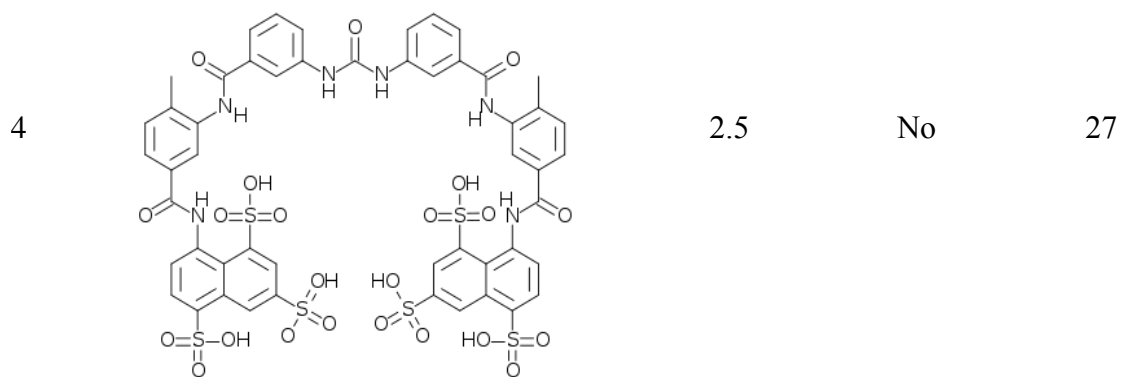
The NCI natural products and challenge sets were screened against the kinase activity of the TRPM7 kinase domain. A total of 5 small molecules were identified as inhibitors of the TRPM7 kinase domain. Compound 1 showed marked selectivity for TRPM7 over eEF2K and showed 80% inhibition of MDA-MB-231 breast cancer cell migration at a 10  $\mu$ M concentration. The inhibitors described here represent a starting point for the development of selective small molecules capable of compromising the kinase activity of TRPM7.

Identified inhibitors	Kinase Assay TRPM7 IC <sub>50</sub> (μM)	Inhibits TRPM7 Auto- Phosphorylation?	Kinase Assay eEF2K IC <sub>50</sub> (μM)	
Hematoporphyrin HCl				
1		0.52	Yes	378
	Iso-hematoporphyrin			
2		2.3	Yes	58
	Stictic Acid			
3		4.5	Yes	27

**Table 3.1 continued, next page.**



Suramin Sodium



Tetrocarcin A

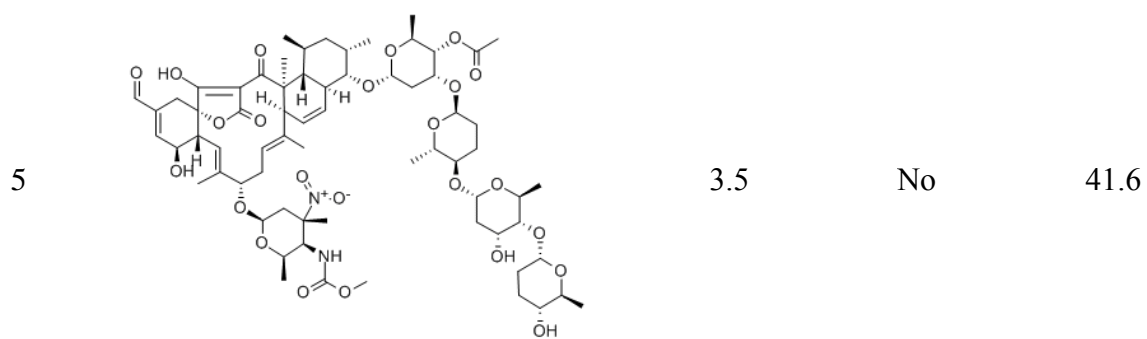


**Table 3.1.** The *in vitro* kinase assay results of the identified compounds.

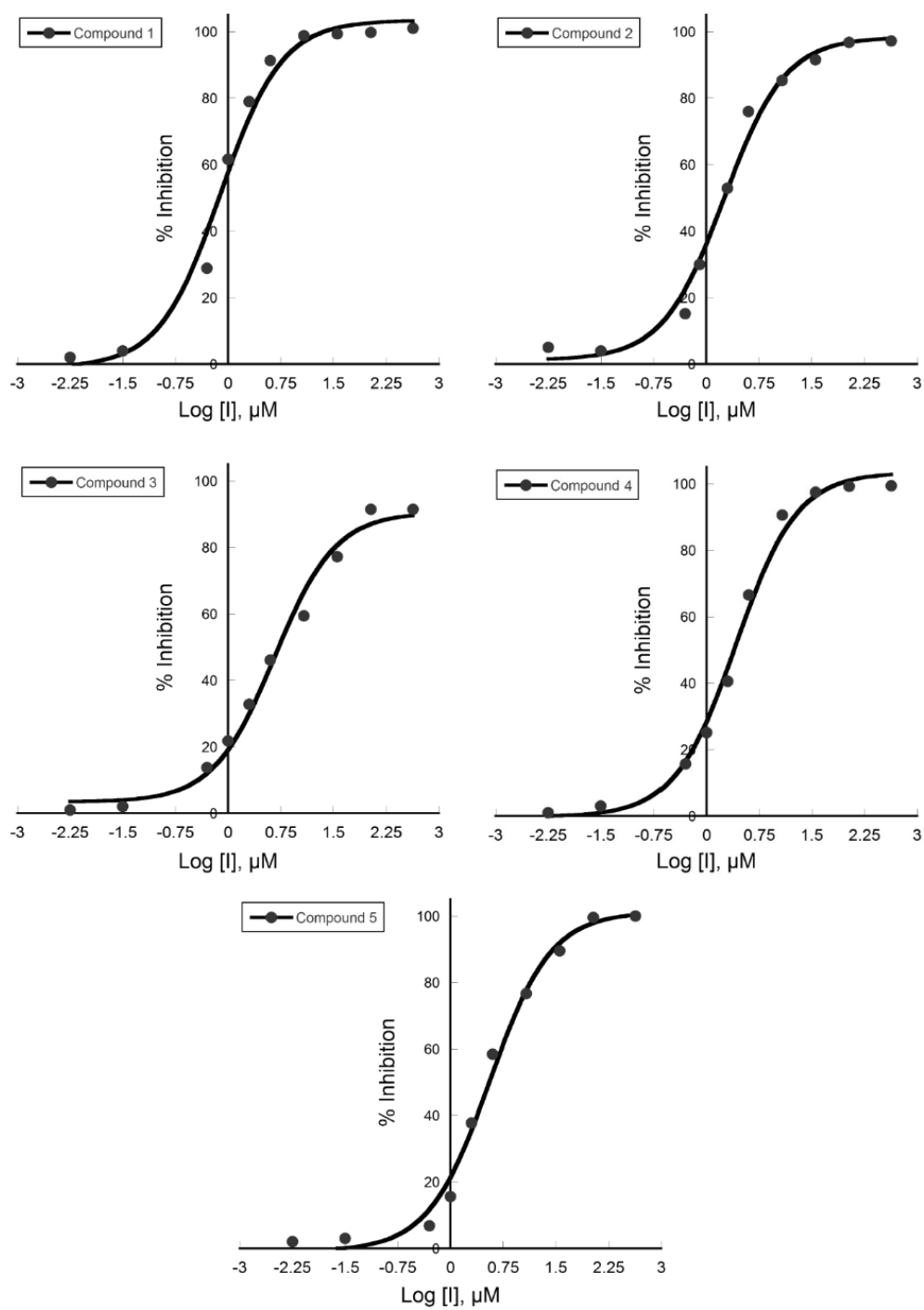


**Figure 3.1. The effect of compounds 1-5 on the ability of TRPM7 kinase domain to phosphorylate its peptide substrate.**

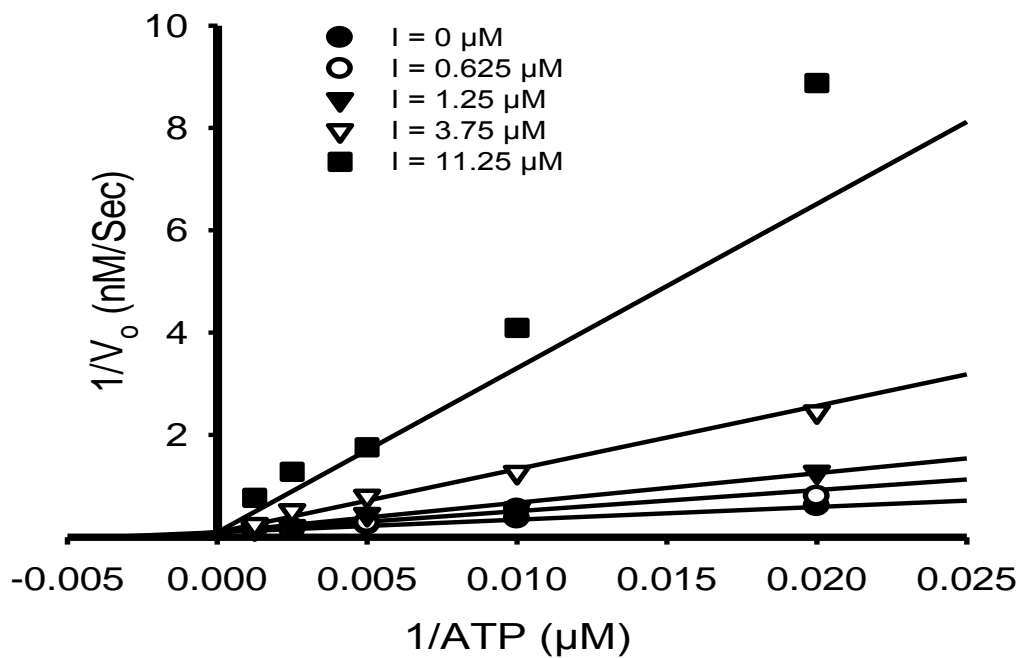


**Figure 3.2. Mechanism of TRPM7 inhibition by compound 1**

Double reciprocal plot of  $1/V_0$  vs  $1/[ATP]$  at varied fixed concentrations of compound 1 (0–11.25  $\mu\text{M}$ ) and 10  $\mu\text{M}$  peptide substrate. Initial velocities were measured using various (50–800  $\mu\text{M}$ ) concentrations of ATP. The data were fitted to a model of linear competitive inhibition according to equation 3.2, where  $k_{\text{cat}}^{\text{app}} = 0.4 \pm 0.02 \text{ s}^{-1}$ ,  $K_m^{\text{app}} = 253 \pm 24 \mu\text{M}$ ,  $K_i^{\text{app}} = 0.7 \pm 0.04 \mu\text{M}$ .

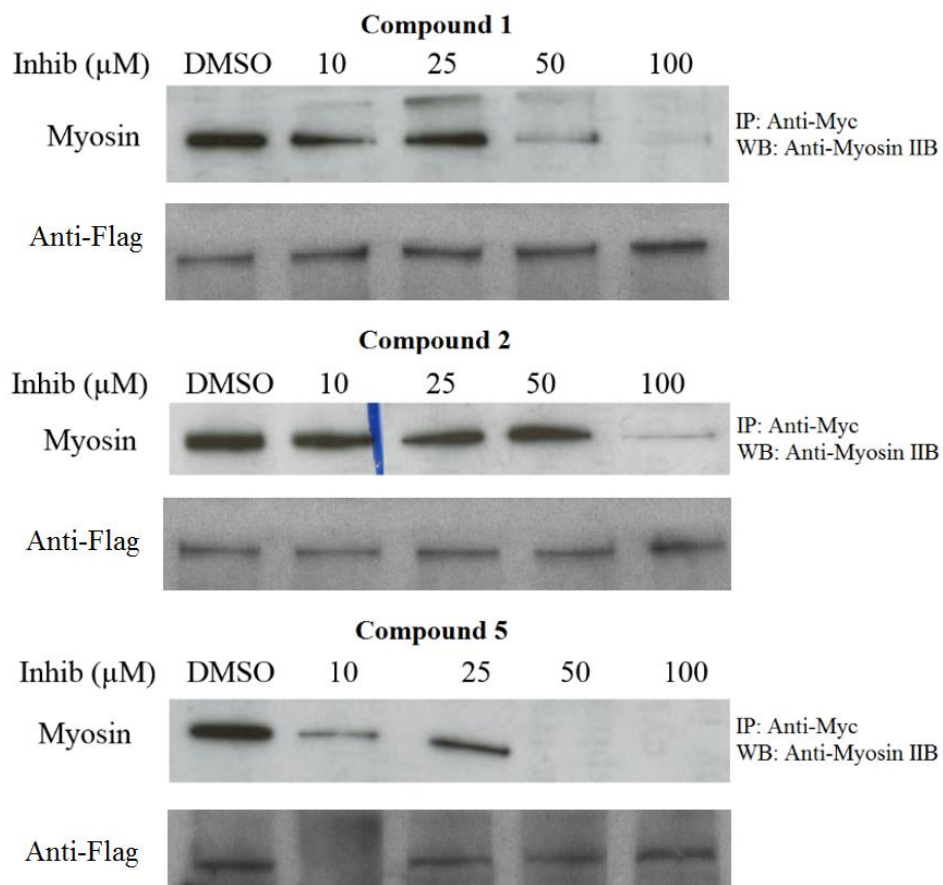


**Figure 3.3. Examining the ability of the tested compounds to modulate TRPM7-myosin interactions in HEK293 cells.**

The effect of compounds 1, 2 and 5 on TRPM7 interaction with myosin IIB was investigated by TRPM7 immunoprecipitation using anti-Myc beads and associating myosin IIB was detected by western blotting.

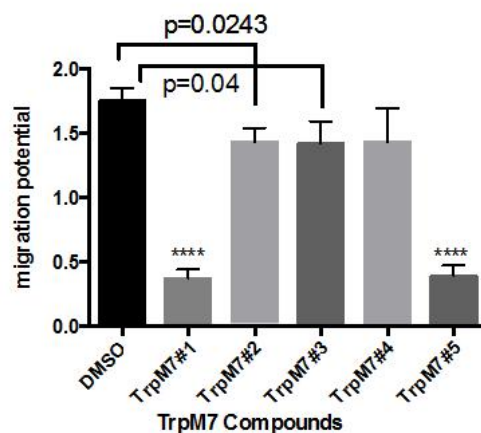
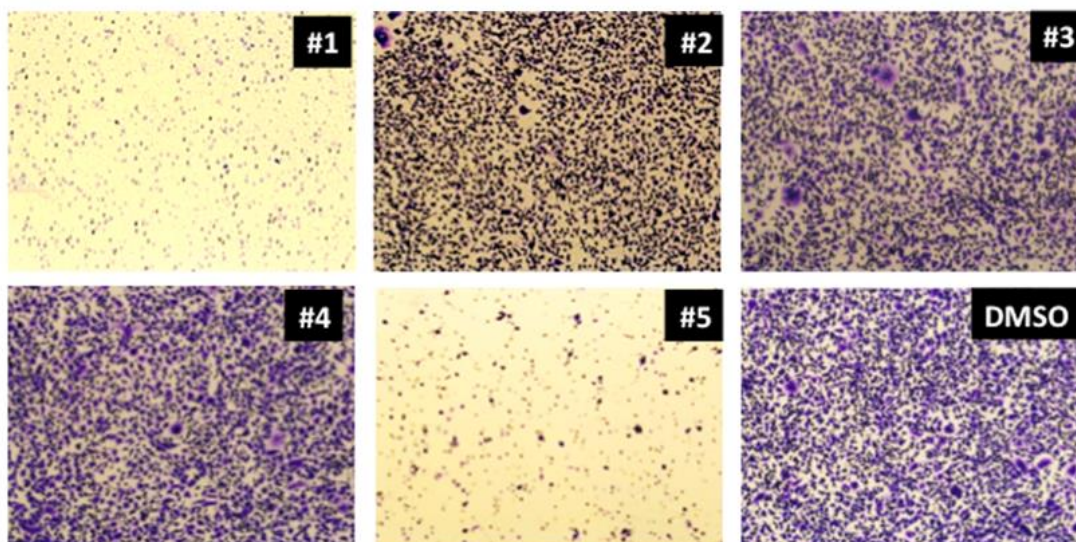


**Figure 3.4. TRPM7 kinase domain inhibitors inhibit MDA-MB-231 breast cancer cell migration.**

Representative images of migrated cells on the underside of a trans-well membrane stained with crystal violet dye. 10  $\mu$ M of compounds 1 and 5 significantly reduces the number of cells that travel through the trans-well pores to successfully reach the underside of the trans-well membrane (migrated cells) in comparison to the untreated cells. This experiment has been independently repeated three times, each one as a triplicate.

## **Chapter 4: Identification of Small Molecule Inhibitors for PERK through Luminescence High Throughput Screening and Characterization of Novel PERK Inhibitors in Pancreatic Cancer Cells<sup>††</sup>**

### **4.1 ABSTRACT**

An adaptive stress response mechanism, termed the unfolded protein response (UPR), is activated in a variety of tumor types to cope with ER stress and maintain protein homeostasis. PERK (PKR-like endoplasmic reticulum kinase) is a key component of the UPR. PERK is a Ser/Thr protein kinase whose active homodimer phosphorylates eukaryotic initiation factor 2 $\alpha$  (eIF2 $\alpha$ ), thereby inhibiting protein translation globally and reducing the load of newly synthesized proteins entering the ER. Many studies reported that the UPR is activated in a variety of tumor types. Previous studies demonstrated that cells with a compromised PERK signaling pathway are sensitive to hypoxic stress *in vitro* and form tumors that grow more slowly *in vivo*. Together, these data suggest a substantial role for PERK and the UPR in tumor cell survival and adaptation to stress. Thus, selective inhibitors of PERK activity may be useful therapeutic candidates for the treatment of cancer. In this study, we discovered potent inhibitors of PERK by high throughput screening of small molecule libraries. Using an HTS approach a number of lead

---

<sup>††</sup> Contributions to the work described in this chapter: Dr. Eun Jeong Cho and Dr. Ashwini K. Devkota (Helped high throughput screening at TI3D); Dr. Ramakrishna Edupuganti (Synthesized PERK specific inhibitor, GSK2606414); Dr. Tamer S. Kaoud, Dr. Clint D.J. Tavares, and Dr. Qiantao Wang (Helped design experiments, and contributed reagents, materials and analysis tool).

compounds were identified with demonstrated ability to inhibit PERK kinase activity *in vitro*. Several potent PERK inhibitors were further tested in a cell-based assay to evaluate modulation of the PERK signaling pathway.

## 4.2 INTRODUCTION

Protein folding is necessary for newly synthesized proteins to attain a correct conformation before exiting from the ER. Accumulation of unfolded or misfolded proteins in the ER occurs when the cell is subject to stress caused by various pathological disturbances. Under such stress the cell will initiate a protective mechanism named the unfolded protein response (UPR) that is specifically designed to restore homeostasis and normal ER function <sup>(56, 57)</sup>. This stress survival mechanism attenuates overall protein translation; however, it enhances the translation of a small number of stress survival proteins such as HIF-1 $\alpha$ , c-Myc and VEGF <sup>(77-80)</sup>. During tumorigenesis, cancer cells need to tolerate cellular stresses such as oxidative stress, nutrient deprivation or disruption of ER redox status. In order to adapt to and overcome the stress, tumor cells remodel transcriptional and translational programs by activating pro-survival signaling pathways. The unfolded stress response (UPR) is responsible for detecting ER stress and reacting to increased levels of unfolded or misfolded proteins in the ER. Tumor cells, which are frequently subjected to increased levels of unfolded proteins, hypoxia and glucose deprivation may be dependent on the UPR for survival <sup>(81)</sup>.

The UPR is initiated by several proteins such as IRE1, ATF6 and PERK. It has long been recognized that the majority of solid tumors contain areas of hypoxia because of

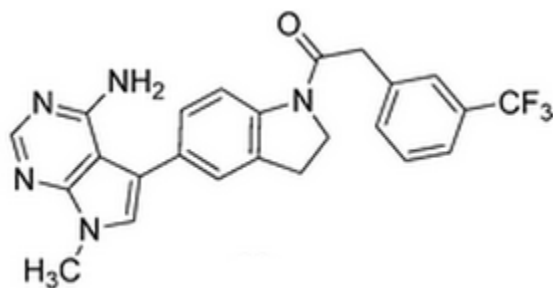
an abnormal tumor vasculature <sup>(115)</sup>. To overcome the effects of hypoxia, tumors take advantage of the UPR by phosphorylating eIF2 $\alpha$  through activation of PERK as an adaptive mechanism. PERK is a serine/threonine kinase that is activated by a cell's UPR, which detects the presence of unfolded proteins in the ER. PERK has been shown to be critical to tumor cell adaptation and angiogenesis in response to hypoxic stress <sup>(80, 118)</sup>. Using PERK<sup>-/-</sup>-MEFs, it was observed that failure of tumor cells to activate the UPR results in increased apoptosis, reduced cell survival and inhibition of tumor growth <sup>(80, 118)</sup>.

Therefore, PERK is a potential candidate protein for targeting tumor stress. Accordingly, PERK became an active target for drug design in academia and the pharmaceutical industry. The goal of this study was to identify inhibitors using high throughput screening that exhibit selective PERK inhibition. Despite PERK being identified as a therapeutic target, no specific small molecule inhibitor that targeted PERK had been reported when we initiated our research. In a recent study, Axten et al. reported a selective 'first in class' inhibitor of PERK (GSK2606414) through screening and lead optimization using the human PERK crystal structure (scheme 4.1) <sup>(124)</sup>. The compound GSK2606414 has an IC<sub>50</sub> of 0.4 nM *in vitro* which was measured using the GST-PERK kinase domain and His-tagged full-length recombinant human eIF2 $\alpha$  substrate. In addition, Axten et al. demonstrated that this compound inhibits PERK activation in a cellular assay (IC<sub>50</sub>=30 nM) and inhibits the growth of a human tumor xenograft in mice.

Small molecule inhibitors are generally discovered in a high throughput assay system where a large number of compounds are screened against a target enzyme in an automated fashion using a suitable assay. High throughput Screening (HTS) is an approach



in drug discovery that has gained widespread popularity. A radiation-based  $^{32}\text{P}$  assay is a common protein kinase assay format. However, radiation-based screening produces numerous challenges for HTS, such as radioactive contamination of the work environment and safety issues, so it is not suitable for HTS. In this study, we optimized a nonradioactive screening method based on luminescence generated by firefly luciferase. The kinase-Glo<sup>TM</sup> luminescent kinase assay (Promega, Madison, WI) determines relative ATP levels remaining in solution following a kinase reaction by luciferase-mediated luminescence. The intensity of the luminescence signal is inversely correlated to kinase activity. Herein we report utilizing a luminescent kinase assay to determine PERK activity in an HTS application using a 384 well plate format. After optimization of enzyme, substrate, and ATP concentrations, we screened small molecule libraries and identified several lead hits. The lead compounds were demonstrated to weakly inhibit PERK autophosphorylation and potently inhibit its activity against eIF2 $\alpha$  *in vitro* and in cellular assay.



**GSK 2606414**

**Scheme 4.1. The first-in-class inhibitor of PERK (GSK2606414).**

## **4.3 MATERIALS AND METHODS**

### **Reagents and equipment**

Competent cells used for amplification and expression were provided by Novagen (Gibbstown, NJ). Yeast extract and tryptone were purchased from US biological (Swampscott, MA). IPTG and DTT were obtained from USB (Cleveland, OH). Most of the buffer components including HEPES, Trizma base (Tris), sodium chloride, potassium chloride, EDTA, EGTA, calcium chloride, magnesium chloride, Brij-35, Triton X-100,  $\beta$ -mercaptoethanol, benzamidine hydrochloride, TPCK and PMSF were purchased from Sigma (St. Louis, MO). Ni-NTA agarose was supplied by Qiagen (Santa Clarita, CA) while all other components used in the protein expression and purification was obtained from Fisher Scientific (Pittsburgh, PA). Amersham Biosciences (Pittsburgh, PA) provided the FPLC system and the columns for purification. P81 cellulose papers were obtained from Whatman (Piscataway, NJ). ATP was purchased from Roche (Indianapolis, IN). Radiolabelled [ $\gamma$ - $^{32}$ P] ATP was obtained from Perkin Elmer (Waltham, MA). ADP was from MP Biomedicals (Solon, OH).

### **PERK Cloning**

The original expression empty vector (GVL2) was kindly provided by Dr. Yan Jessie Zhang (Department of Chemistry and Biochemistry, University of Texas at Austin). This expression vector was derived from pET28a vector (Novagen) containing N-terminal hexahistidine tag and GST tag followed by multiple cloning sites (MCS). Ligation independent cloning (LIC) site was introduced into the MCS by one step PCR reaction

using *pfuUltra* polymerase (Stratagene). The PCR was performed using the following primers: a forward primer, 5'- GGT GGC TCT GGG TCA AGT AAA GGT GGA TAC GGA TCC-3' and a reverse primer, 5'- GCC GGG TCC CTG AAA GAG GAC TTC AAG TGA GCT CGA TTT TGG AGG-3'. The linearized GVL2-3C/LIC vector was then treated for 1 hour at room temperature with T4 DNA polymerase (NEB) in NEB buffer 2 containing 2.5mM dTTP and the reaction was stopped by heat inactivation at 75°C for 20 minutes. The human PERK truncated kinase domain (550-1116 a.a) (GenBank accession number: NM\_004836.5) was amplified by PCR reaction using the forward primer (5'-CAG GGA CCC GGC TCA GGA ATG AGG CAA AGG AAG GAG TCT GAA-3') and the reverse primer (5'-GAC CCA GAG CCA CC TTA TTT-3'). The PCR amplification reaction mixture (50 µl) contained 1X *PfuUltra*<sup>TM</sup> HF reaction buffer (Tris (pH 8.0) and 2 mM Mg<sup>2+</sup>), 200 µM of each dNTP, 0.2 µM each of the forward and reverse primer, 10 ng of DNA template and 1U of *PfuUltra*<sup>TM</sup> HF polymerase. The PCR cycle conditions included initial denaturation at 95 °C for 3 minutes, followed by 35 cycles of denaturation at 94 °C for 30 seconds, primer annealing at 57 °C for 1 minute and extension at 72 °C for 5 minutes, with a final elongation step of 72 °C for 10 minutes. The PCR product was gel purified and ligated into previously prepared linearized GVL2-3C/LIC vector. The ligated product was transformed into the *E. coli* DH5α cells. A single colony was isolated and amplified and the extracted plasmid DNA was verified for sequencing at the ICMB core facilities, UT-Austin, using an applied Biosystems automated DNA sequencer.

### **PERK Expression (550-1116)**

Recombinant human PERK was expressed in *E. coli* strain Rosetta-gami<sup>TM</sup> 2 (DE3) (Novagen). The strain was chosen to facilitate the expression of human PERK since it contains many rare codons (almost 9% of the total codons). Rosetta-gami<sup>TM</sup> 2 (DE3) carries the pRARE2 plasmid that provides tRNAs for seven rare codons. The PERK kinase domain expression construct was transformed into Rosetta-gami<sup>TM</sup> 2 (DE3) chemical competent cells. A single isolated colony was used to inoculate 100 mL of LB media containing 50 µg/mL kanamycin, 34 µg/mL chloramphenicol and 10 µg/mL tetracycline and the culture was grown overnight at 37 °C with shaking at 250 rpm. Next day the overnight culture was diluted 100 fold into 1000 mL 2xYT media containing same concentrations of antibiotics and were grown at 37 °C for 5-6 hours for OD<sub>600</sub> to reach 0.6. Cultures were induced with 0.1 mM IPTG for 16 hours at 25 °C. Then the cells were harvested by centrifugation (5000 rpm for 20 minutes at 4 °C), flash frozen in liquid nitrogen and stored at -80 °C until lysis.

### **PERK Purification (550-1116)**

#### ***Ni-NTA affinity chromatography***

Aliquot of the frozen cell pellet from each liter of culture was resuspended in 50 mL lysis buffer (50 mM Tris pH 8.0, 250 mM NaCl, 10 mM Imidazole, 0.1% β-mercaptoethanol, 1 % triton X-100 (v/v), 1 mM benzamidine, 0.1 mM PMSF, 0.1 mM TPCK and 0.1 mg/mL lysozyme). The suspension was sonicated for a total of 20 minutes at 5 second pulse with 5 second intervals in ice at 4 °C. The lysate was centrifuged for 30

minutes at 16,000 rpm at 4 °C. The supernatant containing the protein fractions were incubated with Ni-NTA beads (Qiagen) for 1 hour at 4 °C. The beads were washed with 100 mL wash buffer (50 mM Tris pH 8.0, 500 mM NaCl, 40 mM Imidazole, 0.1%  $\beta$ -mercaptoethanol, 1 mM benzamidine, 0.1 mM PMSF and 0.1 mM TPCK). The His6-GST-3C-PERK protein was eluted with 20 mLs of elution buffer (50 mM Tris pH 8.0, 500 mM NaCl, 500 mM Imidazole, 0.1%  $\beta$ -mercaptoethanol, 1 mM benzamidine, 0.1 mM PMSF and 0.1 mM TPCK). The concentration was estimated based on the absorbance at 280 nm ( $A_{280}$ ) in spectrophotometer using the extinction coefficient of  $112370 \text{ cm}^{-1}\text{M}^{-1}$  and path length of 1 cm.

### ***3C Protease cleavage***

The His6-GST-3C-PERK protein eluted from Ni-NTA affinity chromatography was dialyzed in 4 L of 3C Cleavage buffer (25 mM HEPES, 200 mM NaCl, 2 mM DTT, 10% Glycerol at pH 7.5). The cleavage was performed by incubating protein in the presence of 1.5 % PreScission protease (kindly provided by Dr. Yan Jessie Zhang, Department of Chemistry and Biochemistry, University of Texas at Austin) at 4 °C overnight with gentle shaking. The cleavage was confirmed by running the protein in 10% SDS-PAGE.

### ***Activation of PERK***

After overnight protease cleavage, the total protein was collected and further incubated with 4 mM ATP and 10 mM  $\text{MgCl}_2$  for additional 3 hours on the ice for activation. The activated PERK was then applied to HiPrep 26/10 Desalting column (GE Healthcare) pre-equilibrated with anion exchange buffer (50 mM Tris pH 8.0, 10 mM

NaCl, 0.1 mM EDTA, and 0.1 mM EGTA, 0.1%  $\beta$ -mercaptoethanol). The excess ATP was removed and the eluted protein fractions from HiPrep 26/10 Desalting column were followed by *Mono-Q* HR 10/10 anion exchange chromatography.

#### ***MonoQ 10/10 anion exchange chromatography***

The cleaved and activated protein was applied to *Mono-Q* HR 10/10 anion exchange column pre-equilibrated with anion exchange buffer (50 mM Tris pH 8.0, 10 mM NaCl, 0.1 mM EDTA, 0.1 mM EGTA, 0.1%  $\beta$ -mercaptoethanol). The column was developed with a gradient of 0.15-1 M NaCl over 17 column volumes at a flow rate of 2 mL/min. The collected peak fractions were analyzed by SDS-PAGE and the fractions containing cleaved PERK were collected and dialyzed against storage buffer (25 mM HEPES, 50 mM KCl, 0.1 mM EDTA, 0.1 mM EGTA, 2 mM DTT, 10% Glycerol at pH 7.5). The dialyzed protein were concentrated using Amicon Ultra-15 centrifugal filter unit (10,000 NMWL) (Millipore), flash frozen in small aliquots in liquid nitrogen and were stored at -80 °C. The concentration of the protein was established based on the absorbance at 280 nm ( $A_{280}$ ) in spectrophotometer using the extinction coefficient of 97,150  $\text{cm}^{-1}\text{M}^{-1}$  and path length of 1 cm.

#### **Expression and purification of eIF2 $\alpha$**

The codon-optimized human eIF2 $\alpha$  (4-314) in pET30a vector (pET30a-heIF2aopt) was generously provided by Dr. Gerhard Wagner (Department of Biological Chemistry and Molecular Pharmacology, Harvard Medical School, Boston, MA). The BL21 (DE3) *E. coli* strain (Invitrogen) was used for protein expression. Cells were co-transformed with

the expression plasmid for the human eIF2 $\alpha$  and the plasmid pG-Tf2 (a kind gift from Dr. Gerhard Wagner) which carries the expression system for GroEL, GroES, and TF. A single isolated colony was used to inoculate 100 mL of LB media containing 50  $\mu$ g/mL kanamycin and 17  $\mu$ g/mL chloramphenicol and the culture was grown overnight at 37 °C with shaking at 250 rpm. Next day the overnight culture was diluted 100 fold into 1000 mL 2xYT media containing same concentrations of antibiotics and were grown at 37 °C for 3-5 hours for OD<sub>600</sub> to reach 0.6-1.0. Cultures were induced with 0.1 mM IPTG for 16 hours at 20 °C. Then the cells were harvested by centrifugation (5000 rpm for 20 minutes at 4 °C), flash frozen in liquid nitrogen and stored at -80 °C until lysis. Aliquot of the frozen cell pellet from each liter of culture was resuspended in 50 mL lysis buffer (50 mM Tris pH 8.0, 250 mM NaCl, 10 mM Imidazole, 0.1%  $\beta$ -mercaptoethanol, 1 % triton X-100 (v/v), 1 mM benzamidine, 0.1 mM PMSF, 0.1 mM TPCK and 0.1 mg/mL lysozyme) and sonicated for a total of 20 minutes at 5 second pulse with 5 second intervals in ice at 4 °C. The lysate was centrifuged for 30 minutes at 16,000 rpm at 4 °C. The supernatant containing the protein fractions were incubated with Ni-NTA beads (Qiagen) for 1 hour at 4 °C. The beads were washed with 100 mL wash buffer (50 mM Tris pH 8.0, 500 mM NaCl, 40 mM Imidazole, 0.1%  $\beta$ -mercaptoethanol, 1 mM benzamidine, 0.1 mM PMSF and 0.1 mM TPCK). The His6 tagged protein was eluted with 20 mL of elution buffer (50 mM Tris pH 8.0, 500 mM NaCl, 500 mM Imidazole, 0.1%  $\beta$ -mercaptoethanol, 1 mM benzamidine, 0.1 mM PMSF and 0.1 mM TPCK). The eluted protein was then loaded into HiLoad 16/60 Superdex-75 (GE Healthcare) gel filtration chromatography that was pre-equilibrated with gel filtration buffer (20 mM HEPES, 200mM NaCl, 2mM DTT, 10%

Glycerol at pH 7.5). The protein was run over 1.2 column volume at a flow rate of 1 mL/min. The collected peak fractions were analyzed by SDS-PAGE and the fractions containing human eIF2 $\alpha$  were collected and dialyzed against storage buffer. The dialyzed protein were concentrated using Amicon Ultra-15 centrifugal filter unit (10,000 NMWL) (Millipore), flash frozen in small aliquots in liquid nitrogen and were stored at -80 °C.

### **Peptide Synthesis**

Peptide substrate for PERK (5-FAM-Arg-Ser-Arg-Arg-Gly-Ser-Leu-Asn-Lys-Ser-Arg-OH) was identified by peptide microarray analysis at Pfizer (Oncology PGRD, La Jolla, CA). This peptide was synthesized, purified by HPLC and purchased from *AnaSpec* (San Jose, CA).

### **Substrate dependence assays**

eIF2 $\alpha$  dependence assays were performed using 20 nM PERK and several concentrations of eIF2 $\alpha$  (0-50  $\mu$ M) in assay buffer containing 25 mM HEPES pH 7.5, 50 mM KCl, 0.1 mM EDTA, 0.1 mM EGTA, 2 mM DTT, 10 mM MgCl<sub>2</sub>, 40  $\mu$ g/ml BSA and 0-1000  $\mu$ M [ $\gamma$ -<sup>32</sup>P] ATP (specific activity = 1000 cpm/pmol) in a final reaction volume of 100  $\mu$ L. The reaction mixture was incubated at 30 °C for 10 minutes before the reaction was initiated by addition of [ $\gamma$ -<sup>32</sup>P] ATP. 10  $\mu$ l aliquots were taken and spotted into P81 phosphocellulose papers at fixed time point intervals. The papers were washed with 50 mM phosphoric acid (3 times for 20 minutes each) and then dried following acetone wash. The amounts of radiolabelled phospho- eIF2 $\alpha$  were determined by counting the associated



counts/min on a scintillation counter (Packard 1500) at an  $\sigma$  value of 2. Kinase activity was determined by calculating the rate of phosphorylation of eIF2 $\alpha$  ( $\mu\text{M}\cdot\text{s}^{-1}$ ), and the data were fitted to equation 4.1.

$$v = \frac{V_{\max}^{\text{app}} [S]}{K_M^{\text{app}} + [S]} \quad \text{Equation 4.1}$$

The parameters are defined as follows:  $v$ , initial velocity;  $V_{\max}^{\text{app}}$ , apparent maximum velocity;  $[S]$ , concentration of varied substrate;  $K_M^{\text{app}}$ , apparent substrate concentration required to achieve half maximal activity.

### **Compound libraries and Screening Facilities**

Compound libraries and automation facilities for high throughput screening (HTS) were provided by Texas Institute for Drug and Diagnostic Development (TI3D) facility at the University of Texas at Austin. TI-3D has several compound libraries for high throughput screening. These include: Chembridge Kinase set of 11,250 compounds, Chembridge fragment set of 4,000 compounds, NCC clinical collection of 446 compounds, Maybridge HitFinder V.9 of 14,400 compounds MicroSource Spectrum of 2,000 compounds, Target focused kinase set of 600 compounds. All compounds were stored at  $-80\text{ }^{\circ}\text{C}$  as 10 mM stock in 100% DMSO.

### **Luminescence assay optimization**

Initially, assays were performed manually in white 96-well plates by varying reagent (enzyme, ATP, or peptide) concentrations or reaction time to determine the

optimum condition. In detail, 60  $\mu\text{L}$  of the assay mixture (enzyme and peptide diluted in assay buffer) was pipetted into a plate, followed by the addition of 40  $\mu\text{L}$  ATP to initiate the enzymatic reaction. After incubating at room temperature for various times, 100  $\mu\text{L}$  of the Kinase-Glo Luminescent Kinase assay kit prepared according to the manufacturer's protocol (Promega) was added and the luminescence was measured 10 minutes later. Finally, the Kinase-Glo Luminescent Kinase Assay (Promega) has been optimized to be done in a 10  $\mu\text{l}$  volume in 384 well plate at room temperature in assay buffer (25 mM HEPES pH7.5, 50 mM KCl, 0.1 mM EDTA, 0.1 mM EGTA, 2 mM DTT, 10 mM  $\text{MgCl}_2$ , 20  $\mu\text{g/ml}$  BSA) containing 20 nM PERK, 200  $\mu\text{M}$  peptide substrate (5-FAM-*RSRRGSLNKSR*) and each tested compound in 0.25% DMSO and 0.01% Triton. The reaction mixtures were incubated at room temperature for 30 minutes before initiation with 1  $\mu\text{M}$  ATP. As controls, either all components except PERK or ATP alone were used. Luminescent kinase assay measures kinase activity by quantitating the amount of ATP remaining in solution following a kinase reaction. After 2 hours, 10  $\mu\text{l}$  of Kinase-Glo assay mix was added. The kinase reaction was quenched and luminescence was measured on an Envision plate reader.

### **High Throughput Screen (HTS)**

A high throughput screening facility was provided by TI-3D (Texas institutes for drug and diagnostic development) at University of Texas-Austin. TI-3D has an automated liquid handling system (Perkin Elmer) which can perform assays in 384 well plates and Envision plate reader (Perkin Elmer) that can read luminescence signal. All the libraries

were screened at 25  $\mu\text{M}$  final concentration except the Chembridge fragment set which was screened at 500  $\mu\text{M}$  and Target focused kinase library that was screened at 3 different concentrations (1, 5, 25  $\mu\text{M}$ ). Assays were conducted in 10  $\mu\text{l}$  reaction volume at room temperature in assay buffer (25 mM HEPES pH7.5, 50 mM KCl, 0.1 mM EDTA, 0.1 mM EGTA, 2 mM DTT, 10 mM  $\text{MgCl}_2$ , 20  $\mu\text{g/ml}$  BSA) containing 20 nM PERK, 200  $\mu\text{M}$  peptide substrate and 1  $\mu\text{M}$  ATP in 0.25% DMSO and 0.01% Triton. Rows 1 and 2 (positive controls) contained enzyme but no compounds whereas rows 23 and 24 (negative controls) contained no enzyme or compounds. Rows 3 to 22 contained enzyme as well as the compounds to be screened. First, 5  $\mu\text{l}$  of assay reaction (all components except ATP and inhibitor) was added to the 384 well plates except for the negative control which contain the same assay mix except the enzyme and peptide. Then 1  $\mu\text{l}$  of the 10X inhibitor or DMSO only (controls) was added to the wells. The enzyme-inhibitor mix was allowed to incubate at room temperature for 30 minutes before starting the reaction with 4  $\mu\text{l}$  of ATP. After adding ATP, the mixture was incubated at room temperature for 2 hours. Then, 10  $\mu\text{l}$  of Kinase-Glo reagent (Promega) was added to each well, and the luminescence signal was read on the Envision plate reader for 10 minutes. Approximately 104 compounds showed greater than 30% inhibition.

### **DMSO tolerance**

Assays to test DMSO tolerance were performed in assay buffer (25 mM HEPES pH 7.5, 50 mM KCl, 0.1 mM EDTA, 0.1 mM EGTA, 2 mM DTT, 10 mM  $\text{MgCl}_2$  and 40  $\mu\text{g/mL}$  BSA) containing 20 nM PERK, 1  $\mu\text{M}$  ATP, 200  $\mu\text{M}$  peptide substrate and different

concentrations of DMSO (0, 1, 2, 3, 5, 10%) in 100  $\mu$ l volume at room temperature. Assays were started with the addition of ATP.

### **Confirmation Screen**

Compounds demonstrating above 30% activity in the rescreen were further confirmed by radioactive screen. Compound final concentrations were 100  $\mu$ M for Fragment library and 1, 5, 25  $\mu$ M for all other libraries. Assays were performed at room temperature in 100  $\mu$ l volume in 96 well plate format. All other assay conditions were maintained similar except that the radioactive assays were performed using protein substrate at 5  $\mu$ M. First, 10  $\mu$ l of compounds were pipetted into the wells of 96 well plates. Then 70  $\mu$ l of the assay mix (enzyme, peptide, and buffer) were added into each wells. The first row contained enzyme but no inhibitors (positive controls) and the last row contained no enzyme or inhibitors (negative control). The enzyme-inhibitor mix was incubated in a volume of 90  $\mu$ L per well in 96-well plate at room temperature for 30 minutes. The reactions were initiated by the addition of 10  $\mu$ L [ $\gamma$ - $^{32}$ P] ATP, adjusting the ATP concentration to 100  $\mu$ M (100-1000 c.p.m.  $\text{pmol}^{-1}$ ) for PERK. The reaction was incubated at room temperature for 10 minutes and then quenched by transferring 80  $\mu$ L of reaction mixture to each well of a P81 96-well filter plate (Unifilter, Whatman) containing 200  $\mu$ L of 0.1 M phosphoric acid solution. The P81 filter plate was washed 7-8 times with 200-300 mL of 0.1 M phosphoric acid solution to get rid of excess ATP, dried with acetone followed by the addition of 20 mL of scintillation cocktail. The counts in each wells were read using MicroBeta®TriLux liquid scintillation counter (Perkin Elmer). For the

compounds that showed greater than 50% activities, dose response assays were performed at several concentrations of the compound to determine IC<sub>50</sub>.

### **In Vitro Kinase Inhibition Assay**

Kinase inhibition assays were conducted at 30 °C in assay buffer (25 mM HEPES buffer-pH 7.5, 50 mM KCl, 0.1 mM EDTA, 0.1 mM EGTA, 2 mM DTT and 10 µg mL<sup>-1</sup> BSA), containing 300 µM [ $\gamma$ -<sup>32</sup>P] ATP (100-1000 c.p.m. pmol<sup>-1</sup>), 11 mM MgCl<sub>2</sub> and different concentrations of each compound in a final total volume of 70 µL, containing 5-10 % DMSO and 0.03% Brij-35 surfactant. Activity was assessed at different compound concentrations by the measurement of initial rates, where the total product formation represented less than 10% of the initial substrate concentrations. Every reaction was initiated by the addition of ATP. At set time points (0.5, 1, 1.5, 2, 4 min), 10 µl aliquots were taken from every reaction and spotted onto 2×2 cm<sup>2</sup> squares of P81 cellulose paper; the papers were washed 3 times for 15 minutes each in 50 mM phosphoric acid (H<sub>3</sub>PO<sub>4</sub>), followed by a pure acetone wash, then dried. The amount of labeled protein was determined by counting the associated c.p.m. on a Packard 1500 scintillation counter at a sigma value of 2. Dose-response curves for data conforming to inhibition were fitted to equation 4.2.

$$V_0 = V_{\infty} - \left( V_{\infty} \frac{i}{i + (K50)} \right) + V'$$

Equation 4.2

## **Cell culture**

HEK293T cells were maintained in DMEM (Invitrogen) supplemented with 2 mM L-glutamine (Invitrogen), 10% (v/v) FBS-US grade (Invitrogen), 100 g mL<sup>-1</sup> streptomycin (Sigma-Aldrich) and 100 U mL<sup>-1</sup> penicillin (Sigma-Aldrich). Cells were cultured at 37 °C in a humidified 5% CO<sub>2</sub> incubator. The pancreatic carcinoma MiaPaCa-2 cell line was obtained from American Type Culture Collection (Manassas VA). MiaPaCa-2 cells were grown in DMEM medium adjusted to contain 4 mmol/L L-glutamine, 4.5 g/L glucose, 10% (v/v) fetal bovine serum, 100 units/mL penicillin, and 100 µg/mL streptomycin. Cell line was maintained in a humidified incubator containing 5% CO<sub>2</sub> at 37 °C.

## **Cell Proliferation Assay**

Cell proliferation was assessed using MTS assay (CellTiter 96<sup>®</sup> AQueous Assay, Promega, WI). Cells were seeded in 96-well plates at a density of 2 X 10<sup>3</sup> cells per well in 100 µl medium. Next day cells were treated with different concentrations of 4 PERK inhibitors (compound 1-4) followed by addition of 0.15 µg/mL tunicamycin to induce ER stress. After 72 hours incubation, 20% MTS reagent was added into the culture medium. After 2-4 hours further incubation, the change in tetrazolium salts into formazan was determined by measuring the absorbance at 490 nm using kinetic microplate reader (Molecular Devices Corporation, Sunnyvale, CA).

## **Colony Formation Assay**

The inhibition of the colony-forming ability of MiaPaCa-2 cells was assayed by seeding cells in complete medium into 100-mm tissue culture plates and cells were allowed to grow to reach 90% confluence. Cells were then treated with various concentration of compounds in complete medium for 1 hour, followed by addition of 5 µg/mL tunicamycin for an additional 6 hours to induce ER-stress. DMSO was used as a control. Treated cells were harvested using trypsin, counted and a specific number of cells (500 cells) were plated in 50 mm petri dishes. They were cultured at 37 °C with 5% CO<sub>2</sub> and saturated humidity conditions for 10 days. After 10 days, the medium was removed and cells were rinsed in PBS, and fixed in 3% (v/v) acetic acid, 10% (v/v) methanol for 2 minutes. Then fixed solution was discarded and 0.2% (w/v) crystal violet staining solution was added and stained for 30 minutes. They were washed with water slowly and dried in the air and colonies were counted manually. Colonies were defined as  $\geq 50$  cells.

## **Western blot analysis**

MiaPaCa-2 cells were treated with DMSO or various concentrations of compound 3 for 1 hour, followed by addition of 5 µg/ml tunicamycin (Sigma) for an additional 5 hours to induce ER-stress. After respective times, the cells were trypsinized and collected by centrifugation. After washing the cells with PBS (Invitrogen), the lysates were prepared in cold RIPA buffer containing protease inhibitors (Roche Diagnostics, Indianapolis, IN). Then cell lysates were cleared and collected by centrifugation. The protein concentration was measured by Bradford analysis (Bio-Rad). Lysates containing 30 µg of total protein

were fractionated on a 10% SDS polyacrylamide gel and transferred to Hybond-P PVDF Membrane (GE Healthcare) using Bio-Rad's Mini-PROTEAN system. The membranes were blocked with 5% dry milk in Tris-buffered saline-Tween 20 (TBST) for 1 hour at room temperature. Blots were incubated with primary antibodies overnight at 4 °C using 1:1000 anti-total PERK (R&D System); 1:1000 anti-total eIF2 $\alpha$ ; 1:1000 anti-phospho eIF2 $\alpha$  (Ser 51); 1:500 anti-ATF4; 1:500 anti-CHOP (Cell Signaling Technology) and anti-actin (Millipore). Either anti-goat (Thermo Scientific) anti-rabbit (Bio-Rad) or anti-mouse (Cell Signaling Technology) horseradish peroxidase-conjugated secondary antibodies, ECL Plus™ and western blotting reagents (GE Healthcare) were employed to develop the blots.

#### **4.4 RESULTS AND DISCUSSION**

##### **Expression and purification of active human PERK and eIF2 $\alpha$**

Human PERK and eIF2 $\alpha$  were purified according to the protocol explained earlier in the Materials and Methods section. His-GST-tagged human PERK (541-1116 a.a) was expressed in a modified pET28a vector using *E. coli* strain Rosetta-gami™ 2(DE3). Purification was accomplished by three successive chromatography steps: 1) Ni-NTA affinity, 2) Cleavage and HiPrep desalting, and 3) Mono Q 10/10 anion exchange. We purified soluble, tag-cleaved human PERK, which has an ability to phosphorylate eIF2 $\alpha$  as well as a peptide substrate. The purity of PERK was verified by running the protein on 10% SDS-PAGE. The final cleaved PERK runs as an 85-kD protein on SDS-PAGE (figure 4.1C). His<sub>6</sub>-tagged human eIF2 $\alpha$  (4-314 a.a) was overexpressed in *E. coli* strain BL21



(DE3) and purified using Ni-NTA affinity chromatography, followed by a gel filtration column. The recombinant human eIF2 $\alpha$  runs as a 37-kD protein in SDS-PAGE (figure 4.1D).

### **Determination of kinetic parameters of PERK**

To analyze the ability of the purified kinase to phosphorylate its substrate, eIF2 $\alpha$ , dose response assays were performed with 20 nM PERK and several concentrations of eIF2 $\alpha$  (0-50  $\mu$ M) as described under '4.3 Materials and Methods'. Initial velocity data at different concentrations of eIF2 $\alpha$  and saturating ATP concentration were fitted using equation 4.1 and kinetic parameters for PERK phosphorylating eIF2 $\alpha$  determined (figure 4.2). The recombinant human PERK expressed in bacteria phosphorylates eIF2 $\alpha$ , with a half maximal activity achieved at  $8.1 \pm 3.2$   $\mu$ M and a catalytic constant of  $k_{\text{cat}}^{\text{app}} = 0.28 \pm 0.035$  s<sup>-1</sup>.

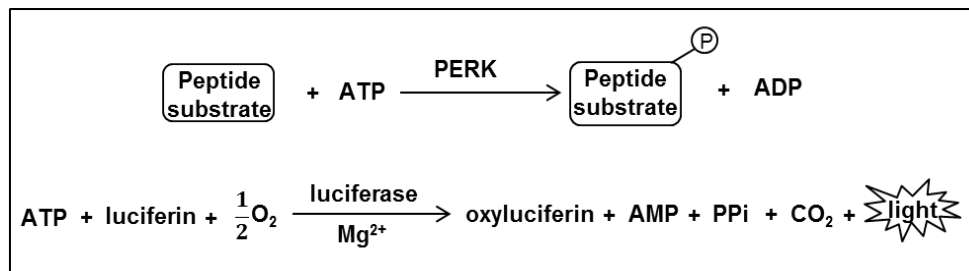
### **Optimization of luminescent kinase assay for screening**

To screen chemical libraries efficiently, a suitable detection technology must be chosen<sup>(146)</sup>. The Kinase-Glo Luminescent Kinase Assay, a nonradioactive, homogeneous, ATP quantitative kit useful for kinase activity detection, is available from Promega (Madison, WI). ATP is a universal substrate for kinases. Thus, we decided to use the Kinase-Glo assay in order to determine kinase activity in an HTS format. In order to optimize the kinase reaction for screening, a set of experiments were conducted to determine the optimal concentration of ATP, substrate, and kinase necessary for the

reaction. We optimized HTS assay conditions using both 96 well plates and 384 well plates (figure 4.3).

The reaction has been optimized to be done in a 10  $\mu$ l volume in 384 well plate at room temperature in assay buffer (25 mM HEPES pH7.5, 50 mM KCl, 0.1 mM EDTA, 0.1 mM EGTA, 2 mM DTT, 10 mM MgCl<sub>2</sub>, 20  $\mu$ g/ml BSA) containing 20 nM PERK, 200  $\mu$ M peptide substrate (5-FAM-*RSRRGSLNKSR*) and each tested compound in 0.25% DMSO and 0.01% Triton. The reaction mixtures were incubated at room temperature for 30 minutes before initiation with 1  $\mu$ M ATP. As controls, either all components except PERK or ATP alone were used. Luminescent kinase assay measures kinase activity by quantitating the amount of ATP remaining in solution following a kinase reaction. After 2 hours, 10  $\mu$ l of Kinase-Glo assay mix was added. The kinase reaction was quenched and luminescence was measured on an Envision plate reader. ATP remaining at the time that the reagent is added is used as a substrate by the luciferase to catalyze the mono-oxygenation of luciferin (Scheme 4.2). The luminescent signal correlates directly to the amount of ATP present and inversely correlates with the amount of kinase activity. High throughput screening assays usually contain small amounts of additives such as DMSO or detergents. Since many small molecule compounds are not soluble in aqueous buffer, addition of small amount of DMSO can enhance the solubility of the compounds. In addition, detergents such as Brij-35 or Triton are also widely used since they can enhance the stability of the enzyme. These additives can bind to the enzyme and interfere the enzyme activity. Therefore DMSO tolerance test was performed by varying DMSO

concentration (0 to 10%) to see if this factor had any effect on the enzymatic activity. As shown in figure 4.4, the presence of DMSO did not affect the enzyme activity.



**Scheme 4.2. Principle of the Kinase-Glo luminescent kinase assay.**

### **High throughput screening of small molecule libraries**

HTS was performed in 384 well plates using the optimized assay conditions, as described earlier. A total of ~30,000 small compounds from both focused and diverse libraries were screened for potential hits. All the libraries were screened at 25  $\mu\text{M}$  final concentration except the Chembridge fragment set which was screened at 500  $\mu\text{M}$ . Compounds showing greater than 50% activity in the assay were considered as hits. Out of 32,096 compounds screened, ~104 compounds showed greater than 50% activity. HTS is often populated with false-hits, which can result from the variability in the assay itself. The suitability of the HTS assay is often determined by a statistical measurement called the  $Z'$  factor which takes into account the mean and standard deviation values for the positive and negative reference controls <sup>(147)</sup>. A  $Z'$  value between 0.5 and 1 is generally considered as an indicator of a quality assay. The calculated  $Z'$  values for our screening

were greater than 0.5 for all plates which suggests that there is a large separation of data points between the baseline and the positive signal.

Both focused and diverse libraries of small compounds were screened for potential hits. The focused library was selected utilizing a ligand-based pharmacophore selection method that ranked compounds based on pharmacophores that promote interaction with the ATP binding site of protein kinases (Chembridge Corporation). A Target focused Kinase set ~600 known kinase inhibitors was also screened. As expected, several hits were obtained from the kinase focused libraries (Chembridge Kinase set and Target focused Kinase set) (figures 4.7 and 4.8). A Fragment library was also screened at 500  $\mu\text{M}$  to yield several hits (figures 4.5). The Fragment library contains simpler and less functionalized compounds (MW <300 Da). As a consequence, hits from the fragment library do not tend to bind tightly ( $K_d$  values in the micro- to milli-molar range). This suggests that kinase-focused libraries may be suitable for targeting PERK. The main task we faced following the screen was to verify the hits. Some compounds may interfere with luminescence leading to false-positive hits, thus, a different type of kinase assay such as a  $^{32}\text{P}$  assay was used for confirmation.

### **Hit confirmation screen by radiometric assay**

Based on the inhibitory activities of the compounds, we prioritized *hits* in the original screens to validate them. Confirmation screen was performed by radioactive assay using the protein substrate, eIF2 $\alpha$ . All enzyme-inhibitor mixtures were incubated for 30 minutes before starting the reaction with [ $\gamma$ - $^{32}\text{P}$ ] ATP. Since some compounds were found

to be insoluble, the final DMSO concentration was increased to 5% to enhance better solubility. Hits were re-screened at concentrations of 0.5 and 25  $\mu\text{M}$  except the fragments, which were tested at 500  $\mu\text{M}$ . Compounds that showed more than 50 % inhibition at 25  $\mu\text{M}$  in the counter screen, were further assessed in dose-response assays in the presence of 0.01% triton X-100. It is known that many compounds form aggregates in aqueous solutions and inhibit the enzyme by non-specifically binding to them <sup>(148-150)</sup>. The presence of small amounts of non-ionic detergent such as triton X-100 can often attenuate the inhibition if the compound is acting by aggregation <sup>(148-150)</sup>. Therefore, the purpose of triton X-100 is to get rid of the promiscuous inhibitors.

Among several hits exhibiting more than 50% inhibition at a concentration of 25  $\mu\text{M}$ , four small molecules inhibited PERK with nanomolar  $\text{IC}_{50}$ . The four inhibitors were all found in the target focused kinase library. Their inhibition rates from both initial and validation screening were calculated as a percentage with respect to the control value (table 4.1 and 4.2). The dose-response curves are plotted and fitted using equation 4.2. As seen in figure 4.9, compound 3 is the most potent inhibitor of PERK with an  $\text{IC}_{50}$  of 19 nM while compounds 1, 2, and 4 show  $\text{IC}_{50}$  values of 68, 300, and 45 nM respectively.

#### **Effect of compounds (1-4) on PERK autophosphorylation**

In addition, we examined whether these compounds are capable of inhibiting PERK autophosphorylation by using a phosphate free form of PERK. As shown in figure 4.10A, phosphate free PERK was successfully prepared by treating with lambda phosphatase *in vitro* and purified through size-exclusion chromatography. To test the capability of the

produced phosphate free PERK to autophosphorylate *in vitro* after removal of the phosphates, 200 nM of phosphate free PERK was exposed to 1 mM <sup>32</sup>P-ATP in the presence of 10 mM MgCl<sub>2</sub> for 0 to 30 minutes and the phosphate addition was visualized by autoradiography. Phosphate free PERK was successfully autophosphorylated *in vitro* (figure 4.10B), confirming that this form of the enzyme is suitable to test the effects of the compound (1-4) on PERK autophosphorylation. Figure 4.11 displays the dose-responsive curves of compounds (1-4) against PERK autophosphorylation. As seen in table 4.3, compounds 1 and 2 inhibited PERK autophosphorylation with IC<sub>50</sub> values of 74 and 140 nM respectively. On the other hand, different mode of inhibition was observed in compound 3 and 4. In particular, compound 3 showed more than 60 fold difference between IC<sub>50</sub> values of PERK autophosphorylation (~1200 nM) and eIF2 $\alpha$  phosphorylation (~19 nM) suggesting that compound 3 appears to have a distinct mode of binding. Our data suggest that compound 3 may be a starting point for the development of potent and selective small molecules capable of inhibiting PERK.

### **Characterization of PERK inhibitors on cellular activity**

In order to confirm that our *in vitro* results using purified enzyme correlates with cellular studies, we examined the ability of compounds (1-4) to inhibit PERK activity in HEK293T cells. PERK activity was assessed in a gel-based assay in the presence of each inhibitor. The effect of each compound on the phosphorylation of eIF2 $\alpha$ , an *in vivo* substrate of PERK, as well as on the autophosphorylation of PERK was tested following stimulation of PERK by a chemical inducer of the UPR, and visualized by western blot

analysis. To validate the ability of the selected anti-p-eIF2 $\alpha$  (Ser51) antibody to detect the phosphorylated form of eIF2 $\alpha$ , we examined the effect of compounds (1-4) on the phosphorylation of recombinant eIF2 $\alpha$  by PERK in-vitro using this antibody in a western blot based assay. As shown in figure 4.12, levels of phosphorylated eIF2 $\alpha$  were significantly decreased when incubated with compounds (1-4) compared to the control.

PERK is up-regulated in cells upon treatment with pharmacological agents that disrupt the Ca<sup>2+</sup> balance (thapsigargin), protein folding (DTT), or N-linked glycosylation (tunicamycin) in the endoplasmic reticulum <sup>(125)</sup>. We used 1  $\mu$ M of thapsigargin <sup>(151, 152)</sup> as an ER stress inducer. As expected, compounds 1-4 showed inhibition of eIF2 $\alpha$  phosphorylation in the HEK293T cells, with compounds 3 and 4 exhibiting almost complete inhibition at a concentration of 5  $\mu$ M (figure 4.13).

A demonstration of an inhibition of PERK autophosphorylation with the 4 inhibitors in HEK293T cells was difficult due to the lack of a reliable phospho-specific antibody to human PERK. Thus, autophosphorylation of PERK was visualized by SDS-PAGE by mobility shift detection of the phosphorylated protein using a total anti-PERK antibody. Treatment of HEK293T cells with 1  $\mu$ M thapsigargin for 2 hours leads to activation and autophosphorylation of PERK. Figure 4.S1 displays an example of the inhibition of PERK upon treatment with compound 3. The level of PERK phosphorylation started to decrease at the concentration of  $\sim$  10  $\mu$ M. Surprisingly, at the higher concentration, expression level of PERK itself was significantly suppressed (figure 4.S1, supplementary materials). Previous studies suggest that many kinases are activated upon cleavage by caspases <sup>(153)</sup>. In fact another eIF2 $\alpha$  kinase, PKR (protein kinase double-

stranded RNA-dependent) is cleaved by mammalian caspase and the cleaved PKR is active in phosphorylating its substrate <sup>(154)</sup>. Likewise, high concentration of PERK inhibitors may trigger more stress in cells and escalated ER stress might cause cleavage or degradation of PERK. Future studies to understand the possible underlying mechanism of this result will be necessary.

### **Investigating the effect of compound 3 (TG101348) in pancreatic cancer cells**

#### *Effect of compound 3 (TG101348) on cell proliferation and colony formation*

It has been reported by Bobrovnikova-Marjon et al. that knockdown of PERK by shRNA in human breast and esophageal carcinoma cells triggers a cell cycle delay, resulting in a significant decrease (50% reduction) in cell proliferation <sup>(155)</sup>. Moreover, PERK-deficient MEF cells generated tumors with a significantly reduced volume (16 fold) relative to PERK-positive MEF cells <sup>(80)</sup> suggesting that PERK promotes cancer cell proliferation and tumor growth.

Therefore, the effectiveness of compound 3 in inhibiting the growth of human pancreatic carcinoma cell lines was investigated. MiaPaCa-2 cells were treated with different doses of compound 3 to determine whether or not this compound might have anti-proliferative effects on pancreatic cancer cells during the log phase of growth. MiaPaCa-2 cells were cultured with increasing concentrations of the compound followed by incubation with the ER stress inducer, tunicamycin for 72 hours. Tunicamycin perturbs ER homeostasis by affecting N-linked glycosylation of proteins. Then cell proliferation was assessed by an MTS assay (Promega). This assay relies on the ability of viable cells



to convert a soluble tetrazolium salt [3-(4, 5-dimethylthiazol-2-yl)-5-(3-carboxymethoxyphenyl)-2-(4-sulfophenyl)-2*H*-tetrazolium, MTS] to a formazan product, which then can be quantitated using a spectrophotometer. Control cells were treated with equivalent concentrations of DMSO in the absence of inhibitors. As shown in figure 4.14, incubation with compound 3 in the presence of tunicamycin for 72 hours significantly inhibited the proliferation of MiaPaCa-2 cells. Treatment of compound 3 resulted in a dose-dependent inhibition of cell proliferation with a 50% inhibitory concentration ( $IC_{50}$ ) value of  $\sim 0.8 \mu\text{M}$  in the presence of tunicamycin ( $0.15 \mu\text{g/ml}$ ). In the absence of tunicamycin, the  $IC_{50}$  value was  $\sim 15 \mu\text{M}$ . Compounds (1,2 and 4) were also effectively anti-proliferative in ER stressed MiaPaCa-2 cells, but higher concentration of these compounds were required to reach 50% inhibition in the absence of ER stress (data not shown). There was no significant cytotoxic effect when MiaPaCa-2 cells were solely treated with tunicamycin ( $0.15 \mu\text{g/ml}$ ) without compounds. The cytotoxic effects of compounds on long-term survival were further confirmed with a clonogenic assay. This assay is also referred to as an anchorage-dependent colony formation assay. It measures the ability of a single cell to grow into a colony (usually defined as  $>50$  cells) and its ability to undergo unlimited division. Cancer cells are characterized by unrestricted growth due to loss of contact inhibition while normal, untransformed cell growth is arrested when they come into contact with each other. Thus, this clonogenic assay is an indirect measure of the tendency of MiaPaCa-2 cells to undergo neoplastic transformation. MiaPaCa-2 cells were treated with varying concentrations (5, 10, 25, 50  $\mu\text{M}$ ) of compound 3 under tunicamycin-induced stress for 6 hours. Next, the medium was aspirated and washed, and

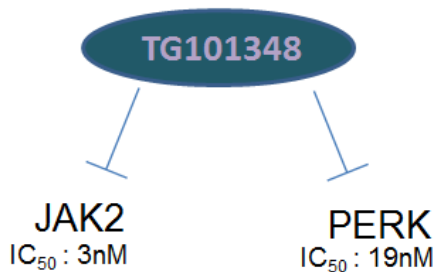
cells were trypsinized. Then, cells were counted, re-plated onto 60 mm dishes at initial cell concentrations of 500 cells/well and allowed to grow for an additional 15 days with inhibitor-free medium. As seen in figure 4.15, during the 15-day culture period, exposure of cells to compound 3 reduced the colony-forming ability relative to cells exposed to tunicamycin alone. Clonogenicity of MiaPaCa-2 cells treated with compound 3 showed 50% inhibition that was clearly evident at 10  $\mu$ M. In addition, treatment with both compound 1 and 2 led to nearly 100% cell death even at the lowest concentration, 5  $\mu$ M (data not shown).

#### ***Effect of compound 3 (TG101348) on PERK downstream signaling pathway***

To further elucidate the mechanism of PERK inhibitor-mediated ER stress response signaling in pancreatic cancer cell lines, we evaluated key UPR signaling molecules by Western blotting. We selected compound 3 for use in cellular studies based on its potency as an inhibitor of PERK activity in MiaPaCa-2 cells. As expected, pre-treatment of MiaPaCa-2 cells with compound 3 in the presence of the ER stress inducer, tunicamycin resulted in the inhibition of PERK activation, as well as PERK expression. In addition, treatment with compound 3 repressed PERK-mediated UPR signaling in a dose-dependent fashion.

It is generally known that tunicamycin activates the UPR through inhibition of N-linked glycosylation, which triggers ER stress due to the accumulation of misfolded proteins. As shown in figure 4.16, tunicamycin alone induced activation of PERK, which was visualized by a mobility shift detection of phosphorylated proteins on SDS-PAGE.

Furthermore, treatment with tunicamycin markedly increased the levels of ATF4 and CHOP. The treatment with compound 3 significantly suppressed the expression of PERK in the MiaPaCa-2 cells and this expression pattern was similar to that seen in figure 4.S1. This decrease in PERK expression by compound 3 may be due to the activation of caspase-driven proteolytic activity associated with cells undergoing apoptosis triggered by ER stress. The molecular mechanism underlying this observation needs to be investigated further. Western blot analysis of MiaPaCa-2 cells treated with compound 3 revealed decreases in downstream targets for PERK signaling, such as ATF4, and CHOP expression, compared to cells treated with tunicamycin alone (figure 4.16), suggesting a cause and effect relationship between compound 3 and down-regulation of UPR signaling. Interestingly, however compound 3 did not inhibit phospho-eIF2 $\alpha$ , even at the highest concentration used. This suggests that other eIF2 $\alpha$  kinases, such as GCN2, PKR and HRI may contribute to the regulation of eIF2 $\alpha$  in pancreatic cancer cells. Collectively, however our results suggest that compound 3 disrupts the regulation of the UPR in pancreatic cancer cells subject to ER stress by tunicamycin. TG101348 is also known to inhibit the non-receptor tyrosine kinase, JAK2<sup>(156-158)</sup>, which is associated with the promotion of growth and division of mammalian cells including blood cell and found in almost every cell type<sup>(158, 159)</sup>. It is essential for signaling through a variety of cytokine receptors, such as those that bind growth hormone, prolactin, erythropoietin, and thrombopoietin<sup>(158-162)</sup>. Therefore the effectiveness of TG101348 may be a result of targeting both JAK2 and PERK (scheme 4.3).



**Scheme 4.3. Dual inhibition of compound 3 (TG101348).**

***Biphasic effects of PERK specific inhibitor (GSK2606414)***

Recently, a group from GlaxoSmithKline developed and discovered a specific PERK inhibitor, GSK 260414, which exhibited antitumor activity against human pancreatic xenograft tumors <sup>(125)</sup>. According to the authors, this PERK inhibitor has an IC<sub>50</sub> of ~0.4 nM *in vitro* and an IC<sub>50</sub> of ~30 nM for inhibition of PERK autophosphorylation in a cellular assay. Moreover this compound is orally available and highly selective for PERK with a selectivity of >385-fold for PERK over a panel of 294 kinases including three other eIF2 $\alpha$  kinases. We synthesized this highly specific PERK inhibitor (GSK2606414) to compare with our inhibitors and to use in control experiments. In the beginning, we synthesized GSK260414 according to Axten et al. and confirmed its structure by <sup>1</sup>H NMR, <sup>13</sup>C NMR and mass spectrometry <sup>(124)</sup>. The ability of GSK2606414 to inhibit PERK was confirmed in an *in vitro* dose response assay. Next we examined its cytotoxicity in human pancreatic cancer cells (MiaPaCa-2) by using an MTS assay to compare with results we obtained from our hits (compound 1-4). MiaPaCa-2 cells were treated with various concentrations of GSK2606414 under stressed condition by tunicamycin and MTS assays

were performed using the same protocol described above. It showed remarkably anti-proliferative activity in ER-stressed MiaPaCa-2 cells at concentrations ranging from 0.05 to 1  $\mu\text{M}$ . The maximum inhibitory effect was observed at 0.5-1  $\mu\text{M}$ . The majority of MiaPaCa-2 cells treated at 500 nM exhibited  $\leq 15\%$  viability compared with their respective controls. Surprisingly, this anti-proliferative effect was reversed when cells were incubated at concentrations greater than 1  $\mu\text{M}$  as shown in figure 4.17 (indicated by red curve).

We found that GSK2606414 possessed an inhibitory effect when added at 0.05–1  $\mu\text{M}$  concentration, but it became growth stimulatory when its concentration was further increased to 25  $\mu\text{M}$ , implying that PERK inhibition by GSK2606414 might trigger a compensatory effect that in turn, leads to a paradoxical and biphasic proliferative response. Furthermore, in the absence of ER stressor, tunicamycin, there were no significant effects of GSK2606414 on cell growth as seen in the blue color in figure 4.17. The rebound effect was also observed in a colony formation assay (figure 4.18). This biphasic response was unexpected since Axten et al. reported an anti-proliferative activity of the PERK inhibitor in a 3-day proliferation assay against multiple human tumor cell lines, including pancreatic cancer cells, as well as primary human microvascular endothelial cells. The authors also did not report significant effects on the growth of any of these cells in the absence of exogenous ER stress inducers, suggesting that the UPR is not induced under normal cell culture conditions.

We wondered whether PERK signaling was also biphasic. Therefore, we assessed the influence of varying doses of GSK2606414 on PERK-dependent signaling in the

MiaPaCa-2 cells by western blotting analysis. As shown in figure 4.19, CHOP showed a biphasic pattern of expression in response to GSK2606414. Indeed, lower concentrations (1, 3  $\mu$ M) of GSK2606414 decreased CHOP protein expression levels compared to the control, whereas higher doses counteracted this effect. We observed a similar result on p-eIF2 $\alpha$  expression; at a GSK2606414 concentration of 3  $\mu$ M expression of p-eIF2 $\alpha$  was minimal. The biphasic pattern of proliferation in tunicamycin-stressed cells correlates with CHOP expression. Generally CHOP is thought to be a pro-apoptotic transcription factor induced by ER stress<sup>(50)</sup>. Hence CHOP expression is generally considered as an ER stress induced cell death marker<sup>(71, 94)</sup>. Our observation raises the possibility that CHOP may promote MiaPaCa-2 cell proliferation in the presence of stress, despite its apoptotic function. As a transcription factor, CHOP itself seems unlikely to be intrinsically apoptotic; it more likely regulates the expression of downstream genes that facilitate either cell death or cell survival depending on the extent of ER stress and cell fate. The compensatory feedback signaling may be triggered through other UPR molecules such as ATF6 and IRE 1, which rescue pancreatic cancer cells from cell death.

Axten et.al reported that the PERK inhibitor inhibited PERK activity in a dose dependent manner with an IC<sub>50</sub> in the range of 10-30 nM as shown by the inhibition of stress-induced PERK autophosphorylation, as well as decreases in the downstream substrates, eIF2 $\alpha$  phosphorylation, ATF4, and CHOP in multiple pancreatic cancer cell lines. It should be noted that the authors tested the GSK compound up to 3  $\mu$ M, and did not report concentrations higher than 3  $\mu$ M. In addition, more recently, Cojocari et.al also synthesized this PERK inhibitor, GSK2606414, and tested it in their cellular experiments

<sup>(163)</sup>. The authors observed its ability to inhibit PERK autophosphorylation and downstream eIF2 $\alpha$  phosphorylation following exposure to hypoxia (0.2% O<sub>2</sub>) or thapsigargin (300 nM) in the colon cancer cells (HCT116) and pancreatic ductal carcinoma cells (KP4). The GSK2606414 strongly decreased hypoxia- or thapsigargin-induced expression of CHOP in HCT116 cells. However, the compound was ineffective at inhibiting CHOP expression in KP4 cells, but surprisingly sensitized them to thapsigargin-induced ER stress in a concentration dependent manner. Under normal growth conditions however, GSK2606414 did not affect the proliferation of KP4 cells <sup>(163)</sup>.

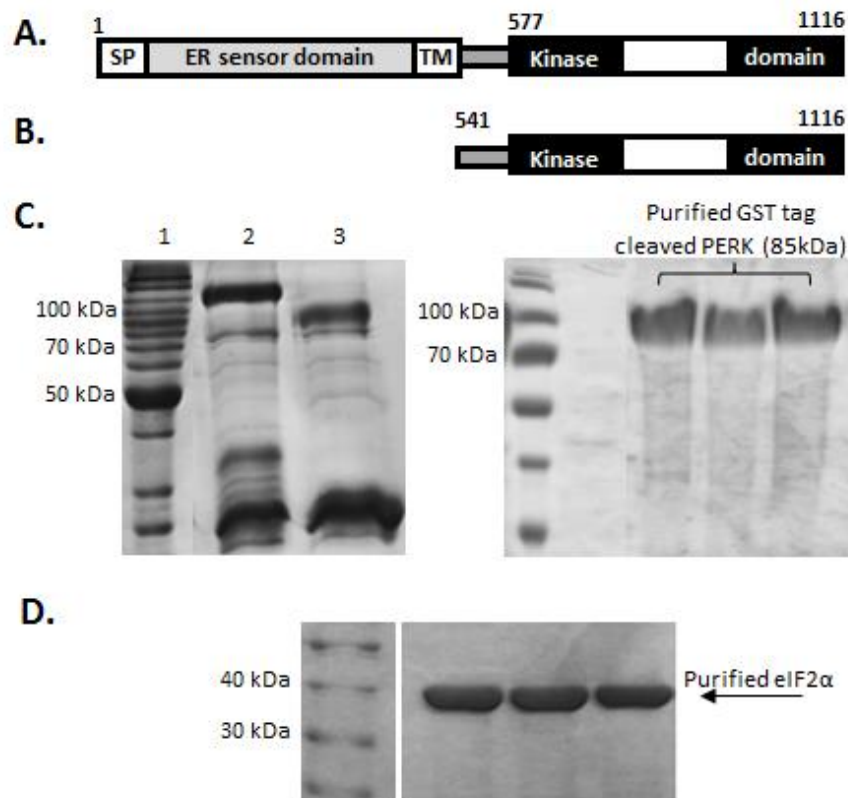
Based on results from ourselves and others pancreatic cells tend to be insensitive to PERK inhibition under normal cell culture conditions. No other group has reported a paradoxical biphasic effects of GSK2606414 in the literature. Therefore, the possible underlying molecular mechanism of this biphasic phenomenon needs to be further investigated.

#### **4.5 CONCLUSION**

Both focused and diverse libraries consisting of almost 30,000 small compounds were screened against PERK through luminescent kinase assay. Approximately, 60 hits were identified from the initial high throughput screening and further validated using a radioactive based kinase assay. A total of four small molecules were selected as potential inhibitors of PERK with nanomolar IC<sub>50</sub>'s. Compound 3, TG101348 showed the most marked inhibitory potency *in vitro* and is a known inhibitor of the kinase JAK2. Its biological effect was further examined in a pancreatic cancer cell line. TG101348 induced

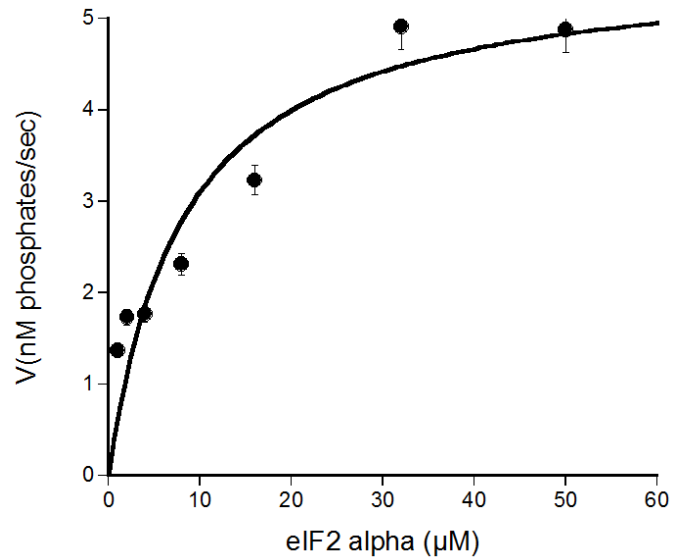
the dose-dependent degradation of PERK as well as the down-regulation of UPR signaling (e.g. the induction of ATF4 and CHOP). Furthermore, TG101348 suppressed pancreatic cancer cell proliferation. Pancreatic cancer cells subject to tunicamycin-induced ER stress exhibit a biphasic response to the PERK specific inhibitor GSK2606414. The basis for this observation is unknown, but suggests the potential for synthetic-lethal targeting of cancer cells utilizing PERK as an adaptive stress response. Further studies to understand the possible underlying molecular mechanism will be required. The inhibitors described here represent starting points for the development of potent and selective small molecules capable of compromising UPR signaling by inhibiting PERK.





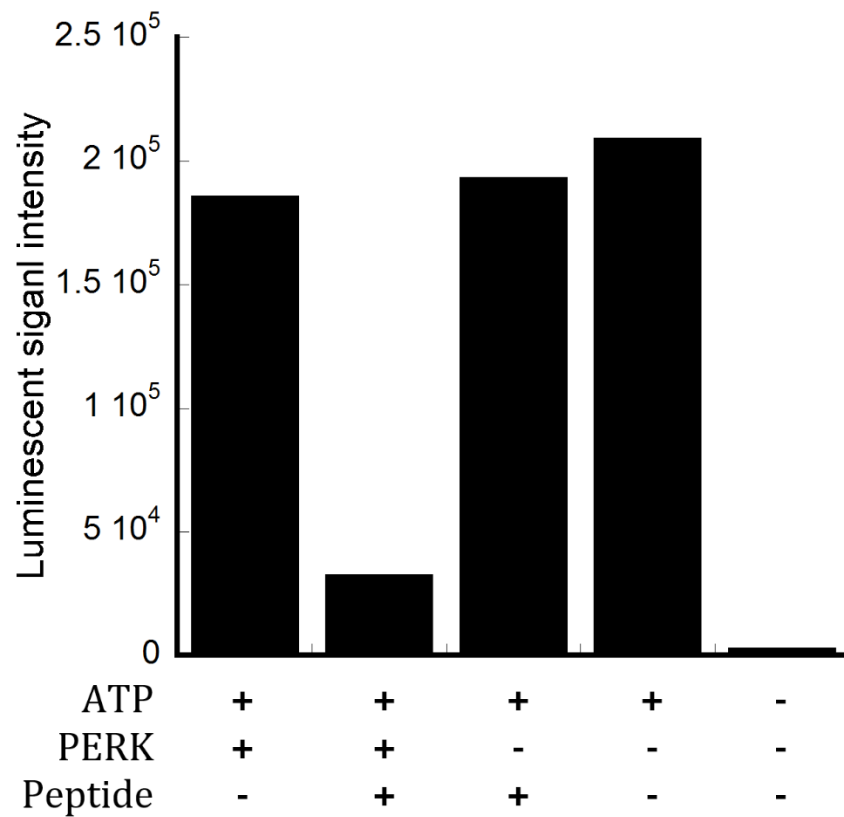
**Figure 4.1. Purification of human PERK catalytic domain and eIF2 $\alpha$  that were expressed in *E. coli*.**

**A**, Schematic representation of the full length of PERK. **B**, Schematic representation of the expressed form of the catalytic domain of PERK. This PERK catalytic domain was expressed in *E. coli*. **C**, *Left gel*, samples from Ni-NTA affinity chromatography were resolved by 10% SDS-PAGE: Lane 1, BenchMark™ protein ladder (Invitrogen); Lane 2, Protein eluted from Ni-NTA agarose affinity chromatography; Lane 3, Elution fraction from the Ni-NTA column was incubated with PreScission protease, resulting in GST-tag cleaved PERK. *Right gel*, Purified tagless PERK catalytic domain runs as an 85 kDa protein on 10% SDS-PAGE. **D**, Human eIF2 $\alpha$  (4-314 a.a) overexpressed in the bacterial cells (BL21) was subjected to Ni-NTA agarose affinity chromatography followed by Superdex 200 gel filtration chromatography. Purified eIF2 $\alpha$  runs as a 37 kDa protein on 10% SDS-PAGE.



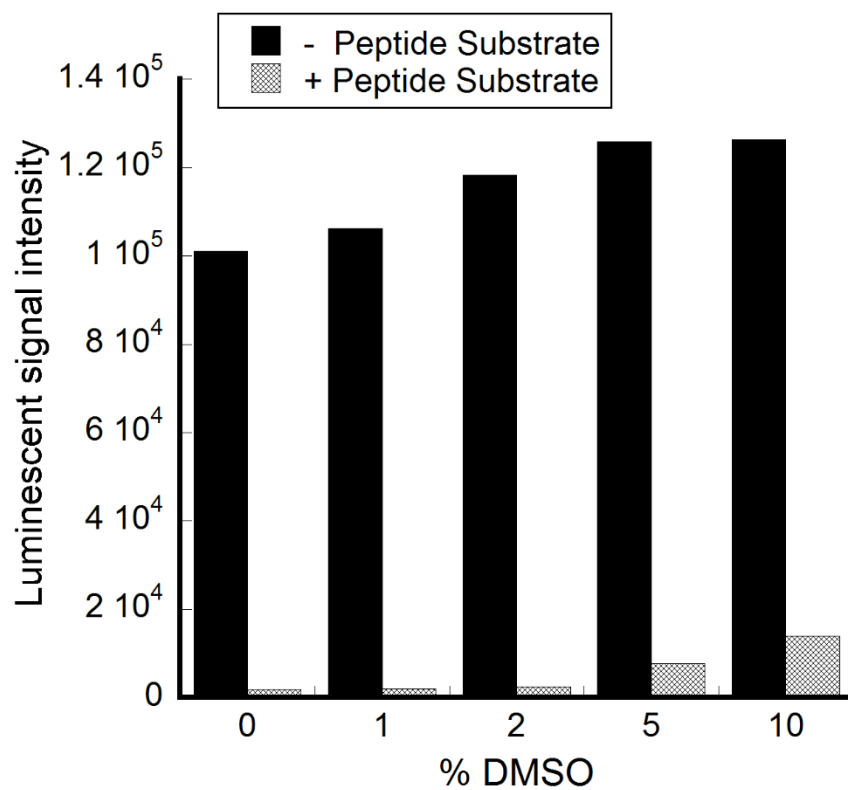
**Figure 4.2. Analysis of the kinase activity of PERK.**

Human eIF2 $\alpha$  dependence assays were performed using 20 nM PERK and 0-50  $\mu$ M eIF2 $\alpha$  in a suitable buffer as described under '4.3. Materials and Methods'. The data were fitted to Michaelis Menten equation 4.1, where  $K_M^{\text{app}} = 8.1 \pm 3.2 \mu\text{M}$  and  $V_{\text{max}}^{\text{app}} = 5.6 \pm 0.7 \text{ nM}\cdot\text{s}^{-1}$ . Kinase activity was determined by measuring the rate of phosphorylation of eIF2 $\alpha$  ( $\text{nM}\cdot\text{s}^{-1}$ ).



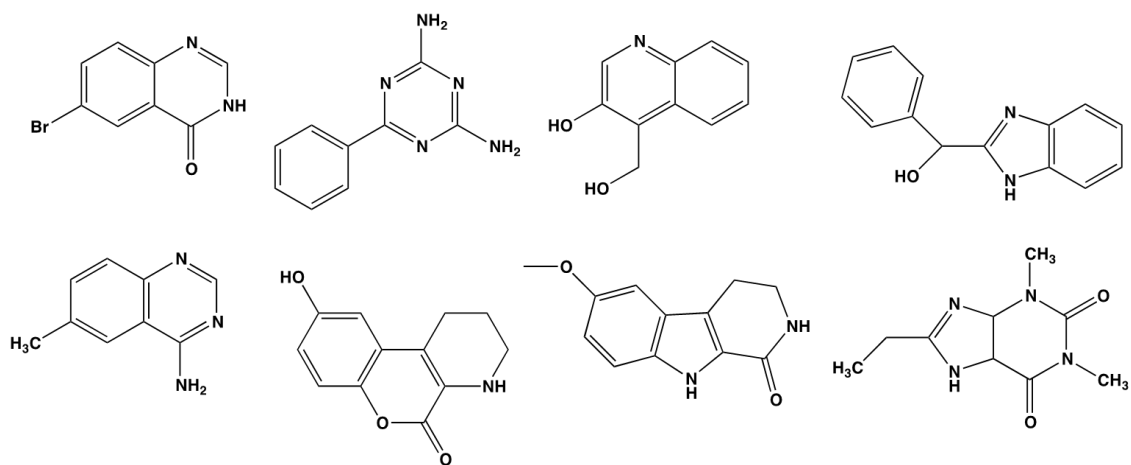
**Figure 4.3. Optimization of luminescent kinase assay.**

HTS assay conditions were optimized in 384 well plates. Assays were conducted in a 10  $\mu$ l reaction volume at room temperature in the assay buffer as described under ‘4.3 Materials and Methods’. Assay mixtures were prepared with or without enzyme in the presence or absence of 200  $\mu$ M of peptide and 1  $\mu$ M ATP. Positive control = assay buffer only. Negative controls =no enzyme or no peptide or ATP only.

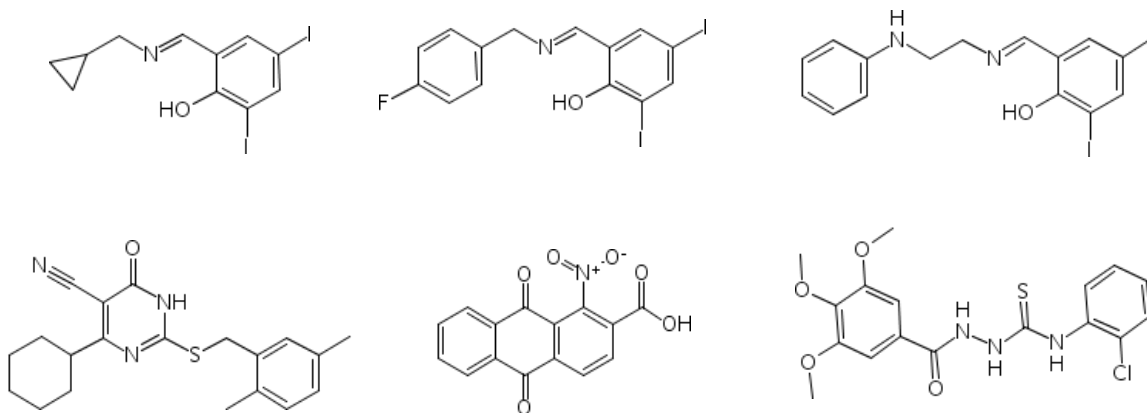


**Figure 4.4. Assay stability in the presence of different concentrations of DMSO.**

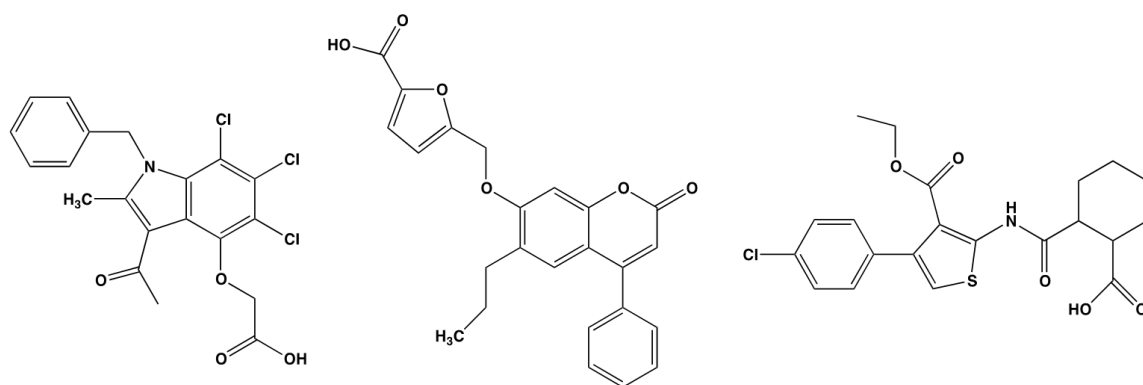
Assay mixtures were prepared with or without 200  $\mu$ M of peptide in the presence of 20 nM PERK, 1  $\mu$ M ATP and above indicated concentrations of DMSO (0-10%).



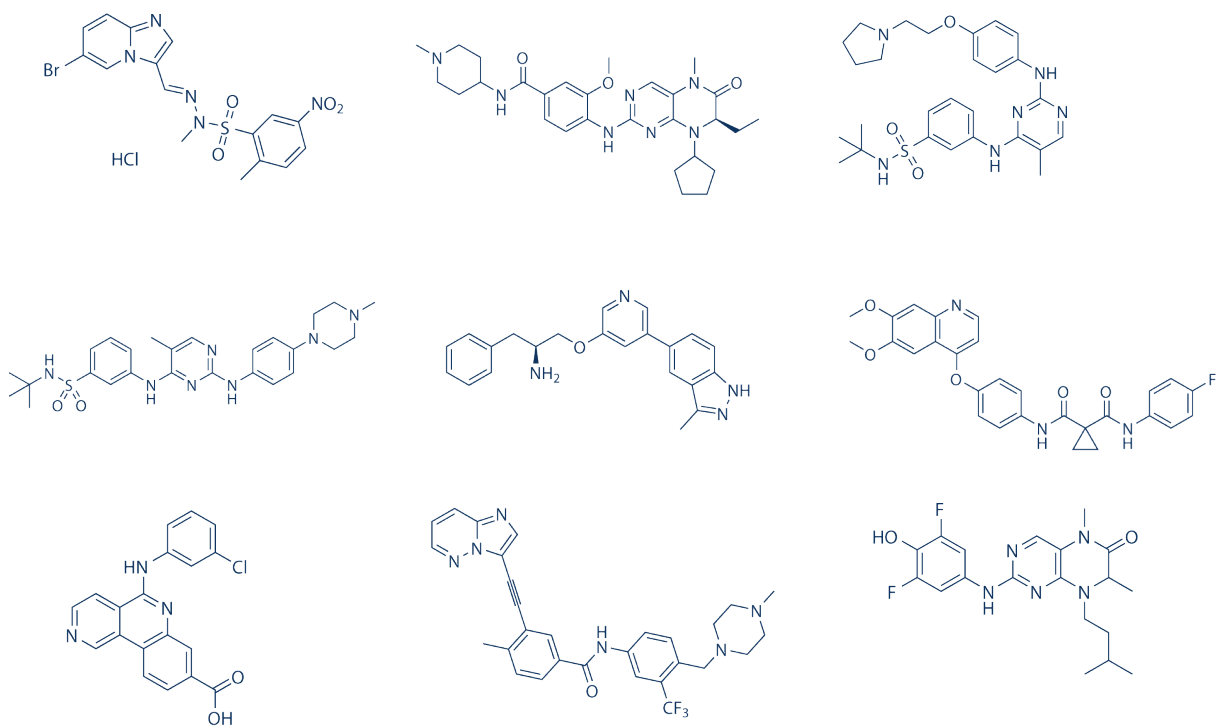
**Figure 4.5. Examples of hits from Fragment library (Chembridge).**



**Figure 4.6. Examples of hits from Maybridge library.**

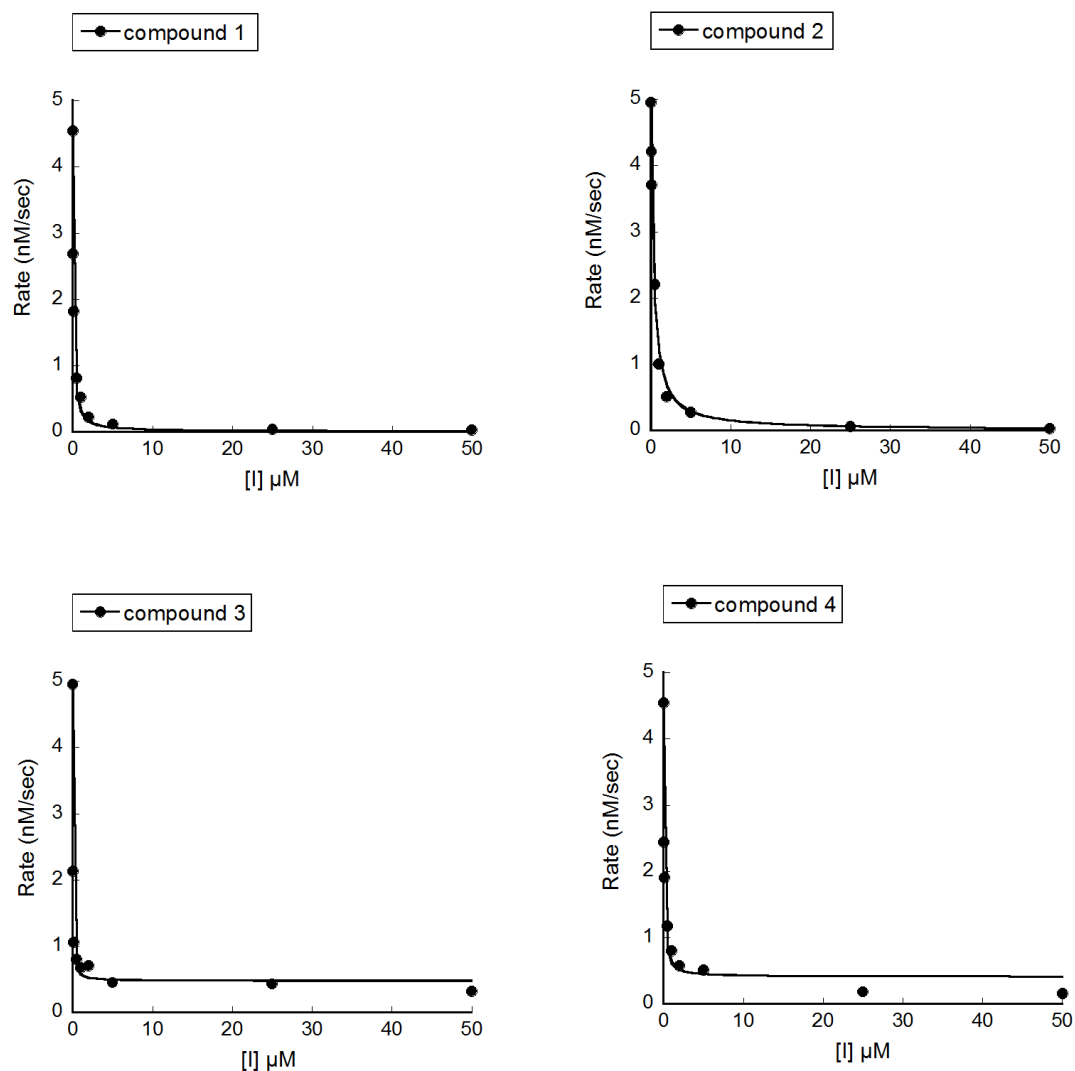


**Figure 4.7. Examples of hits from kinase-biased library (Chembridge).**



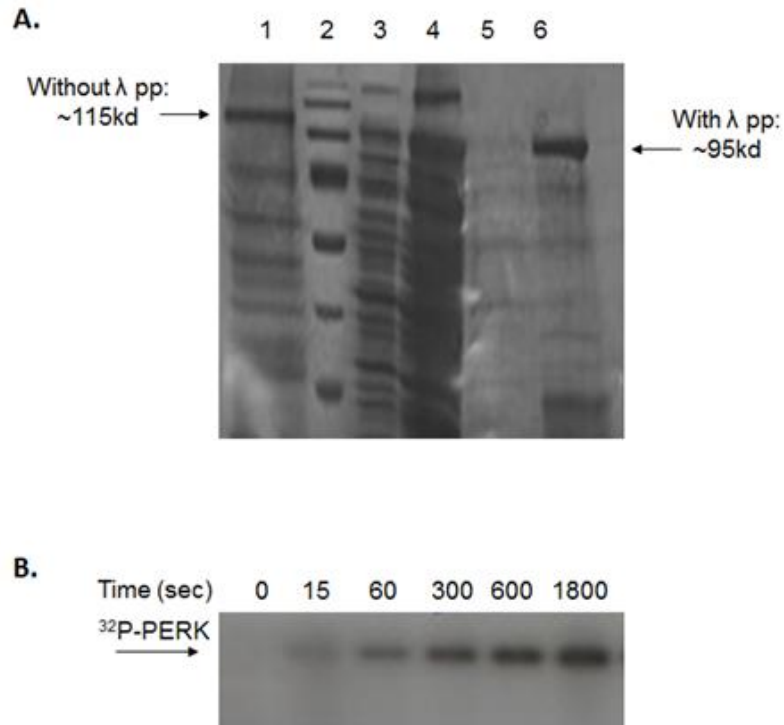
**Figure 4.8. Examples of hits from Target focused kinase set.**





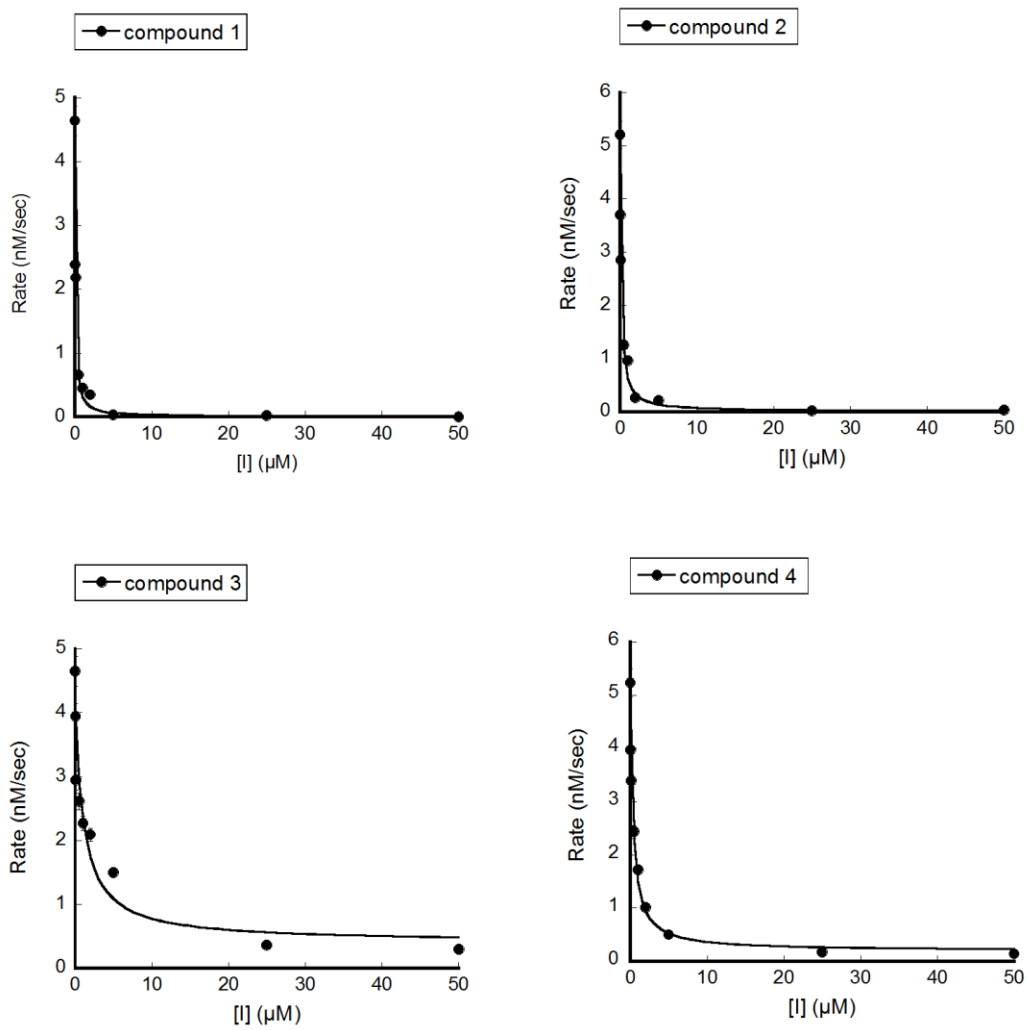
**Figure 4.9. The effect of compounds 1-4 on the ability of PERK kinase domain to phosphorylate eIF2 $\alpha$  substrate.**

20 nM active PERK kinase domain was assayed with 8  $\mu$ M of eIF2 $\alpha$  substrate. Activity was assessed at different inhibitor concentrations by the measurement of initial rates at 30  $^{\circ}$ C in 25 mM HEPES pH 7.5, 0.1 mM EDTA, 0.1 mM EGTA, 2 mM DTT, 0.05 M KCl, 10 mM MgCl<sub>2</sub> and 0.2 mM [ $\gamma$ -<sup>32</sup>P] ATP. The reaction was started by the addition of radio labeled ATP. These 4 compounds are potent inhibitors towards PERK (IC<sub>50</sub> for compounds 1-4 inhibiting eIF2 $\alpha$  phosphorylation were 68, 300, 19 and 45 nM respectively). The lines are the best fits of each data set to equation 4.2.



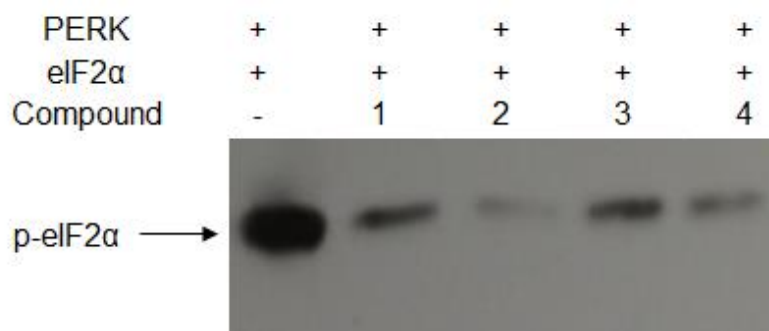
**Figure 4.10. Preparation of phosphate-free PERK kinase domain by treatment with lambda phosphatase.**

**A,** Human PERK kinase domain (541-1116 a.a) overexpressed in the bacterial cells (BL21) was subjected to Ni-NTA agarose affinity chromatography and treated with lambda phosphatase *in vitro* at room temperature. Lane 1, PERK without lambda phosphatase treatment; Lane 2, BenchMark™ protein ladder (Invitrogen); Lane 3, Flow-through 1; Lane 4, Flow-through 2; Lane 5, Wash; Lane 6, Eluted PERK with lambda phosphatase treatment. **B,** Autophosphorylation of phosphate-free PERK



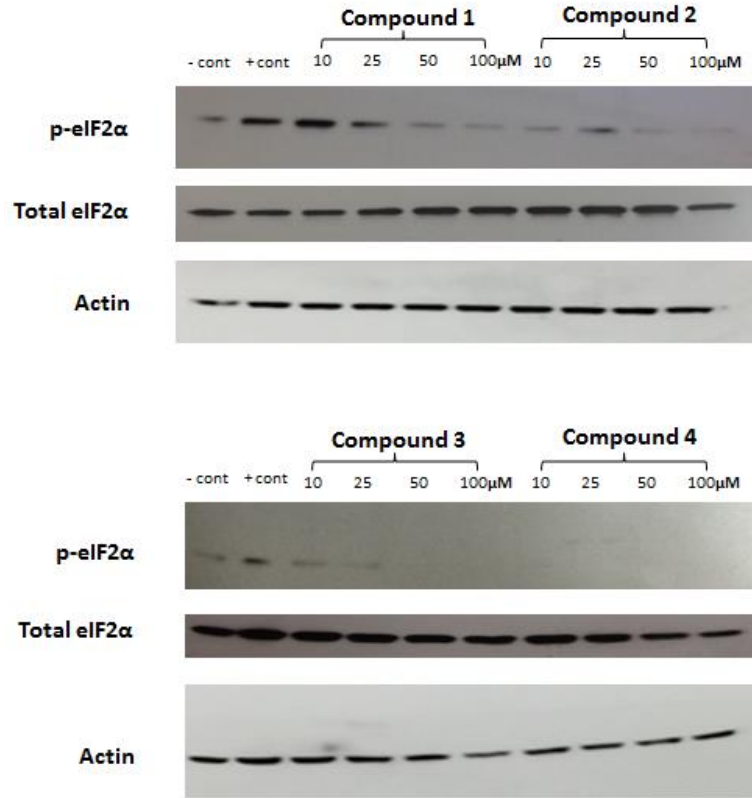
**Figure 4.11. The effect of compounds 1-4 on the ability of PERK kinase domain to autophosphorylate.**

Initial velocities of PERK autophosphorylation was measured using 50 nM phosphate free, inactive PERK at 30 °C in 25 mM HEPES pH 7.5, 0.1 mM EDTA, 0.1 mM EGTA, 2 mM DTT, 0.05 M KCl, 10 mM MgCl<sub>2</sub> and 10 μM [ $\gamma$ -<sup>32</sup>P] ATP. IC<sub>50</sub> for compounds 1-4 inhibiting PERK autophosphorylation were 74, 142, 1186 and 398 nM respectively. The lines are the best fits of each data set to equation 4.2.



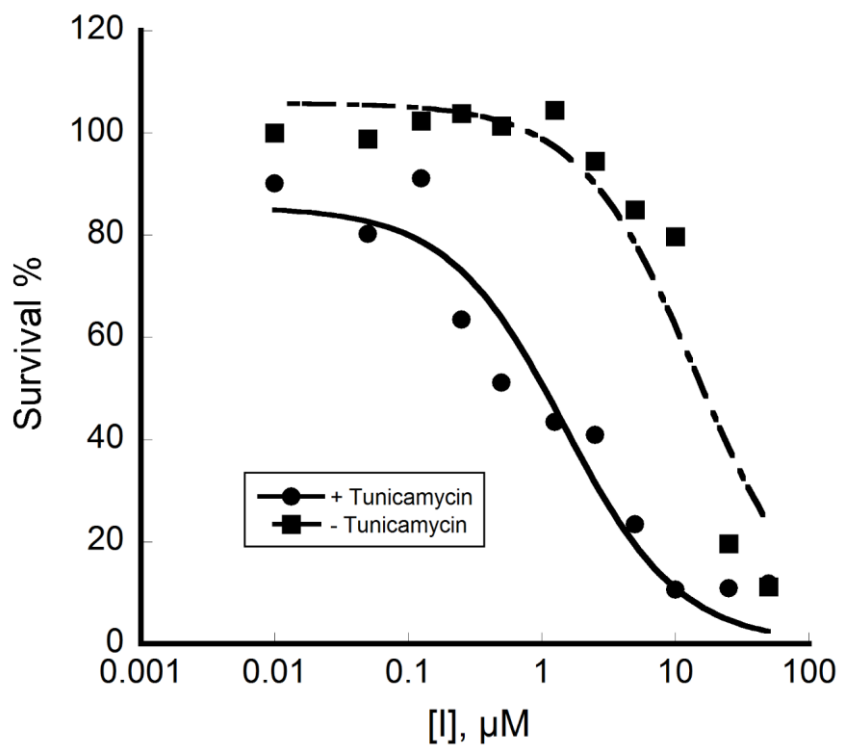
**Figure 4.12. Test the compounds (1-4) on the phosphorylation of eIF2 $\alpha$  *in vitro*.**

PERK kinase domain (20 nM) was incubated with eIF2 $\alpha$  (8  $\mu$ M) and ATP (1 mM) in the assay buffer containing 25 mM HEPES pH 7.5, 50 mM KCl, 0.1 mM EDTA, 0.1 mM EGTA, 2 mM DTT, 10 mM MgCl<sub>2</sub>, 40  $\mu$ g/ml BSA for 10 minutes in the presence of 10  $\mu$ M of compounds (1-4). Phosphorylated eIF2 $\alpha$  was detected by western blot using anti-p-eIF2 $\alpha$  antibody.



**Figure 4.13. Cellular effect of compounds (1-4) on the phosphorylation of eIF2 $\alpha$  in HEK293T cells.**

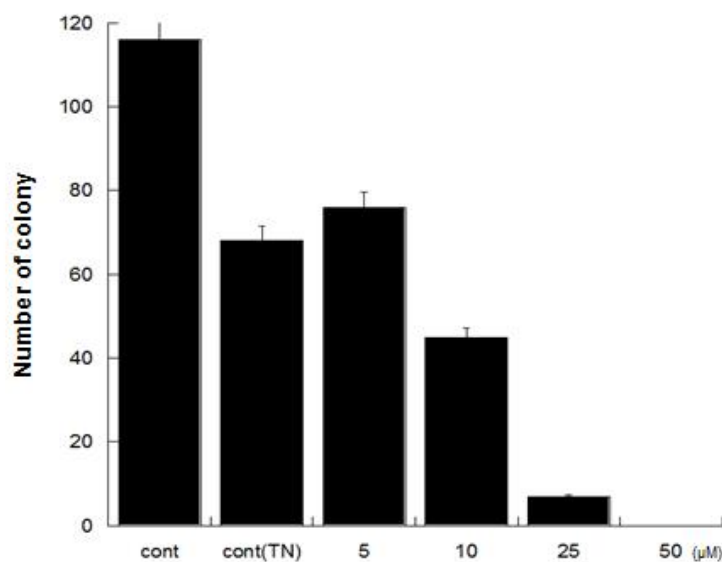
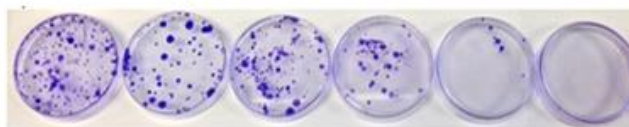
HEK293T cells were pre-treated with different concentrations of each compound (10-100  $\mu$ M) followed by UPR induction for 1 hour (1  $\mu$ M thapsigargin). Cell lysates were analyzed by western blot.



**Figure 4.14. Compound 3 induces apoptotic death of pancreatic cancer cells.**

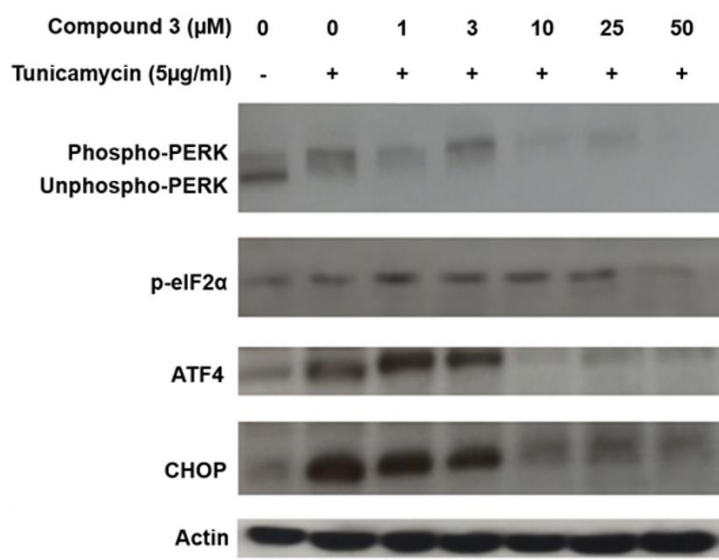
Compound 3 reduces the number of viable MiaPaCa-2 cells in culture. The cells were treated with an increasing concentrations of compound 3 in the presence or absence of tunicamycin (0.15 μg/mL) for 72 hours, and the fraction of viable cells were determined by MTS assay (Promega) according to the protocol described in ‘4.3 Materials and Methods’. The 50% inhibitory concentration (IC<sub>50</sub>) value was obtained using equation 4.2.

Compound 3 ( $\mu\text{M}$ )	0	0	5	10	25	50
Tunicamycin ( $5\mu\text{g/ml}$ )	-	+	+	+	+	+



**Figure 4.15. Compound 3 inhibits colony formation of MiaPaCa-2 cells.**

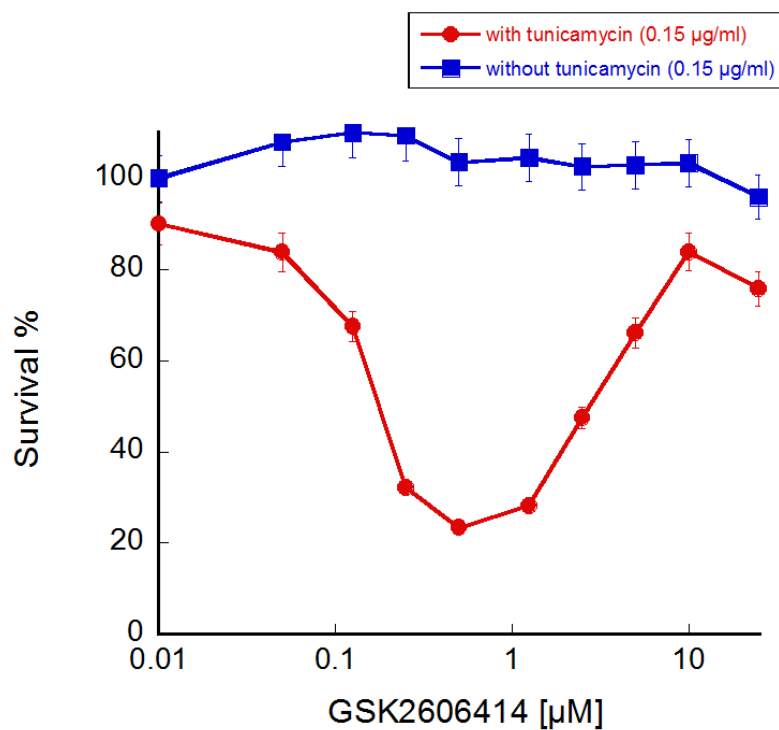
MiaPaCa-2 cells were treated with various concentrations of compound 3 in complete medium for 1 hour, followed by addition of  $5\mu\text{g/ml}$  tunicamycin for an additional 6 hours to induce ER stress. Treated cells were harvested using trypsinization, and re-plated (500 cells/ dish) and cultured at  $37\text{ }^\circ\text{C}$  with  $5\%$   $\text{CO}_2$  for 10 days. Images of the colonies formed after 10 days were taken after staining with  $0.2\%$  crystal violet. The colonies then were counted.



**Figure 4.16. Cellular effect of compound 3 on PERK signaling.**

MiaPaCa-2 cells were pre-treated with different concentrations of compound 3 (1-50  $\mu\text{M}$ ) followed by UPR induction for 5 hours (5  $\mu\text{g/ml}$  tunicamycin). Cell lysates were analyzed by western blot.

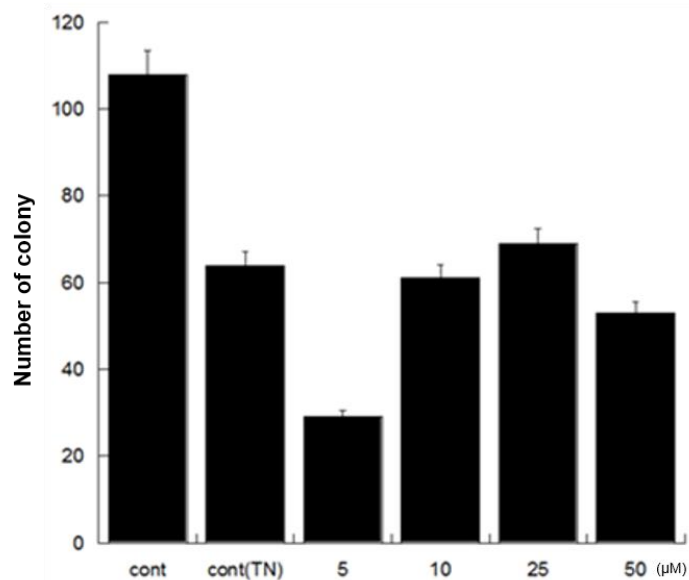
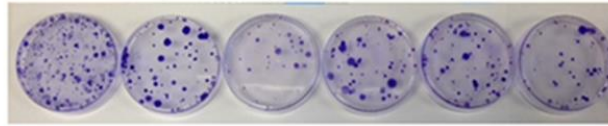




**Figure 4.17. PERK inhibition by GSK2606414 induces biphasic response in pancreatic cancer cell proliferation under ER stress.**

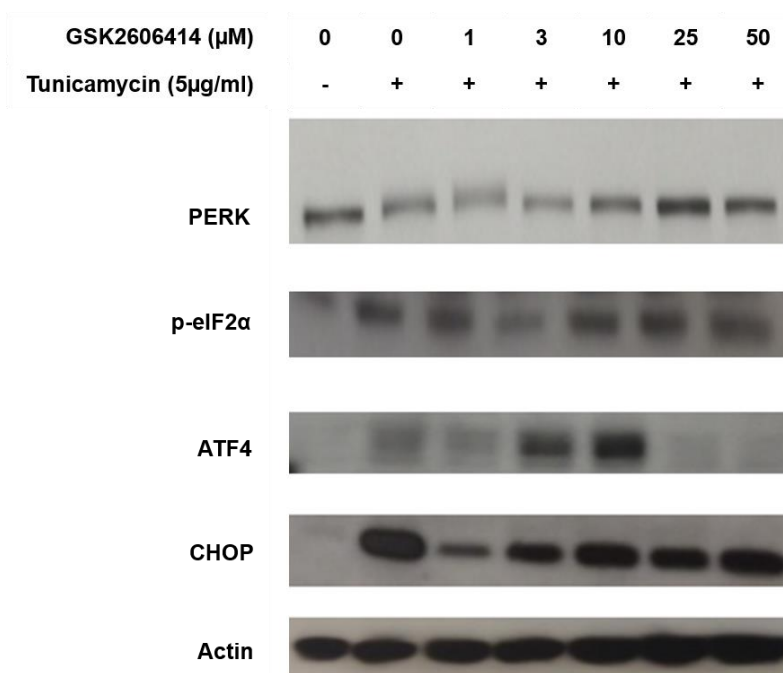
GSK2606414 triggers biphasic response in the number of viable MiaPaCa-2 cells in culture. The cells were treated with increasing concentrations of GSK2606414 in the presence (red) or absence of 0.15 µg/ml tunicamycin (blue) for 72 hours, and the fraction of viable cells were determined by MTS assay (Promega).

GSK2606414 ( $\mu\text{M}$ )	0	0	5	10	25	50
Tunicamycin ( $5\mu\text{g/ml}$ )	-	+	+	+	+	+



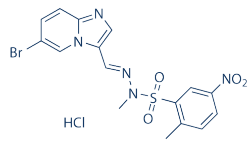
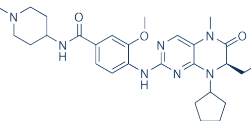
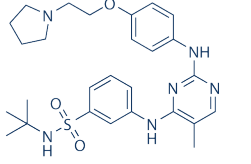
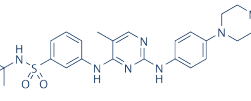
**Figure 4.18. GSK2606414 induces biphasic response in colony formation of MiaPaCa-2 cells.**

MiaPaCa-2 cells were treated with various concentrations of GSK2606414 in complete medium for 1 hour, followed by addition of  $5\mu\text{g/mL}$  tunicamycin for an additional 6 hours to induce ER stress. Treated cells were harvested using trypsinization, and replated (500 cells/ dish) and cultured at  $37\text{ }^{\circ}\text{C}$  with  $5\% \text{CO}_2$  for 10 days. Images of the colonies formed after 10 days were taken after staining with  $0.2\%$  crystal violet. The colonies then were counted.

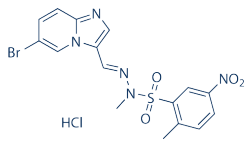
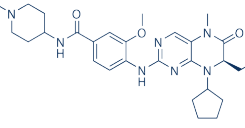
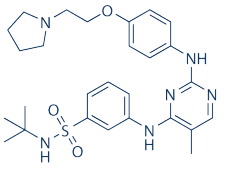
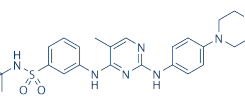


**Figure 4.19. Cellular effect of GSK2606414 on PERK signaling.**

MiaPaCa-2 cells were pre-treated with different concentrations of GSK2606414 (1-50  $\mu\text{M}$ ) followed by UPR induction for 5 hours (5  $\mu\text{g/ml}$  tunicamycin). Cell lysates were analyzed by western blot.

Compound	Structure	Inhibition (%)			Known Target
		25μM	5μM	1μM	
1	 HCl	100	100	97.9	PI3K DNA-PK
2		100	100	100	Plk1 Plk2 Plk3
3		100	82.1	57.9	Jak2 Flt3 Ret
4		92.9	64.3	51	Jak2 Jak3 Flt3 Ret

**Table 4.1. Inhibition rates of 4 hits from initial HTS using luminescent kinase assay.**

Compound	Structure	Inhibition (%)		Known Target
		5 $\mu$ M	0.5 $\mu$ M	
1		95	80	PI3K DNA-PK
2		93	71	Plk1 Plk2 Plk3
3		79	59	Jak2 Flt3 Ret
4		60	50	Jak2 Jak3 Flt3 Ret

**Table 4.2. Inhibition rates of 4 hits from validation screening using radiometric kinase assay.**

	<b>IC<sub>50</sub> for eIF2<math>\alpha</math> phosphorylation (<math>\mu</math>M)</b>	<b>IC<sub>50</sub> for PERK autophosphorylation (<math>\mu</math>M)</b>
Compound 1	0.068 $\pm$ 0.005	0.074 $\pm$ 0.009
Compound 2	0.3 $\pm$ 0.002	0.142 $\pm$ 0.014
Compound 3	0.019 $\pm$ 0.004	1.186 $\pm$ 0.6
Compound 4	0.045 $\pm$ 0.01	0.398 $\pm$ 0.11

**Table 4.3. Summary of PERK inhibition.**

## 4.6 SUPPLEMENTARY MATERIALS

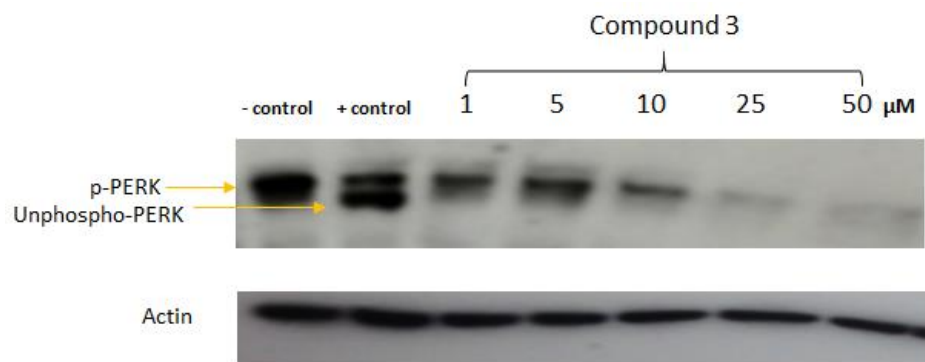


**Figure 4.S1. Cellular effect of compound 3 on the phosphorylation of PERK in HEK293T cells.**

HEK293T cells were pre-treated with different concentrations of compounds (1-50  $\mu\text{M}$ ) followed by UPR induction for 1 hour (1  $\mu\text{M}$  thapsigargin). Cell lysates were probed for PERK by western blot.

## References

1. Middelbeek, J., Clark, K., Venselaar, H., Huynen, M. A., and van Leeuwen, F. N. The alpha-kinase family: an exceptional branch on the protein kinase tree, *Cell Mol Life Sci* 67, 875-890.
2. Krapivinsky, G., Mochida, S., Krapivinsky, L., Cibulsky, S. M., and Clapham, D. E. (2006) The TRPM7 ion channel functions in cholinergic synaptic vesicles and affects transmitter release, *Neuron* 52, 485-496.
3. Venkatachalam, K., and Montell, C. (2007) TRP channels, *Annual review of biochemistry* 76, 387-417.
4. Tian, S. L., Jiang, H., and Shi, J. (2009) [TRPM7: a membrane protein with ion channel and kinase activities], *Sheng Li Ke Xue Jin Zhan* 40, 253-257.
5. Takezawa, R., Schmitz, C., Demeuse, P., Scharenberg, A. M., Penner, R., and Fleig, A. (2004) Receptor-mediated regulation of the TRPM7 channel through its endogenous protein kinase domain, *Proc Natl Acad Sci U S A* 101, 6009-6014.
6. Runnels, L. W., Yue, L., and Clapham, D. E. (2001) TRP-PLIK, a bifunctional protein with kinase and ion channel activities, *Science* 291, 1043-1047.
7. Ryazanov, A. G., Pavur, K. S., and Dorovkov, M. V. (1999) Alpha-kinases: a new class of protein kinases with a novel catalytic domain, *Curr Biol* 9, R43-45.
8. Nadler, M. J., Hermosura, M. C., Inabe, K., Perraud, A. L., Zhu, Q., Stokes, A. J., Kurosaki, T., Kinet, J. P., Penner, R., Scharenberg, A. M., and Fleig, A. (2001) LTRPC7 is a Mg<sub>2</sub>ATP-regulated divalent cation channel required for cell viability, *Nature* 411, 590-595.
9. Montell, C. (2005) The TRP superfamily of cation channels, *Sci STKE* 2005, re3.
10. Wolf, F. I. (2004) TRPM7: channeling the future of cellular magnesium homeostasis?, *Sci STKE* 2004, pe23.
11. Penner, R., and Fleig, A. (2007) The Mg<sup>2+</sup> and Mg(2+)-nucleotide-regulated channel-kinase TRPM7, *Handb Exp Pharmacol*, 313-328.
12. Monteilh-Zoller, M. K., Hermosura, M. C., Nadler, M. J., Scharenberg, A. M., Penner, R., and Fleig, A. (2003) TRPM7 provides an ion channel mechanism for cellular entry of trace metal ions, *J Gen Physiol* 121, 49-60.
13. Demeuse, P., Penner, R., and Fleig, A. (2006) TRPM7 channel is regulated by magnesium nucleotides via its kinase domain, *J Gen Physiol* 127, 421-434.
14. Schmitz, C., Perraud, A. L., Johnson, C. O., Inabe, K., Smith, M. K., Penner, R., Kurosaki, T., Fleig, A., and Scharenberg, A. M. (2003) Regulation of vertebrate cellular Mg<sup>2+</sup> homeostasis by TRPM7, *Cell* 114, 191-200.
15. Kozak, J. A., Matsushita, M., Nairn, A. C., and Cahalan, M. D. (2005) Charge screening by internal pH and polyvalent cations as a mechanism for activation, inhibition, and rundown of TRPM7/MIC channels, *J Gen Physiol* 126, 499-514.
16. Inoue, K., Branigan, D., and Xiong, Z. G. (2010) Zinc-induced neurotoxicity mediated by transient receptor potential melastatin 7 channels, *J Biol Chem* 285, 7430-7439.



17. Jiang, J., Li, M., and Yue, L. (2005) Potentiation of TRPM7 inward currents by protons, *J Gen Physiol* 126, 137-150.
18. Jiang, X., Newell, E. W., and Schlichter, L. C. (2003) Regulation of a TRPM7-like current in rat brain microglia, *J Biol Chem* 278, 42867-42876.
19. Runnels, L. W., Yue, L., and Clapham, D. E. (2002) The TRPM7 channel is inactivated by PIP(2) hydrolysis, *Nat Cell Biol* 4, 329-336.
20. Langeslag, M., Clark, K., Moolenaar, W. H., van Leeuwen, F. N., and Jalink, K. (2007) Activation of TRPM7 channels by phospholipase C-coupled receptor agonists, *J Biol Chem* 282, 232-239.
21. Tsuruda, P. R., Julius, D., and Minor, D. L., Jr. (2006) Coiled coils direct assembly of a cold-activated TRP channel, *Neuron* 51, 201-212.
22. Fujiwara, Y., and Minor, D. L., Jr. (2008) X-ray crystal structure of a TRPM assembly domain reveals an antiparallel four-stranded coiled-coil, *J Mol Biol* 383, 854-870.
23. Hanano, T., Hara, Y., Shi, J., Morita, H., Umebayashi, C., Mori, E., Sumimoto, H., Ito, Y., Mori, Y., and Inoue, R. (2004) Involvement of TRPM7 in cell growth as a spontaneously activated Ca<sup>2+</sup> entry pathway in human retinoblastoma cells, *J Pharmacol Sci* 95, 403-419.
24. Ryazanova, L. V., Rondon, L. J., Zierler, S., Hu, Z., Galli, J., Yamaguchi, T. P., Mazur, A., Fleig, A., and Ryazanov, A. G. (2010) TRPM7 is essential for Mg(2+) homeostasis in mammals, *Nat Commun* 1, 109.
25. Nicotera, P., and Bano, D. (2003) The enemy at the gates. Ca<sup>2+</sup> entry through TRPM7 channels and anoxic neuronal death, *Cell* 115, 768-770.
26. Aarts, M., Iihara, K., Wei, W. L., Xiong, Z. G., Arundine, M., Cerwinski, W., MacDonald, J. F., and Tymianski, M. (2003) A key role for TRPM7 channels in anoxic neuronal death, *Cell* 115, 863-877.
27. Wolf, F. I., and Trapani, V. TRPM7 and magnesium, metabolism, mitosis: An old path with new pebbles, *Cell Cycle* 9, 3399.
28. Yee, N. S., Zhou, W., and Liang, I. C. Transient receptor potential ion channel Trpm7 regulates exocrine pancreatic epithelial proliferation by Mg<sup>2+</sup>-sensitive Socs3a signaling in development and cancer, *Dis Model Mech* 4, 240-254.
29. Montezano, A. C., Zimmerman, D., Yusuf, H., Burger, D., Chignalia, A. Z., Wadhera, V., van Leeuwen, F. N., and Touyz, R. M. Vascular smooth muscle cell differentiation to an osteogenic phenotype involves TRPM7 modulation by magnesium, *Hypertension* 56, 453-462.
30. Drennan, D., and Ryazanov, A. G. (2004) Alpha-kinases: analysis of the family and comparison with conventional protein kinases, *Progress in biophysics and molecular biology* 85, 1-32.
31. Matsushita, M., Kozak, J. A., Shimizu, Y., McLachlin, D. T., Yamaguchi, H., Wei, F. Y., Tomizawa, K., Matsui, H., Chait, B. T., Cahalan, M. D., and Nairn, A. C. (2005) Channel function is dissociated from the intrinsic kinase activity and autophosphorylation of TRPM7/ChaK1, *J Biol Chem* 280, 20793-20803.

32. Yamaguchi, H., Matsushita, M., Nairn, A. C., and Kuriyan, J. (2001) Crystal structure of the atypical protein kinase domain of a TRP channel with phosphotransferase activity, *Mol Cell* 7, 1047-1057.
33. Crawley, S. W., and Cote, G. P. (2009) Identification of dimer interactions required for the catalytic activity of the TRPM7 alpha-kinase domain, *Biochem J* 420, 115-122.
34. Clark, K., Middelbeek, J., Morrice, N. A., Figdor, C. G., Lasonder, E., and van Leeuwen, F. N. (2008) Massive autophosphorylation of the Ser/Thr-rich domain controls protein kinase activity of TRPM6 and TRPM7, *PLoS One* 3, e1876.
35. Clark, K., Middelbeek, J., Dorovkov, M. V., Figdor, C. G., Ryazanov, A. G., Lasonder, E., and van Leeuwen, F. N. (2008) The alpha-kinases TRPM6 and TRPM7, but not eEF-2 kinase, phosphorylate the assembly domain of myosin IIA, IIB and IIC, *FEBS Lett* 582, 2993-2997.
36. Clark, K., Langeslag, M., van Leeuwen, B., Ran, L., Ryazanov, A. G., Figdor, C. G., Moolenaar, W. H., Jalink, K., and van Leeuwen, F. N. (2006) TRPM7, a novel regulator of actomyosin contractility and cell adhesion, *EMBO J* 25, 290-301.
37. Clark, K., Middelbeek, J., Lasonder, E., Dulyaninova, N. G., Morrice, N. A., Ryazanov, A. G., Bresnick, A. R., Figdor, C. G., and van Leeuwen, F. N. (2008) TRPM7 regulates myosin IIA filament stability and protein localization by heavy chain phosphorylation, *J Mol Biol* 378, 790-803.
38. Dorovkov, M. V., and Ryazanov, A. G. (2004) Phosphorylation of annexin I by TRPM7 channel-kinase, *J Biol Chem* 279, 50643-50646.
39. Jiang, J., Li, M. H., Inoue, K., Chu, X. P., Seeds, J., and Xiong, Z. G. (2007) Transient receptor potential melastatin 7-like current in human head and neck carcinoma cells: role in cell proliferation, *Cancer Res* 67, 10929-10938.
40. Kim, B. J., Park, K. J., Kim, H. W., Choi, S., Jun, J. Y., Chang, I. Y., Jeon, J. H., So, I., and Kim, S. J. (2009) Identification of TRPM7 channels in human intestinal interstitial cells of Cajal, *World J Gastroenterol* 15, 5799-5804.
41. Guilbert, A., Gautier, M., Dhennin-Duthille, I., Haren, N., Sevestre, H., and Ouadid-Ahidouch, H. (2009) Evidence that TRPM7 is required for breast cancer cell proliferation, *Am J Physiol Cell Physiol* 297, C493-502.
42. Dhennin-Duthille, I., Gautier, M., Faouzi, M., Guilbert, A., Brevet, M., Vaudry, D., Ahidouch, A., Sevestre, H., and Ouadid-Ahidouch, H. (2011) High expression of transient receptor potential channels in human breast cancer epithelial cells and tissues: correlation with pathological parameters, *Cell Physiol Biochem* 28, 813-822.
43. Guilbert, A., Gautier, M., Dhennin-Duthille, I., Rybarczyk, P., Sahni, J., Sevestre, H., Scharenberg, A. M., and Ouadid-Ahidouch, H. (2013) Transient receptor potential melastatin 7 is involved in oestrogen receptor-negative metastatic breast cancer cells migration through its kinase domain, *European journal of cancer* 49, 3694-3707.
44. Middelbeek, J., Kuipers, A. J., Henneman, L., Visser, D., Eidhof, I., van Horsen, R., Wieringa, B., Canisius, S. V., Zwart, W., Wessels, L. F., Sweep, F. C., Bult,

- P., Span, P. N., van Leeuwen, F. N., and Jalink, K. (2012) TRPM7 is required for breast tumor cell metastasis, *Cancer Res* 72, 4250-4261.
45. Nguyen, D. X., Bos, P. D., and Massague, J. (2009) Metastasis: from dissemination to organ-specific colonization, *Nature reviews. Cancer* 9, 274-284.
  46. Hanahan, D., and Weinberg, R. A. (2011) Hallmarks of cancer: the next generation, *Cell* 144, 646-674.
  47. Davis, F. M., Azimi, I., Faville, R. A., Peters, A. A., Jalink, K., Putney, J. W., Jr., Goodhill, G. J., Thompson, E. W., Roberts-Thomson, S. J., and Monteith, G. R. (2013) Induction of epithelial-mesenchymal transition (EMT) in breast cancer cells is calcium signal dependent, *Oncogene*.
  48. Meng, X., Cai, C., Wu, J., Cai, S., Ye, C., Chen, H., Yang, Z., Zeng, H., Shen, Q., and Zou, F. (2013) TRPM7 mediates breast cancer cell migration and invasion through the MAPK pathway, *Cancer Lett* 333, 96-102.
  49. Wang, S., and Kaufman, R. J. (2012) The impact of the unfolded protein response on human disease, *The Journal of cell biology* 197, 857-867.
  50. Sanchez-Lopez, E., Zimmerman, T., Gomez del Pulgar, T., Moyer, M. P., Lacal Sanjuan, J. C., and Cebrian, A. (2013) Choline kinase inhibition induces exacerbated endoplasmic reticulum stress and triggers apoptosis via CHOP in cancer cells, *Cell death & disease* 4, e933.
  51. Wang, W. A., Groenendyk, J., and Michalak, M. (2014) Endoplasmic reticulum stress associated responses in cancer, *Biochim Biophys Acta*.
  52. Lee, J., and Ozcan, U. (2014) Unfolded protein response signaling and metabolic diseases, *J Biol Chem* 289, 1203-1211.
  53. Vandewynckel, Y. P., Laukens, D., Geerts, A., Bogaerts, E., Paridaens, A., Verhelst, X., Janssens, S., Heindryckx, F., and Van Vlierberghe, H. (2013) The paradox of the unfolded protein response in cancer, *Anticancer research* 33, 4683-4694.
  54. Hetz, C., Chevet, E., and Harding, H. P. (2013) Targeting the unfolded protein response in disease, *Nature reviews. Drug discovery* 12, 703-719.
  55. Hetz, C. (2013) The biological meaning of the UPR, *Nature reviews. Molecular cell biology* 14, 404.
  56. Feldman, D. E., Chauhan, V., and Koong, A. C. (2005) The unfolded protein response: a novel component of the hypoxic stress response in tumors, *Mol Cancer Res* 3, 597-605.
  57. Kim, I., Xu, W., and Reed, J. C. (2008) Cell death and endoplasmic reticulum stress: disease relevance and therapeutic opportunities, *Nat Rev Drug Discov* 7, 1013-1030.
  58. Cornejo, V. H., and Hetz, C. (2013) The unfolded protein response in Alzheimer's disease, *Seminars in immunopathology* 35, 277-292.
  59. DuRose, J. B., Tam, A. B., and Niwa, M. (2006) Intrinsic capacities of molecular sensors of the unfolded protein response to sense alternate forms of endoplasmic reticulum stress, *Mol Biol Cell* 17, 3095-3107.

60. Onn, A., and Ron, D. Modeling the endoplasmic reticulum unfolded protein response, *Nat Struct Mol Biol* 17, 924-925.
61. Harding, H. P., Zhang, Y., Bertolotti, A., Zeng, H., and Ron, D. (2000) Perk is essential for translational regulation and cell survival during the unfolded protein response, *Mol Cell* 5, 897-904.
62. Sano, R., and Reed, J. C. (2013) ER stress-induced cell death mechanisms, *Biochim Biophys Acta* 1833, 3460-3470.
63. Tan, S., Wei, X., Song, M., Tao, J., Yang, Y., Khatoun, S., Liu, H., Jiang, J., and Wu, B. (2014) PUMA mediates ER stress-induced apoptosis in portal hypertensive gastropathy, *Cell death & disease* 5, e1128.
64. Xu, C., Bailly-Maitre, B., and Reed, J. C. (2005) Endoplasmic reticulum stress: cell life and death decisions, *The Journal of clinical investigation* 115, 2656-2664.
65. Ryno, L. M., Wiseman, R. L., and Kelly, J. W. (2013) Targeting unfolded protein response signaling pathways to ameliorate protein misfolding diseases, *Current opinion in chemical biology* 17, 346-352.
66. Cnop, M., Foufelle, F., and Velloso, L. A. (2012) Endoplasmic reticulum stress, obesity and diabetes, *Trends in molecular medicine* 18, 59-68.
67. Eizirik, D. L., Miani, M., and Cardozo, A. K. (2013) Signalling danger: endoplasmic reticulum stress and the unfolded protein response in pancreatic islet inflammation, *Diabetologia* 56, 234-241.
68. Chan, S. M., Sun, R. Q., Zeng, X. Y., Choong, Z. H., Wang, H., Watt, M. J., and Ye, J. M. (2013) Activation of PPARalpha ameliorates hepatic insulin resistance and steatosis in high fructose-fed mice despite increased endoplasmic reticulum stress, *Diabetes* 62, 2095-2105.
69. Engin, F., Yermalovich, A., Nguyen, T., Hummasti, S., Fu, W., Eizirik, D. L., Mathis, D., and Hotamisligil, G. S. (2013) Restoration of the unfolded protein response in pancreatic beta cells protects mice against type 1 diabetes, *Science translational medicine* 5, 211ra156.
70. Bertolotti, A., Zhang, Y., Hendershot, L. M., Harding, H. P., and Ron, D. (2000) Dynamic interaction of BiP and ER stress transducers in the unfolded-protein response, *Nat Cell Biol* 2, 326-332.
71. Ma, Y., Brewer, J. W., Diehl, J. A., and Hendershot, L. M. (2002) Two distinct stress signaling pathways converge upon the CHOP promoter during the mammalian unfolded protein response, *J Mol Biol* 318, 1351-1365.
72. Ma, Y., and Hendershot, L. M. (2004) The role of the unfolded protein response in tumour development: friend or foe?, *Nature reviews. Cancer* 4, 966-977.
73. Zhao, L., and Ackerman, S. L. (2006) Endoplasmic reticulum stress in health and disease, *Current opinion in cell biology* 18, 444-452.
74. Koumenis, C., Naczki, C., Koritzinsky, M., Rastani, S., Diehl, A., Sonenberg, N., Koromilas, A., and Wouters, B. G. (2002) Regulation of protein synthesis by hypoxia via activation of the endoplasmic reticulum kinase PERK and phosphorylation of the translation initiation factor eIF2alpha, *Molecular and cellular biology* 22, 7405-7416.

75. Zhang, J., Zhao, F., Zhao, Y., Wang, J., Pei, L., Sun, N., and Shi, J. Hypoxia induces an increase in intracellular magnesium via TRPM7 channels in rat hippocampal neurons in vitro, *J Biol Chem*.
76. Rao, R. V., Ellerby, H. M., and Bredesen, D. E. (2004) Coupling endoplasmic reticulum stress to the cell death program, *Cell Death Differ* 11, 372-380.
77. Martineau, Y., Le Bec, C., Monbrun, L., Allo, V., Chiu, I. M., Danos, O., Moine, H., Prats, H., and Prats, A. C. (2004) Internal ribosome entry site structural motifs conserved among mammalian fibroblast growth factor 1 alternatively spliced mRNAs, *Mol Cell Biol* 24, 7622-7635.
78. Vagner, S., Gensac, M. C., Maret, A., Bayard, F., Amalric, F., Prats, H., and Prats, A. C. (1995) Alternative translation of human fibroblast growth factor 2 mRNA occurs by internal entry of ribosomes, *Mol Cell Biol* 15, 35-44.
79. Bernstein, J., Sella, O., Le, S. Y., and Elroy-Stein, O. (1997) PDGF2/c-sis mRNA leader contains a differentiation-linked internal ribosomal entry site (D-IRES), *J Biol Chem* 272, 9356-9362.
80. Blais, J. D., Addison, C. L., Edge, R., Falls, T., Zhao, H., Wary, K., Koumenis, C., Harding, H. P., Ron, D., Holcik, M., and Bell, J. C. (2006) Perk-dependent translational regulation promotes tumor cell adaptation and angiogenesis in response to hypoxic stress, *Molecular and cellular biology* 26, 9517-9532.
81. Park, E. H., Lee, J. M., Blais, J. D., Bell, J. C., and Pelletier, J. (2005) Internal translation initiation mediated by the angiogenic factor Tie2, *J Biol Chem* 280, 20945-20953.
82. Gordan, J. D., Thompson, C. B., and Simon, M. C. (2007) HIF and c-Myc: sibling rivals for control of cancer cell metabolism and proliferation, *Cancer cell* 12, 108-113.
83. Blais, J. D., Filipenko, V., Bi, M., Harding, H. P., Ron, D., Koumenis, C., Wouters, B. G., and Bell, J. C. (2004) Activating transcription factor 4 is translationally regulated by hypoxic stress, *Molecular and cellular biology* 24, 7469-7482.
84. Dey, M., Velyvis, A., Li, J. J., Chiu, E., Chiovitti, D., Kay, L. E., Sicheri, F., and Dever, T. E. Requirement for kinase-induced conformational change in eukaryotic initiation factor 2alpha (eIF2alpha) restricts phosphorylation of Ser51, *Proc Natl Acad Sci U S A* 108, 4316-4321.
85. Pomar, N., Berlanga, J. J., Campuzano, S., Hernandez, G., Elias, M., and de Haro, C. (2003) Functional characterization of *Drosophila melanogaster* PERK eukaryotic initiation factor 2alpha (eIF2alpha) kinase, *Eur J Biochem* 270, 293-306.
86. Hinnebusch, A. G. (2005) eIF2alpha kinases provide a new solution to the puzzle of substrate specificity, *Nat Struct Mol Biol* 12, 835-838.
87. Donnelly, N., Gorman, A. M., Gupta, S., and Samali, A. (2013) The eIF2alpha kinases: their structures and functions, *Cell Mol Life Sci* 70, 3493-3511.
88. Harding, H. P., Zhang, Y., and Ron, D. (1999) Protein translation and folding are coupled by an endoplasmic-reticulum-resident kinase, *Nature* 397, 271-274.

89. Ma, K., Vattem, K. M., and Wek, R. C. (2002) Dimerization and release of molecular chaperone inhibition facilitate activation of eukaryotic initiation factor-2 kinase in response to endoplasmic reticulum stress, *J Biol Chem* 277, 18728-18735.
90. Yan, W., Frank, C. L., Korth, M. J., Sopher, B. L., Novoa, I., Ron, D., and Katze, M. G. (2002) Control of PERK eIF2alpha kinase activity by the endoplasmic reticulum stress-induced molecular chaperone P58IPK, *Proc Natl Acad Sci U S A* 99, 15920-15925.
91. Su, Q., Wang, S., Gao, H. Q., Kazemi, S., Harding, H. P., Ron, D., and Koromilas, A. E. (2008) Modulation of the eukaryotic initiation factor 2 alpha-subunit kinase PERK by tyrosine phosphorylation, *J Biol Chem* 283, 469-475.
92. Avivar-Valderas, A., Salas, E., Bobrovnikova-Marjon, E., Diehl, J. A., Nagi, C., Debnath, J., and Aguirre-Ghiso, J. A. (2011) PERK integrates autophagy and oxidative stress responses to promote survival during extracellular matrix detachment, *Molecular and cellular biology* 31, 3616-3629.
93. Cui, W., Li, J., Ron, D., and Sha, B. (2011) The structure of the PERK kinase domain suggests the mechanism for its activation, *Acta crystallographica. Section D, Biological crystallography* 67, 423-428.
94. Woo, C. W., Kutzler, L., Kimball, S. R., and Tabas, I. (2012) Toll-like receptor activation suppresses ER stress factor CHOP and translation inhibition through activation of eIF2B, *Nat Cell Biol* 14, 192-200.
95. Fernandez, J., Yaman, I., Sarnow, P., Snider, M. D., and Hatzoglou, M. (2002) Regulation of internal ribosomal entry site-mediated translation by phosphorylation of the translation initiation factor eIF2alpha, *J Biol Chem* 277, 19198-19205.
96. Fernandez, J., Bode, B., Koromilas, A., Diehl, J. A., Krukovets, I., Snider, M. D., and Hatzoglou, M. (2002) Translation mediated by the internal ribosome entry site of the cat-1 mRNA is regulated by glucose availability in a PERK kinase-dependent manner, *J Biol Chem* 277, 11780-11787.
97. Saito, A., Ochiai, K., Kondo, S., Tsumagari, K., Murakami, T., Cavener, D. R., and Imaizumi, K. (2011) Endoplasmic reticulum stress response mediated by the PERK-eIF2(alpha)-ATF4 pathway is involved in osteoblast differentiation induced by BMP2, *J Biol Chem* 286, 4809-4818.
98. Masuda, M., Miyazaki-Anzai, S., Levi, M., Ting, T. C., and Miyazaki, M. (2013) PERK-eIF2alpha-ATF4-CHOP signaling contributes to TNFalpha-induced vascular calcification, *Journal of the American Heart Association* 2, e000238.
99. Han, J., Back, S. H., Hur, J., Lin, Y. H., Gildersleeve, R., Shan, J., Yuan, C. L., Krokowski, D., Wang, S., Hatzoglou, M., Kilberg, M. S., Sartor, M. A., and Kaufman, R. J. (2013) ER-stress-induced transcriptional regulation increases protein synthesis leading to cell death, *Nature cell biology* 15, 481-490.
100. DeZwaan-McCabe, D., Riordan, J. D., Arensdorf, A. M., Icardi, M. S., Dupuy, A. J., and Rutkowski, D. T. (2013) The stress-regulated transcription factor CHOP

- promotes hepatic inflammatory gene expression, fibrosis, and oncogenesis, *PLoS genetics* 9, e1003937.
101. Wang, X., Liao, Y., Yap, P. L., Png, K. J., Tam, J. P., and Liu, D. X. (2009) Inhibition of protein kinase R activation and upregulation of GADD34 expression play a synergistic role in facilitating coronavirus replication by maintaining de novo protein synthesis in virus-infected cells, *Journal of virology* 83, 12462-12472.
  102. Cullinan, S. B., Zhang, D., Hannink, M., Arvisais, E., Kaufman, R. J., and Diehl, J. A. (2003) Nrf2 is a direct PERK substrate and effector of PERK-dependent cell survival, *Mol Cell Biol* 23, 7198-7209.
  103. Cullinan, S. B., and Diehl, J. A. (2004) PERK-dependent activation of Nrf2 contributes to redox homeostasis and cell survival following endoplasmic reticulum stress, *J Biol Chem* 279, 20108-20117.
  104. Harding, H. P., Zeng, H., Zhang, Y., Jungries, R., Chung, P., Plesken, H., Sabatini, D. D., and Ron, D. (2001) Diabetes mellitus and exocrine pancreatic dysfunction in *perk*<sup>-/-</sup> mice reveals a role for translational control in secretory cell survival, *Mol Cell* 7, 1153-1163.
  105. Zhang, W., Feng, D., Li, Y., Iida, K., McGrath, B., and Cavener, D. R. (2006) PERK EIF2AK3 control of pancreatic beta cell differentiation and proliferation is required for postnatal glucose homeostasis, *Cell Metab* 4, 491-497.
  106. Zhang, P., McGrath, B., Li, S., Frank, A., Zambito, F., Reinert, J., Gannon, M., Ma, K., McNaughton, K., and Cavener, D. R. (2002) The PERK eukaryotic initiation factor 2 alpha kinase is required for the development of the skeletal system, postnatal growth, and the function and viability of the pancreas, *Molecular and cellular biology* 22, 3864-3874.
  107. Harding, H. P., Zyryanova, A. F., and Ron, D. (2012) Uncoupling proteostasis and development in vitro with a small molecule inhibitor of the pancreatic endoplasmic reticulum kinase, PERK, *J Biol Chem* 287, 44338-44344.
  108. Wang, R., McGrath, B. C., Kopp, R. F., Roe, M. W., Tang, X., Chen, G., and Cavener, D. R. (2013) Insulin secretion and Ca<sup>2+</sup> dynamics in beta-cells are regulated by PERK (EIF2AK3) in concert with calcineurin, *J Biol Chem* 288, 33824-33836.
  109. Gao, Y., Sartori, D. J., Li, C., Yu, Q. C., Kushner, J. A., Simon, M. C., and Diehl, J. A. (2012) PERK is required in the adult pancreas and is essential for maintenance of glucose homeostasis, *Molecular and cellular biology* 32, 5129-5139.
  110. Dever, T. E. (1999) Translation initiation: adept at adapting, *Trends Biochem Sci* 24, 398-403.
  111. Satoh, S., Hijikata, M., Handa, H., and Shimotohno, K. (1999) Caspase-mediated cleavage of eukaryotic translation initiation factor subunit 2alpha, *The Biochemical journal* 342 ( Pt 1), 65-70.

112. Pavitt, G. D., Ramaiah, K. V., Kimball, S. R., and Hinnebusch, A. G. (1998) eIF2 independently binds two distinct eIF2B subcomplexes that catalyze and regulate guanine-nucleotide exchange, *Genes & development* 12, 514-526.
113. Jackson, R. J., Hellen, C. U., and Pestova, T. V. (2010) The mechanism of eukaryotic translation initiation and principles of its regulation, *Nature reviews. Molecular cell biology* 11, 113-127.
114. Fan, S., Li, Y., Yue, P., Khuri, F. R., and Sun, S. Y. (2010) The eIF4E/eIF4G interaction inhibitor 4EGI-1 augments TRAIL-mediated apoptosis through c-FLIP Down-regulation and DR5 induction independent of inhibition of cap-dependent protein translation, *Neoplasia* 12, 346-356.
115. Koumenis, C., and Wouters, B. G. (2006) "Translating" tumor hypoxia: unfolded protein response (UPR)-dependent and UPR-independent pathways, *Mol Cancer Res* 4, 423-436.
116. Jenner, R. G., Maillard, K., Cattini, N., Weiss, R. A., Boshoff, C., Wooster, R., and Kellam, P. (2003) Kaposi's sarcoma-associated herpesvirus-infected primary effusion lymphoma has a plasma cell gene expression profile, *Proc Natl Acad Sci U S A* 100, 10399-10404.
117. Fels, D. R., and Koumenis, C. (2006) The PERK/eIF2alpha/ATF4 module of the UPR in hypoxia resistance and tumor growth, *Cancer Biol Ther* 5, 723-728.
118. Bi, M., Naczki, C., Koritzinsky, M., Fels, D., Blais, J., Hu, N., Harding, H., Novoa, I., Varia, M., Raleigh, J., Scheuner, D., Kaufman, R. J., Bell, J., Ron, D., Wouters, B. G., and Koumenis, C. (2005) ER stress-regulated translation increases tolerance to extreme hypoxia and promotes tumor growth, *EMBO J* 24, 3470-3481.
119. Virrey, J. J., Dong, D., Stiles, C., Patterson, J. B., Pen, L., Ni, M., Schonthal, A. H., Chen, T. C., Hofman, F. M., and Lee, A. S. (2008) Stress chaperone GRP78/BiP confers chemoresistance to tumor-associated endothelial cells, *Mol Cancer Res* 6, 1268-1275.
120. Wouters, B. G., and Koritzinsky, M. (2008) Hypoxia signalling through mTOR and the unfolded protein response in cancer, *Nat Rev Cancer* 8, 851-864.
121. Arsham, A. M., Howell, J. J., and Simon, M. C. (2003) A novel hypoxia-inducible factor-independent hypoxic response regulating mammalian target of rapamycin and its targets, *J Biol Chem* 278, 29655-29660.
122. Gingras, A. C., Raught, B., Gygi, S. P., Niedzwiecka, A., Miron, M., Burley, S. K., Polakiewicz, R. D., Wyslouch-Cieszyńska, A., Aebersold, R., and Sonenberg, N. (2001) Hierarchical phosphorylation of the translation inhibitor 4E-BP1, *Genes Dev* 15, 2852-2864.
123. Hay, N., and Sonenberg, N. (2004) Upstream and downstream of mTOR, *Genes Dev* 18, 1926-1945.
124. Axten, J. M., Medina, J. R., Feng, Y., Shu, A., Romeril, S. P., Grant, S. W., Li, W. H., Heerding, D. A., Minthorn, E., Mencken, T., Atkins, C., Liu, Q., Rabindran, S., Kumar, R., Hong, X., Goetz, A., Stanley, T., Taylor, J. D., Sigethy, S. D., Tomberlin, G. H., Hassell, A. M., Kahler, K. M., Shewchuk, L. M., and



- Gampe, R. T. (2012) Discovery of 7-methyl-5-(1-([3-(trifluoromethyl)phenyl]acetyl)-2,3-dihydro-1H-indol-5-yl)-7H-pyrrolo[2,3-d]pyrimidin-4-amine (GSK2606414), a potent and selective first-in-class inhibitor of protein kinase R (PKR)-like endoplasmic reticulum kinase (PERK), *Journal of medicinal chemistry* 55, 7193-7207.
125. Atkins, C., Liu, Q., Minthorn, E., Zhang, S. Y., Figueroa, D. J., Moss, K., Stanley, T. B., Sanders, B., Goetz, A., Gaul, N., Choudhry, A. E., Alsaïd, H., Jucker, B. M., Axten, J. M., and Kumar, R. (2013) Characterization of a novel PERK kinase inhibitor with antitumor and antiangiogenic activity, *Cancer Res* 73, 1993-2002.
  126. Wolf, F. I., and Cittadini, A. (1999) Magnesium in cell proliferation and differentiation, *Front Biosci* 4, D607-617.
  127. Schlingmann, K. P., Waldegger, S., Konrad, M., Chubanov, V., and Gudermann, T. (2007) TRPM6 and TRPM7--Gatekeepers of human magnesium metabolism, *Biochim Biophys Acta* 1772, 813-821.
  128. Jin, J., Desai, B. N., Navarro, B., Donovan, A., Andrews, N. C., and Clapham, D. E. (2008) Deletion of Trpm7 disrupts embryonic development and thymopoiesis without altering Mg<sup>2+</sup> homeostasis, *Science* 322, 756-760.
  129. Ryazanova, L. V., Dorovkov, M. V., Ansari, A., and Ryazanov, A. G. (2004) Characterization of the protein kinase activity of TRPM7/ChaK1, a protein kinase fused to the transient receptor potential ion channel, *J Biol Chem* 279, 3708-3716.
  130. Su, L. T., Agapito, M. A., Li, M., Simonson, W. T., Huttenlocher, A., Habas, R., Yue, L., and Runnels, L. W. (2006) TRPM7 regulates cell adhesion by controlling the calcium-dependent protease calpain, *J Biol Chem* 281, 11260-11270.
  131. Sun, H. S., Jackson, M. F., Martin, L. J., Jansen, K., Teves, L., Cui, H., Kiyonaka, S., Mori, Y., Jones, M., Forder, J. P., Golde, T. E., Orser, B. A., Macdonald, J. F., and Tymianski, M. (2009) Suppression of hippocampal TRPM7 protein prevents delayed neuronal death in brain ischemia, *Nat Neurosci* 12, 1300-1307.
  132. Wei, W. L., Sun, H. S., Olah, M. E., Sun, X., Czerwinska, E., Czerwinski, W., Mori, Y., Orser, B. A., Xiong, Z. G., Jackson, M. F., Tymianski, M., and MacDonald, J. F. (2007) TRPM7 channels in hippocampal neurons detect levels of extracellular divalent cations, *Proc Natl Acad Sci U S A* 104, 16323-16328.
  133. Noble, M. E., Endicott, J. A., and Johnson, L. N. (2004) Protein kinase inhibitors: insights into drug design from structure, *Science* 303, 1800-1805.
  134. Li, Q., and Zhu, G. D. (2002) Targeting serine/threonine protein kinase B/Akt and cell-cycle checkpoint kinases for treating cancer, *Curr Top Med Chem* 2, 939-971.
  135. Arora, S., Yang, J. M., Kinzy, T. G., Utsumi, R., Okamoto, T., Kitayama, T., Ortiz, P. A., and Hait, W. N. (2003) Identification and characterization of an inhibitor of eukaryotic elongation factor 2 kinase against human cancer cell lines, *Cancer Res* 63, 6894-6899.
  136. Friday, B. B., and Adjei, A. A. (2008) Advances in targeting the Ras/Raf/MEK/Erk mitogen-activated protein kinase cascade with MEK inhibitors for cancer therapy, *Clin Cancer Res* 14, 342-346.

137. Wilsbacher, J. L., Juang, Y. C., Khokhlatchev, A. V., Gallagher, E., Binns, D., Goldsmith, E. J., and Cobb, M. H. (2006) Characterization of mitogen-activated protein kinase (MAPK) dimers, *Biochemistry* 45, 13175-13182.
138. Callaway, K. A., Rainey, M. A., Riggs, A. F., Abramczyk, O., and Dalby, K. N. (2006) Properties and regulation of a transiently assembled ERK2.Ets-1 signaling complex, *Biochemistry* 45, 13719-13733.
139. Kaoud, T. S., Devkota, A. K., Harris, R., Rana, M. S., Abramczyk, O., Warthaka, M., Lee, S., Girvin, M. E., Riggs, A. F., and Dalby, K. N. Activated ERK2 is a monomer in vitro with or without divalent cations and when complexed to the cytoplasmic scaffold PEA-15, *Biochemistry* 50, 4568-4578.
140. Alexey G. Ryazanov, B. E. T. (2011) EEK2 ASSAYS FOR IDENTIFYING COMPOUNDS THAT INHIBIT EEK2 ACTIVITY.
141. Perraud, A. L., Zhao, X., Ryazanov, A. G., and Schmitz, C. The channel-kinase TRPM7 regulates phosphorylation of the translational factor eEF2 via eEF2-k, *Cell Signal* 23, 586-593.
142. Tavares, C. D., O'Brien, J. P., Abramczyk, O., Devkota, A. K., Shores, K. S., Ferguson, S. B., Kaoud, T. S., Warthaka, M., Marshall, K. D., Keller, K. M., Zhang, Y., Brodbelt, J. S., Ozpolat, B., and Dalby, K. N. (2012) Calcium/calmodulin stimulates the autophosphorylation of elongation factor 2 kinase on Thr-348 and Ser-500 to regulate its activity and calcium dependence, *Biochemistry* 51, 2232-2245.
143. Devkota, A. K., Tavares, C. D., Warthaka, M., Abramczyk, O., Marshall, K. D., Kaoud, T. S., Gorgulu, K., Ozpolat, B., and Dalby, K. N. (2012) Investigating the kinetic mechanism of inhibition of elongation factor 2 kinase by NH125: evidence of a common in vitro artifact, *Biochemistry* 51, 2100-2112.
144. Bacac, M., and Stamenkovic, I. (2008) Metastatic cancer cell, *Annu Rev Pathol* 3, 221-247.
145. Valastyan, S., Reinhardt, F., Benaich, N., Calogrias, D., Szasz, A. M., Wang, Z. C., Brock, J. E., Richardson, A. L., and Weinberg, R. A. (2009) A pleiotropically acting microRNA, miR-31, inhibits breast cancer metastasis, *Cell* 137, 1032-1046.
146. Koresawa, M., and Okabe, T. (2004) High-throughput screening with quantitation of ATP consumption: a universal non-radioisotope, homogeneous assay for protein kinase, *Assay Drug Dev Technol* 2, 153-160.
147. Zhang, J. H., Chung, T. D., and Oldenburg, K. R. (1999) A Simple Statistical Parameter for Use in Evaluation and Validation of High Throughput Screening Assays, *J Biomol Screen* 4, 67-73.
148. Feng, B. Y., and Shoichet, B. K. (2006) A detergent-based assay for the detection of promiscuous inhibitors, *Nat Protoc* 1, 550-553.
149. McGovern, S. L., Helfand, B. T., Feng, B., and Shoichet, B. K. (2003) A specific mechanism of nonspecific inhibition, *J Med Chem* 46, 4265-4272.
150. Ryan, A. J., Gray, N. M., Lowe, P. N., and Chung, C. W. (2003) Effect of detergent on "promiscuous" inhibitors, *J Med Chem* 46, 3448-3451.

151. Kaoud, T. S., Mitra, S., Lee, S., Taliaferro, J., Cantrell, M., Linse, K. D., Van Den Berg, C. L., and Dalby, K. N. (2011) Development of JNK2-selective peptide inhibitors that inhibit breast cancer cell migration, *ACS Chem Biol* 6, 658-666.
152. Liang, S. H., Zhang, W., McGrath, B. C., Zhang, P., and Cavener, D. R. (2006) PERK (eIF2alpha kinase) is required to activate the stress-activated MAPKs and induce the expression of immediate-early genes upon disruption of ER calcium homeostasis, *Biochem J* 393, 201-209.
153. Fischer, U., Janicke, R. U., and Schulze-Osthoff, K. (2003) Many cuts to ruin: a comprehensive update of caspase substrates, *Cell death and differentiation* 10, 76-100.
154. Saelens, X., Kalai, M., and Vandenabeele, P. (2001) Translation inhibition in apoptosis: caspase-dependent PKR activation and eIF2-alpha phosphorylation, *J Biol Chem* 276, 41620-41628.
155. Bobrovnikova-Marjon, E., Grigoriadou, C., Pytel, D., Zhang, F., Ye, J., Koumenis, C., Cavener, D., and Diehl, J. A. (2010) PERK promotes cancer cell proliferation and tumor growth by limiting oxidative DNA damage, *Oncogene* 29, 3881-3895.
156. Zhou, T., Georgeon, S., Moser, R., Moore, D. J., Caflisch, A., and Hantschel, O. (2014) Specificity and mechanism-of-action of the JAK2 tyrosine kinase inhibitors ruxolitinib and SAR302503 (TG101348), *Leukemia* 28, 404-407.
157. Verstovsek, S. (2011) Janus-activated kinase 2 inhibitors: a new era of targeted therapies providing significant clinical benefit for Philadelphia chromosome-negative myeloproliferative neoplasms, *Journal of clinical oncology : official journal of the American Society of Clinical Oncology* 29, 781-783.
158. Sayyah, J., and Sayeski, P. P. (2009) Jak2 inhibitors: rationale and role as therapeutic agents in hematologic malignancies, *Current oncology reports* 11, 117-124.
159. Steelman, L. S., Pohnert, S. C., Shelton, J. G., Franklin, R. A., Bertrand, F. E., and McCubrey, J. A. (2004) JAK/STAT, Raf/MEK/ERK, PI3K/Akt and BCR-ABL in cell cycle progression and leukemogenesis, *Leukemia* 18, 189-218.
160. Zouein, F. A., Duhe, R. J., and Booz, G. W. (2011) JAKs go nuclear: emerging role of nuclear JAK1 and JAK2 in gene expression and cell growth, *Growth factors* 29, 245-252.
161. Silvennoinen, O., Saharinen, P., Paukku, K., Takaluoma, K., and Kovanen, P. (1997) Cytokine receptor signal transduction through Jak tyrosine kinases and Stat transcription factors, *APMIS : acta pathologica, microbiologica, et immunologica Scandinavica* 105, 497-509.
162. Levine, R. L., and Wernig, G. (2006) Role of JAK-STAT signaling in the pathogenesis of myeloproliferative disorders, *Hematology / the Education Program of the American Society of Hematology. American Society of Hematology. Education Program*, 233-239, 510.
163. Cojocari, D., Vellanki, R. N., Sit, B., Uehling, D., Koritzinsky, M., and Wouters, B. G. (2013) New small molecule inhibitors of UPR activation demonstrate that

PERK, but not IRE1alpha signaling is essential for promoting adaptation and survival to hypoxia, *Radiotherapy and oncology : journal of the European Society for Therapeutic Radiology and Oncology* 108, 541-547.